

**POMK regulates dystroglycan function via LARGE1-mediated
elongation of matriglycan**

**Ameya S. Walimbe¹, Hidehiko Okuma¹, Soumya Joseph¹, Tiandi Yang¹, Takahiro
Yonekawa¹, Jeffrey M. Hord¹, David Venzke¹, Mary E. Anderson¹, Silvia Torelli², Adnan
Manzur², Megan Devereaux¹, Marco Cuellar¹, Sally Prouty¹, Saul Ocampo Landa¹, Liping
Yu³, Junyu Xiao⁵, Jack E. Dixon⁶, Francesco Muntoni^{2, 4}, and Kevin P. Campbell^{1*}**

¹Howard Hughes Medical Institute, Senator Paul D. Wellstone Muscular Dystrophy Specialized
Research Center, Department of Molecular Physiology and Biophysics and Department of
Neurology, Roy J. and Lucille A. Carver College of Medicine, The University of Iowa, Iowa
City, Iowa 52242, USA

²Dubowitz Neuromuscular Centre, UCL Great Ormond Street Institute of Child Health & Great
Ormond Street Hospital, London, United Kingdom.

³Medical Nuclear Magnetic Resonance Facility, University of Iowa Roy J. and Lucille A. Carver
College of Medicine, B291 Carver Biomedical Research Building, 285 Newton Road, Iowa City,
IA 52242, USA

⁴National Institute for Health Research Great Ormond Street Hospital Biomedical Research
Centre, UCL Great Ormond Street Institute of Child Health, London, United Kingdom.

⁵The State Key Laboratory of Protein and Plant Gene Research, School of Life Sciences,
Academy for Advanced Interdisciplinary Studies, Peking-Tsinghua Center for Life Sciences,
Peking University, Beijing, 100871, China

⁶Department of Pharmacology, Department of Cellular and Molecular Medicine, Department of
Chemistry and Biochemistry, University of California, San Diego, La Jolla, CA 92093, USA

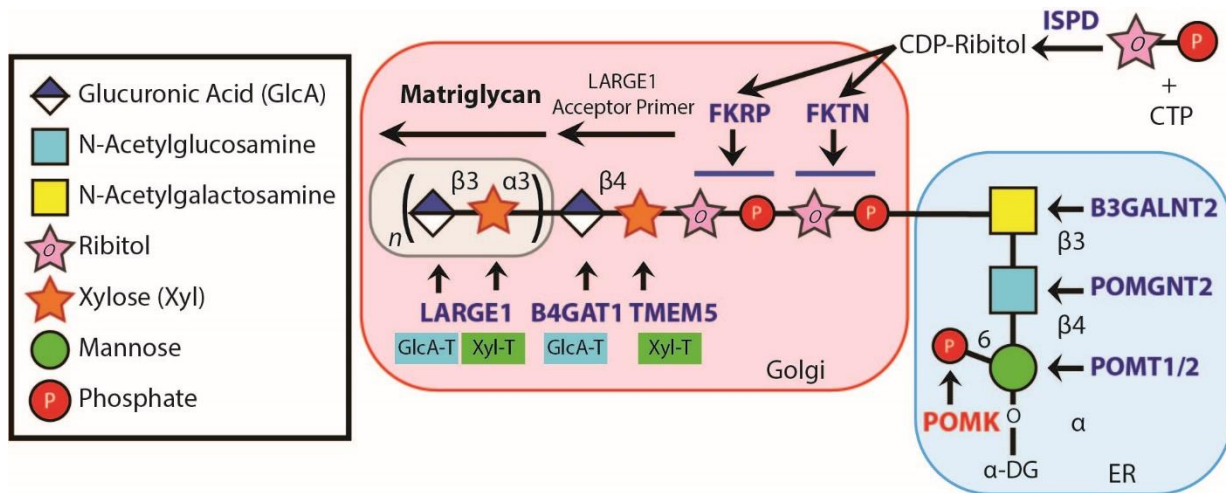
* Corresponding author

27 **Abstract**

28 Matriglycan [-GlcA- β 1,3-Xyl- α 1,3-]_n serves as a scaffold in many tissues for extracellular matrix
29 proteins containing laminin-G domains including laminin, agrin, and perlecan. Like-
30 acetylglucosaminyltransferase-1 (LARGE1) synthesizes and extends matriglycan on α -
31 dystroglycan (α -DG) during skeletal muscle differentiation and regeneration; however, the
32 mechanisms which regulate matriglycan elongation are unknown. Here, we show that Protein O-
33 Mannose Kinase (POMK), which phosphorylates mannose of core M3 (GalNac- β 1,3-GlcNac-
34 β 1,4-Man) preceding matriglycan synthesis, is required for LARGE1-mediated generation of
35 full-length matriglycan on α -DG (~150 kDa). In the absence of *Pomk* gene expression in mouse
36 skeletal muscle, LARGE1 synthesizes a very short matriglycan resulting in a ~90 kDa α -DG
37 which binds laminin but cannot prevent eccentric contraction-induced force loss or muscle
38 pathology. Solution NMR spectroscopy studies demonstrate that LARGE1 directly interacts with
39 core M3 and binds preferentially to the phosphorylated form. Collectively, our study
40 demonstrates that phosphorylation of core M3 by POMK enables LARGE1 to elongate
41 matriglycan on α -DG, thereby preventing muscular dystrophy.

42 Introduction

43 The extracellular matrix (ECM) is essential for development, regeneration and
44 physiological function in many tissues, and abnormalities in ECM structure can lead to disease
45 (*Rowe et al., 2008; Hudson et al., 2003*). The heteropolysaccharide [-GlcA- β 1,3-Xyl- α 1,3-]_n
46 (called matriglycan) is a scaffold for ECM proteins containing laminin-G (LG) domains (e.g.
47 laminin, agrin, and perlecan) (*Yoshida-Moriguchi et al., 2015; Hohenester, 2019; Michele et al,*
48 *2002; Ohtsubo et al., 2006*) and has the remarkable capacity to be tuned during skeletal muscle
49 development and regeneration (*Goddeeris et al., 2013*). Over eighteen genes are involved in the
50 synthesis of the post translational modification terminating in matriglycan (*Figure 1*), and
51 defects in this process cause dystroglycanopathies, congenital and limb-girdle muscular
52 dystrophies that can be accompanied by brain and eye defects. Like-
53 acetylglucosaminyltransferase-1 (LARGE1) synthesizes matriglycan on the cell-surface
54 glycoprotein, α -dystroglycan (α -DG) (*Inamori et al., 2012*). Addition of matriglycan enables α -
55 DG to serve as the predominant ECM receptor in skeletal muscle and brain (*Yoshida-Moriguchi*
56 *et al., 2015; Hohenester, 2019; Jae et al., 2013; Yoshida-Moriguchi et al., 2010; Yoshida-*
57 *Moriguchi et al., 2013*). Crystal structure studies have shown that a single glucuronic acid-
58 xylose disaccharide (GlcA-Xyl) repeat binds to laminin- α 2 LG4 domain (*Briggs et al., 2016;*
59 *Hohenester et al., 1999*), and there is a direct correlation between the number of GlcA-Xyl
60 repeats on α -DG and its binding capacity for ECM ligands (*Goddeeris et al., 2013; Inamori et*
61 *al., 2012*). During skeletal muscle differentiation, LARGE1 elongates matriglycan to its full
62 length for normal skeletal muscle function (*Goddeeris et al., 2013*). However, little is known
63 about the mechanisms which control matriglycan elongation.

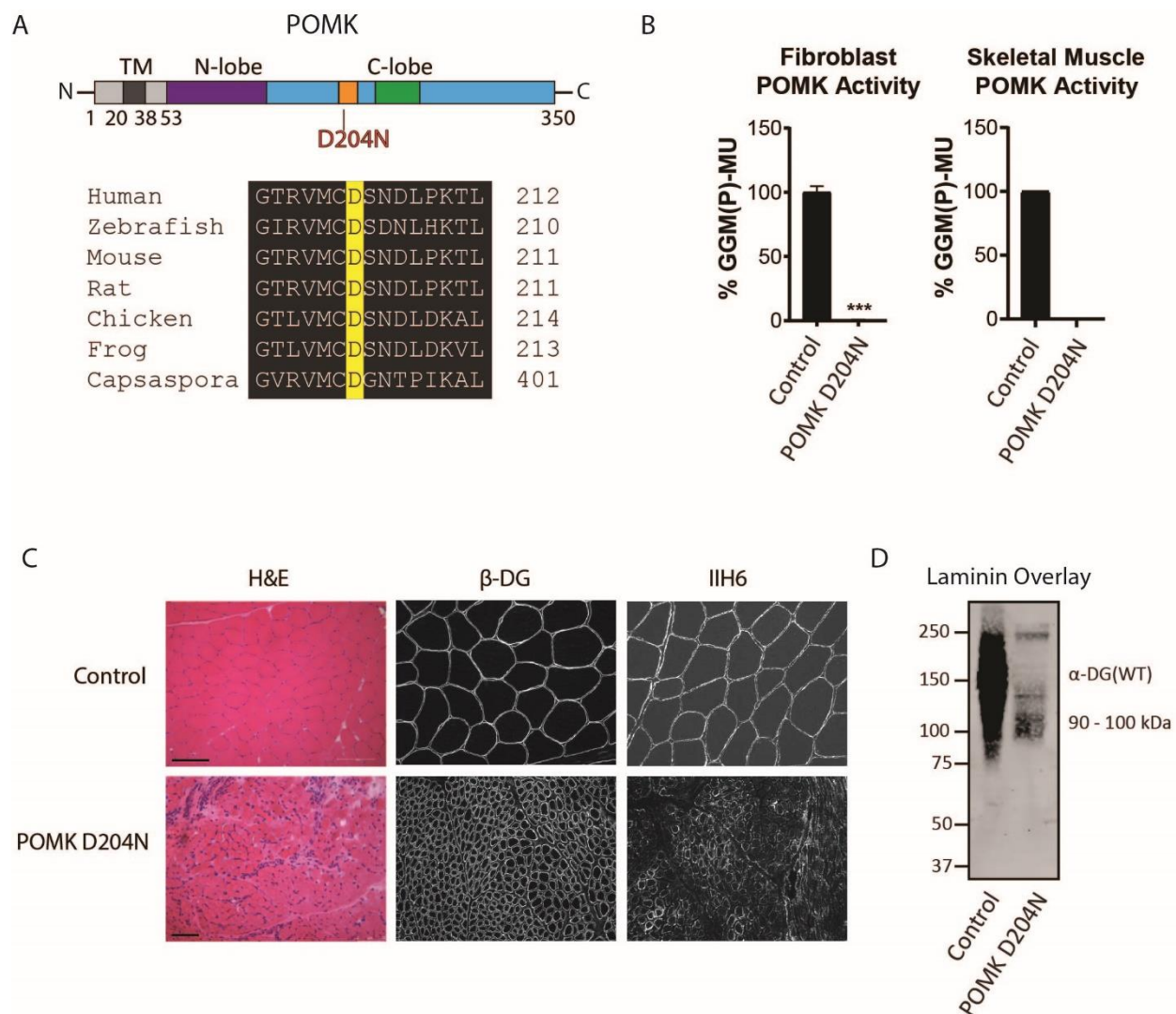


64
 65 **Figure 1.** Synthesis of the α -DG Laminin-Binding Modification and Enzymes Involved.
 66 Synthesis of the laminin-binding modification begins with the addition of the core M3
 67 trisaccharide (GalNAc- β 3-GlcNAc- β 4-Man) on α -DG by the sequential actions of Protein O-
 68 Mannosyltransferase-1 and 2 (POMT1/2), Protein O-linked mannose N-
 69 acetylglucosaminyltransferase 2 (POMGNT2), and β 1,3-N-acetylgalactosaminyltransferase 2
 70 B3GALNT2, in the ER. POMK phosphorylates the C6 hydroxyl of mannose after synthesis of
 71 core M3. The phosphorylated core M3 is further elongated in the Golgi by Fukutin (FKTN),
 72 Fukutin-Related Protein (FKRP), Transmembrane Protein 5 (TMEM5), β 1-4-
 73 glucuronyltransferase-1 (B4GAT1), and Like-acetylglucosaminyltransferase-1 (LARGE1).
 74 Isoprenoid Synthase Domain-Containing (ISPD) produces cytidine diphosphate (CDP)-Ribitol in
 75 the cytosol, and this serves as a sugar donor for the reactions catalyzed by FKTN and FKRP.
 76 LARGE1 synthesizes matriglycan, which directly interacts with the LG domains of matrix
 77 ligands.

78 Complete loss-of-function mutations in the dystroglycanopathy genes abrogate synthesis
79 of the post translational modification terminating in matriglycan. Such mutations preclude
80 addition of matriglycan and, thereby, cause the most severe form of dystroglycanopathy, Walker-
81 Warburg Syndrome (WWS), which is lethal *in utero* or within a day or two of birth (*Yoshida-
82 Moriguchi et al., 2015; Hohenester, 2019; Michele et al., 2002; Ohtsubo et al., 2006*). Protein
83 *O*-Mannose Kinase (POMK) is a glycosylation-specific kinase that phosphorylates mannose of
84 the core M3 trisaccharide (GalNac- β 1,3-GlcNac- β 1,4-Man) during synthesis of the *O*-mannose-
85 linked polysaccharide ending in matriglycan (*Yoshida-Moriguchi et al., 2015; Hohenester et
86 al., 2019; Jae et al., 2013; Yoshida-Moriguchi et al., 2013; Zhu et al., 2016*). Interestingly,
87 unlike with other dystroglycanopathy genes there are patients with complete loss-of-function
88 mutations in POMK who suffer from mild forms of dystroglycanopathy (*Di Costanzo et al.,
89 2014; von Renesse et al., 2014*), suggesting some expression of matriglycan without POMK.
90 Here, we have used a multidisciplinary approach to show that phosphorylation of core M3 by
91 POMK is not necessary for the LARGE1-mediated synthesis of a short, non-extended form of
92 matriglycan on α -DG (~90 kDa) with reduced laminin binding capacity; however, POMK
93 activity is required for LARGE1 to generate full-length matriglycan on α -DG (~150 kDa). In the
94 absence of the phosphorylated core M3, the non-extended matriglycan on ~90 kDa α -DG binds
95 laminin and maintains specific force but cannot prevent eccentric contraction-induced force loss
96 or skeletal muscle pathology. Furthermore, solution NMR studies demonstrated that LARGE1
97 directly interacts with core M3, binding preferentially to the phosphorylated form. Therefore, our
98 study shows that phosphorylation of core M3 by POMK enables LARGE1 to elongate
99 matriglycan on α -DG. Collectively, our work demonstrates a requirement for POMK in the
100 LARGE1-mediated synthesis of full-length matriglycan and proper skeletal muscle function.

101 **Results**

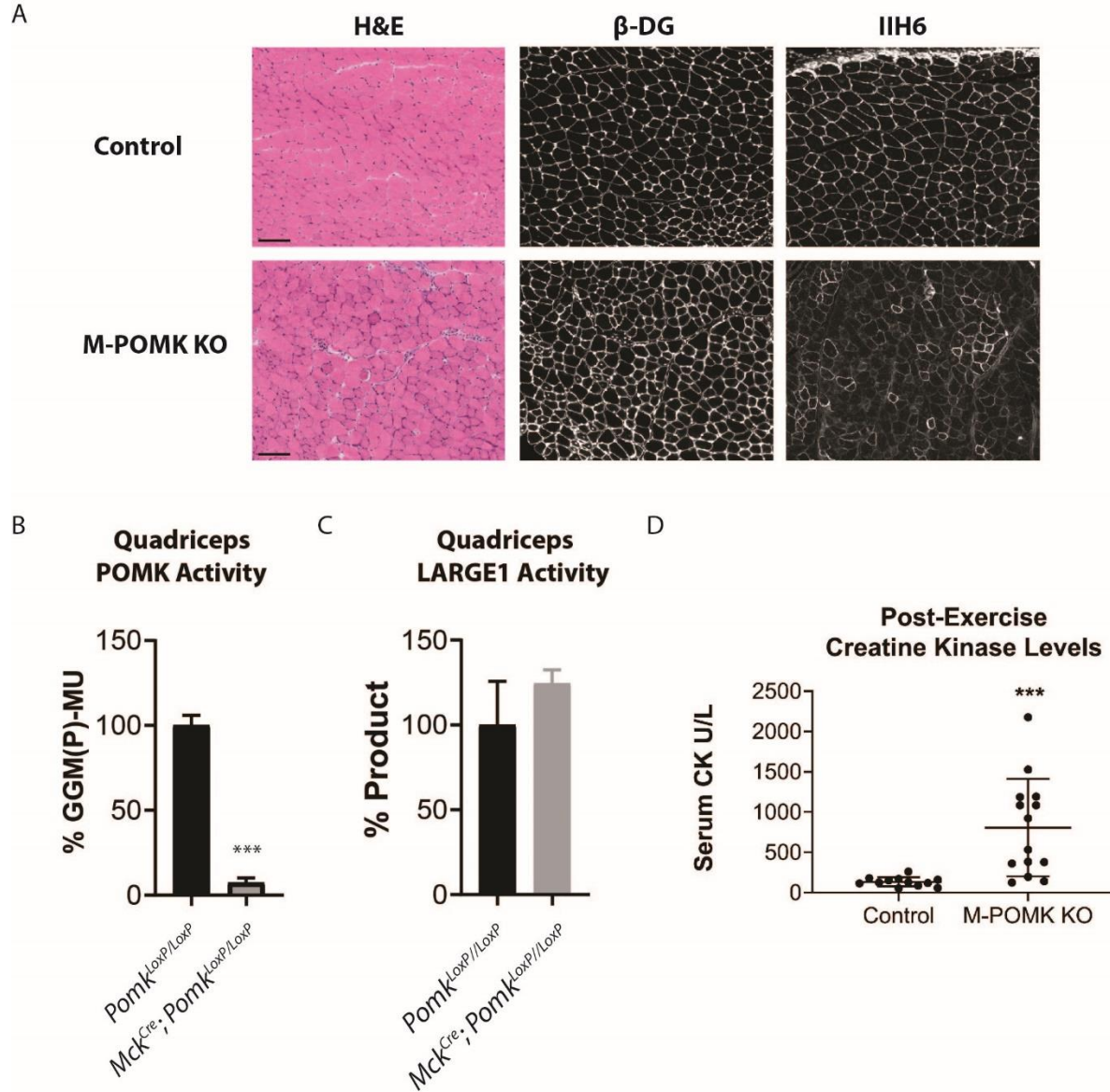
102 To determine if matriglycan can be expressed in the absence of POMK function, and
103 therefore better understand the role of POMK in matriglycan synthesis, we studied skeletal
104 muscle from a patient (NH13-284) with a POMK (D204N) mutation (**Figure 2A**) and congenital
105 muscular dystrophy (CMD) accompanied by structural brain malformations. D204 serves as the
106 catalytic base in the phosphorylation reaction catalyzed by the kinase (**Figure 2A; Figure 2-**
107 **Figure Supplement 1**), and its mutation is predicted to eliminate POMK activity (**Figure 2-**
108 **Figure Supplement 1**) (Zhu et al., 2016). POMK activity from skin fibroblasts and skeletal
109 muscle of patient NH13-284 (POMK D204N) was undetectable when compared to control
110 fibroblasts and muscle, respectively (**Figure 2B**). Fibroblast LARGE1 activity and skeletal
111 muscle B4GAT1 activity of patient NH13-284 were similar to those of a control (**Figure 2-**
112 **Figure Supplement 2A, 2B**). Immunofluorescence analyses of POMK D204N muscle
113 demonstrated partial immunoreactivity to IIIH6 (anti-matriglycan), while the transmembrane
114 subunit of DG, β -DG, was expressed normally in POMK D204N muscle (**Figure 2C**). Flow
115 cytometry using IIIH6 also demonstrated partial immunoreactivity in POMK D204N fibroblasts
116 (**Figure 2-Figure Supplement 2C**). To test the effect of the POMK mutation on ligand binding
117 we performed a laminin overlay using laminin-111. Control human skeletal muscle showed the
118 typical broad band of α -DG laminin binding centered at ~150 kDa range; in contrast, laminin
119 binding at ~90 to 100 kDa range with reduced intensity was observed in POMK D204N skeletal
120 muscle (**Figure 2D**).



121
 122 **Figure 2.** Characterization of a Patient with a Loss-of-Function Mutation in POMK. **A**, (above)
 123 Human POMK consists of a transmembrane domain (TM) and a kinase domain (N-lobe and C-
 124 lobe). The kinase domain contains the catalytic loop (orange) and activation segment (green).
 125 (below) Alignment of protein sequences flanking the D204N mutation. The mutation alters a
 126 highly conserved aspartate that is the catalytic base of the phosphorylation reaction catalyzed by
 127 the kinase. **B**, POMK activity in control and patient NH13-284 (POMK D204N) fibroblasts (left)
 128 and skeletal muscle (right). n=3 experiments were performed in fibroblasts. Triple asterisks:
 129 statistical significance with Student's unpaired t-test (p-value<0.0001). Due to limited skeletal
 130 muscle, n=1 experiment was performed. **C**, Histology and immunofluorescence of control and
 131 POMK D204N skeletal muscle using I1H6 (anti-matriglycan) and a β -DG antibody. (Scale bars:
 132 Control- 200 μ M, POMK D204N- 75 μ M). **D**, Laminin overlay of control and POMK D204N
 133 skeletal muscle.

134 To understand the biochemical basis of the ~90 to 100 kDa laminin binding in the
135 absence of POMK activity, we targeted *Pomk* using LoxP sites and *Cre* driven by the *muscle*
136 *creatine kinase (Mck)* promoter, or both the *Mck* promoter and the *paired box 7 (Pax7)* promoter
137 (**Figure 3-Figure Supplement 1, 2**) (**Brüning et al., 1998; Keller et al., 2004**) to generate
138 muscle-specific *Pomk*-null mouse models. Histologic analyses of *Mck^{Cre}; Pax7^{Cre}; Pomk^{LoxP/LoxP}*
139 (M-POMK KO) quadriceps muscles revealed hallmarks of a mild muscular dystrophy (**Figure**
140 **3A**). Quadriceps muscle extracts of *Mck^{Cre}; Pomk^{LoxP/LoxP}* mice showed reduced POMK activity
141 compared to *Pomk^{LoxP/LoxP}* muscle but had similar levels of LARGE1 activity (**Figure 3B, 3C**).
142 M-POMK KO mice also showed reductions in 2-limb grip strength and body weight and
143 elevations in post-exercise creatine kinase (CK) levels compared to littermate control
144 *Pomk^{LoxP/LoxP}* mice (**Figure 3D; Figure 3-Figure Supplement 3**). Immunofluorescence analysis
145 of M-POMK KO muscle showed that β -DG is expressed at the skeletal-muscle sarcolemma
146 (**Figure 3A**); however, like patient NH13-284 IIH6 immunoreactivity persisted in M-POMK KO
147 muscle, but at a reduced intensity (**Figure 3A**).

148

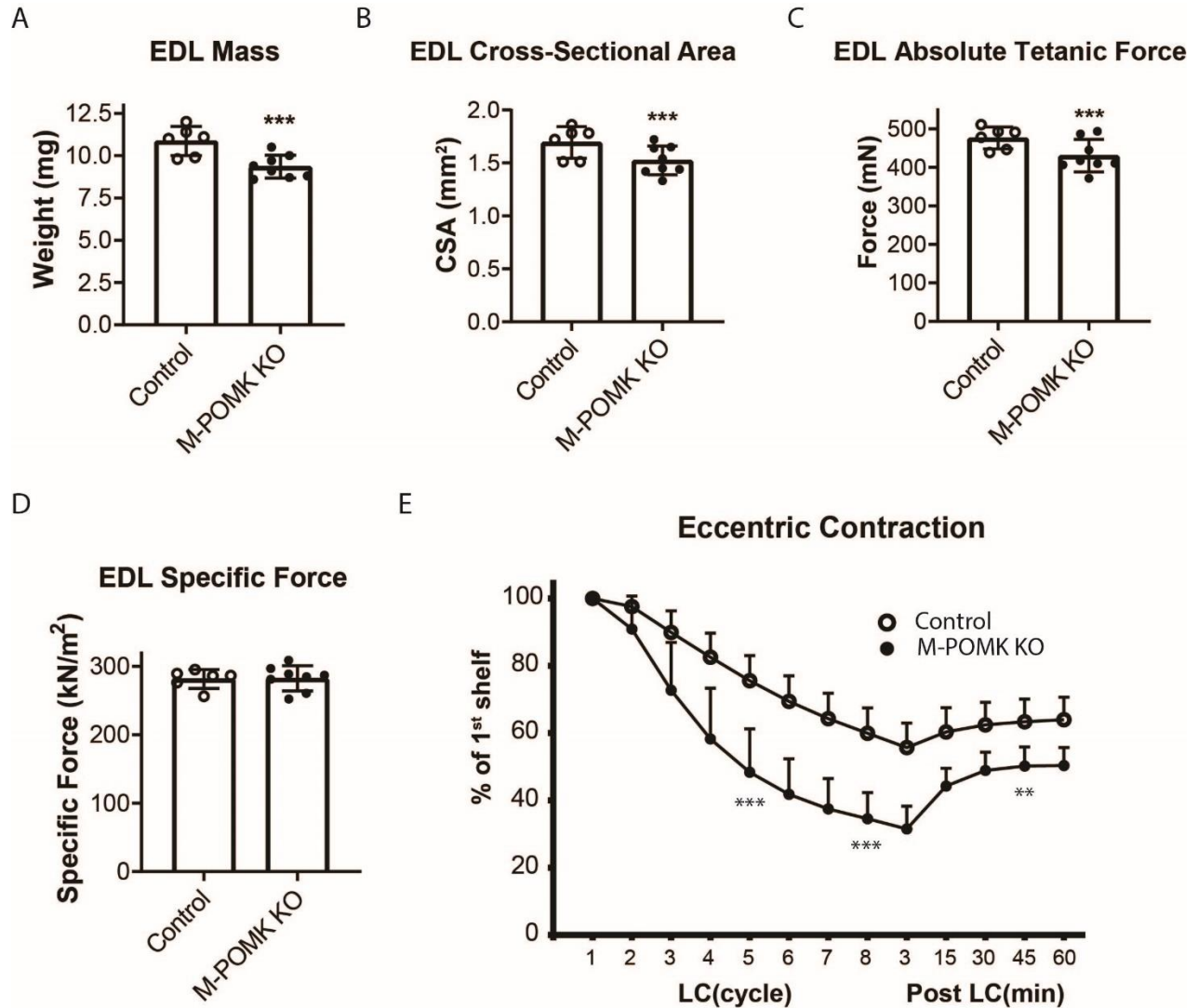


149

Figure 3. Mice with a Muscle-Specific Loss of POMK Develop Hallmarks of a Mild Muscular Dystrophy. **A**, H&E and immunofluorescence analyses using IIH6 (anti-matriglycan) and an anti- β -DG antibody of quadriceps muscles of 4-6-week-old *Pomk^{LoxP/LoxP}* (control) and *Mck^{Cre}; Pax7^{Cre}; Pomk^{LoxP/LoxP}* (M-POMK KO) mice. Scale bars: 100 μ M. **B**, POMK and **C**, LARGE1 activity in extracts of *Mck^{Cre}; Pomk^{LoxP/LoxP}* and *Pomk^{LoxP/LoxP}* quadriceps skeletal muscles. Triple asterisks indicate statistical significance using Student's unpaired t-test (p-value<0.0001, three replicates). **D**, Creatine kinase levels of 8-week old M-POMK KO and Control mice. P-values were calculated with Student's unpaired t-test. Triple asterisks: statistical significance with p-value < 0.05 (p-value=0.0008), n=12 Control and 14 M-POMK KO mice.

159 We next examined *ex vivo* force production in extensor digitorum muscles (EDL)
160 muscles of 18-20 week-old control and M-POMK KO mice. EDL muscle mass and cross-
161 sectional area (CSA) were reduced in M-POMK KO mice compared to control mice (**Figure 4A**,
162 **4B**). Additionally, M-POMK KO EDL absolute isometric tetanic force production was
163 significantly lower than that of controls (**Figure 4C**). However, when normalized to muscle
164 CSA, force production was comparable to control values (**Figure 4D**). We also sought to
165 determine if M-POMK KO muscle could withstand repeated eccentric contractions. EDL
166 muscles of M-POMK KO mice demonstrated greater force deficits after five and eight
167 lengthening contractions (LC) and recovered to a lower level after 45 minutes compared to
168 control EDL (**Figure 4E**). Together, the isometric and eccentric contractile studies suggest that
169 the M-POMK KO EDL muscles display a specific force similar to controls (**Figure 4D**);
170 however, muscle integrity is compromised following the stress of repeated eccentric
171 contractions, as displayed by the slow, but progressive decline in force production and hampered
172 recovery (**Figure 4E**). Thus, the current results demonstrate that the short matriglycan in POMK-
173 deficient skeletal muscle can maintain specific force but cannot prevent eccentric contraction-
174 induced force loss or muscle pathology.

175



176 **Figure 4.** *Mck^{Cre}; Pax7^{Cre}; Pomk^{LoxP/LoxP}* EDL Demonstrates Eccentric Contraction-Induced
 177 Force Loss. **A**, Mass (milligrams) of *Pomk^{LoxP/LoxP}* (Control) and *Mck^{Cre}; Pax7^{Cre}; Pomk^{LoxP/LoxP}*
 178 (M-POMK KO) EDL muscles tested for force production. ***Statistical significance with
 179 Student's unpaired t-test with p-value<0.05 (p=0.0031). **B**, Cross-sectional area (CSA) of EDL
 180 muscles. ***Statistical significance using Student's unpaired t-test with p-value<0.05
 181 (p=0.0463). **C**, Maximum Absolute Tetanic Force production by Control and M-POMK KO
 182 EDL muscles. ***Statistical significance using Student's unpaired t-test with a p-value<0.05
 183 (p=0.0395). **D**, Specific Force Production in Control and M-POMK KO extensor digitorum
 184 longus (EDL) muscles. (p=0.921). **E**, Force deficit and force recovery in *Pomk^{LoxP/LoxP}* (Control,
 185 n=3 mice) and (M-POMK KO, n=4 mice) mice after eccentric contractions. Individual extensor
 186 digitorum longus (EDL) muscles from 18-20-week-old male mice were tested and are
 187 represented by open (Control) or closed (M-POMK KO) circles. ***Statistical significance using
 188 Student's unpaired t-test (p-value<0.0001) compared to Control EDL at given LC cycle.
 189 **Statistical significance using Student's unpaired t-test (p-value=0.0027) compared to Control
 190 EDL at given LC cycle. Error bars represent SD.
 191

192 Biochemical analysis of control and M-POMK KO muscle showed a typical, lower
193 molecular weight (MW) α -DG with anti-core DG antibody (**Figure 5A**), however, on laminin
194 overlay, we observed laminin binding at 90-100 kDa (**Figure 5B**), similar to POMK D204N
195 skeletal muscle (**Figure 2D**). IIH6 also showed binding at 90-100 kDa (**Figure 5C**). Solid-phase
196 binding analyses of M-POMK KO and *Mck^{Cre}; Pomk^{LoxP/LoxP}* skeletal muscle demonstrated a
197 reduced binding capacity (relative B_{max}) for laminin-111 compared to control muscle (**Figure 5-**
198 **Figure Supplement 1A**), but higher than that of *Large^{myd}* muscle, which lacks matriglycan due to
199 a deletion in *Large*.

200 To determine if matriglycan is responsible for the laminin binding at 90-100 kDa in
201 POMK-null muscle, we treated glycoproteins enriched from skeletal muscles of M-POMK KO
202 and *Mck^{Cre}; Pomk^{LoxP/LoxP}* mice with two exoglycosidases, α -Xylosidase and β -Glucuronidase,
203 which in combination digest matriglycan (**Figure 5-Figure Supplement 1B, 2A, 2B**) (**Briggs et**
204 **al., 2016**). Laminin overlay and solid phase analysis showed a reduction in laminin binding from
205 these muscles after dual exoglycosidase digestion (**Figure 5D, 5E; Figure 5- Figure**
206 **Supplement 2A, 2B**).

207

208

209

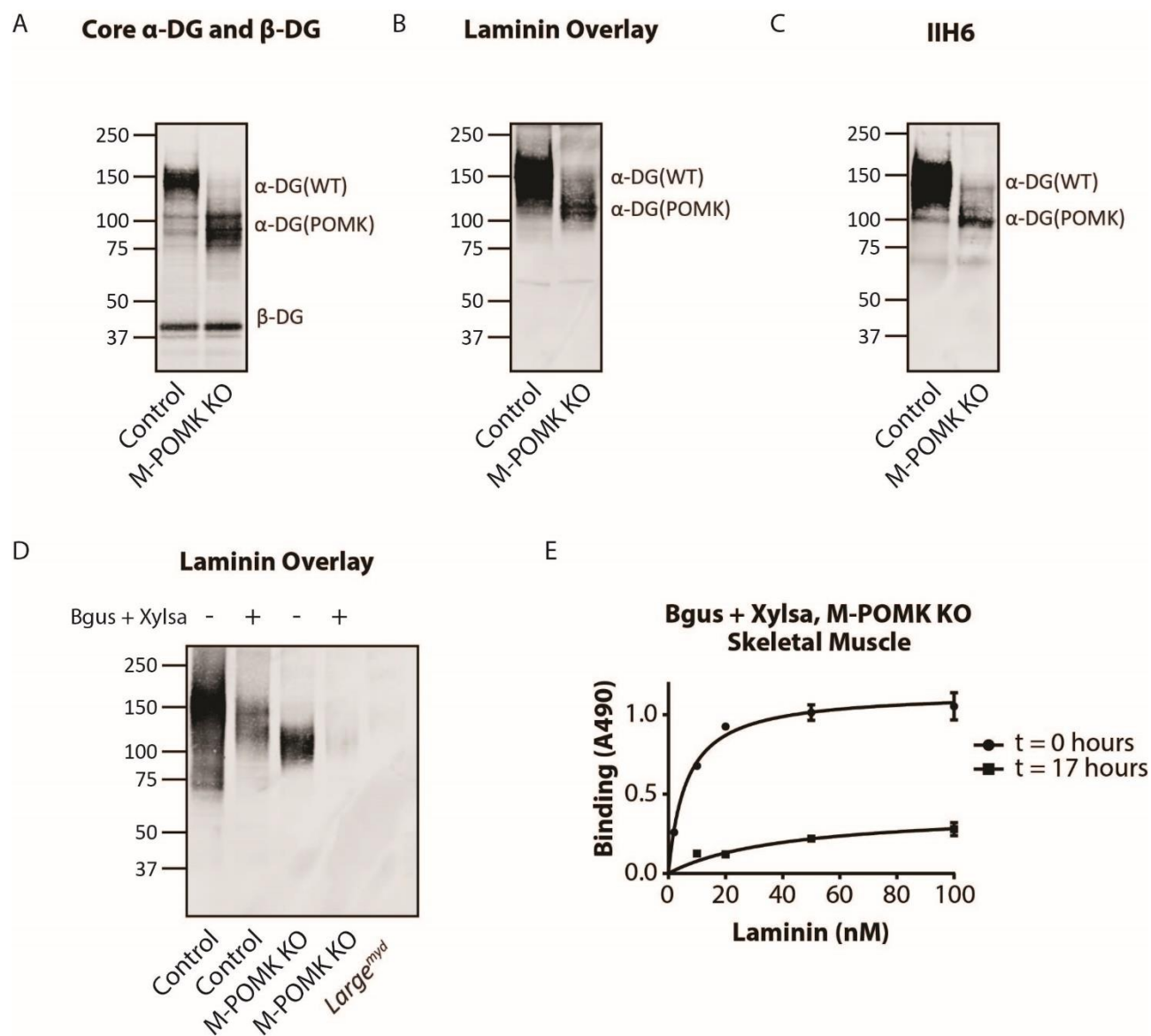
210

211

212

213

214

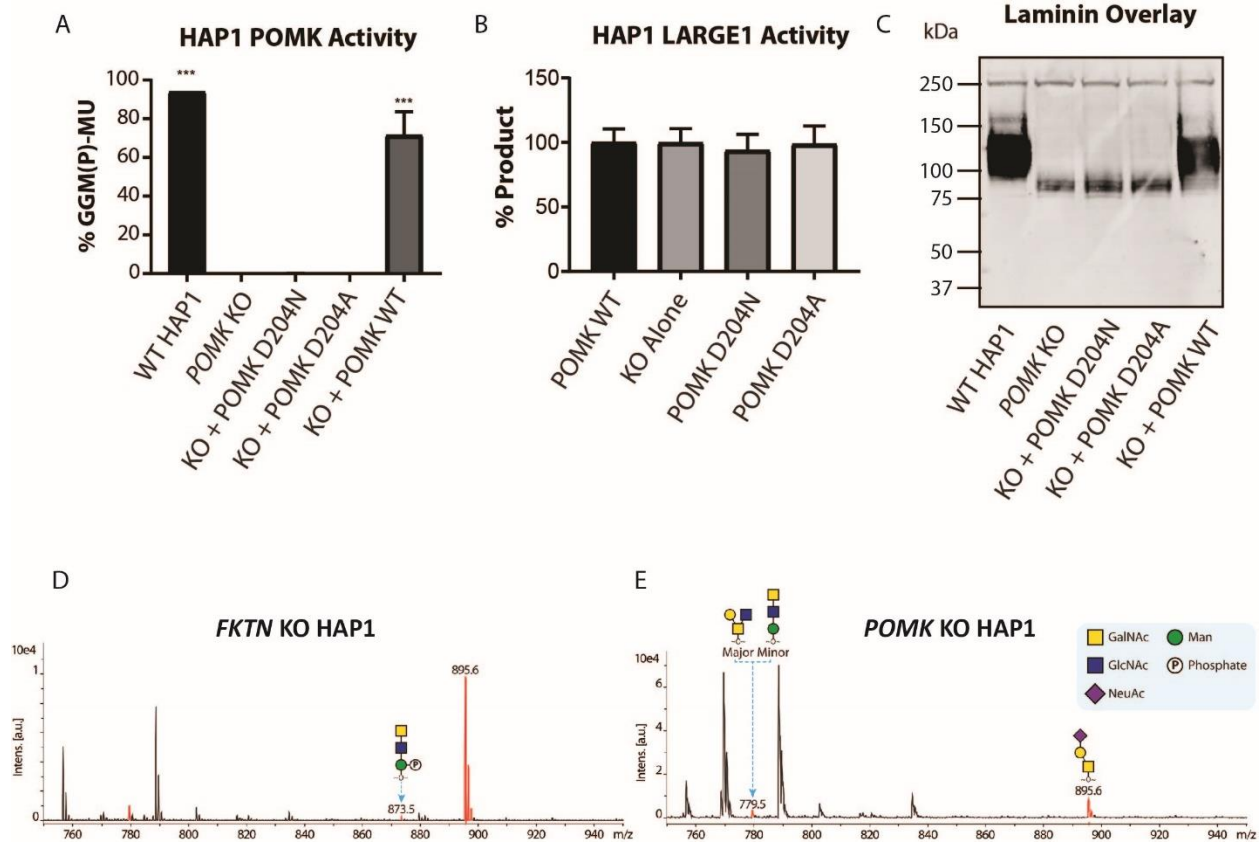


215

216 **Figure 5.** Mice with a Muscle-Specific Loss of POMK Express Matriglycan. **A**, Biochemical
 217 analysis of Control and M-POMK KO skeletal muscle. Glycoproteins were enriched from
 218 quadriceps skeletal muscles of mice using wheat-germ agglutinin (WGA)-agarose.
 219 Immunoblotting was performed with antibody AF6868, which recognizes core α -DG and β -DG
 220 (three replicates). **B**, Laminin overlay of quadriceps muscles of Control and M-POMK KO mice
 221 (three replicates). **C**, IHH6 immunoblotting of Control and M-POMK KO quadriceps muscle.
 222 **D, E**, Laminin overlay (**D**) and Solid phase analysis (**E**) of skeletal muscles of M-POMK KO
 223 mice treated in combination with two exoglycosidases, α -xylosidase (Xylsa) and β -glucuronidase
 224 (Bgus) for 17 hours (three replicates).

225 To study the role of POMK further, we used human *POMK* KO HAP1 cells, which have
226 undetectable levels of POMK activity and expression (**Figure 6A; Figure 6- Figure Supplement**
227 **1A**) (*Zhu et al., 2016*). A mass spectrometry (MS)-based glycomic analysis of *O*-glycans carried
228 by recombinantly-expressed DG mucin-like domain indicated the near complete absence of an
229 MS peak at m/z 873.5 corresponding to phosphorylated core M3 *O*-glycan (**Figure 6D, 6E;**
230 **Figure 6- Figure Supplement 2A, 2B**), consistent with an undetectable level of POMK activity
231 in *POMK* KO HAP1 cells. Compared to WT HAP1 cells, immunoblots of *POMK* KO HAP1
232 cells showed a reduction in IIH6 immunoreactivity, a decrease in MW of core α -DG, and the
233 presence of laminin binding at ~90 kDa on laminin overlay (**Figure 6C; Figure 6-Figure**
234 **Supplement 1B, 1C**). Laminin binding on overlay was rescued only after adenoviral transduction
235 with wild-type (WT) POMK (POMK WT), but not with POMK containing D204N (POMK
236 D204N) or D204A (POMK D204A) mutations (**Figure 6C**). POMK D204N also lacked POMK
237 activity *in vitro* but showed normal B4GAT1, B3GALNT2, and LARGE1 activity, thus
238 confirming the pathogenicity of the D204N mutation (**Figure 6A, 6B; Figure 6- Figure**
239 **Supplement 1D, 1E**).

240

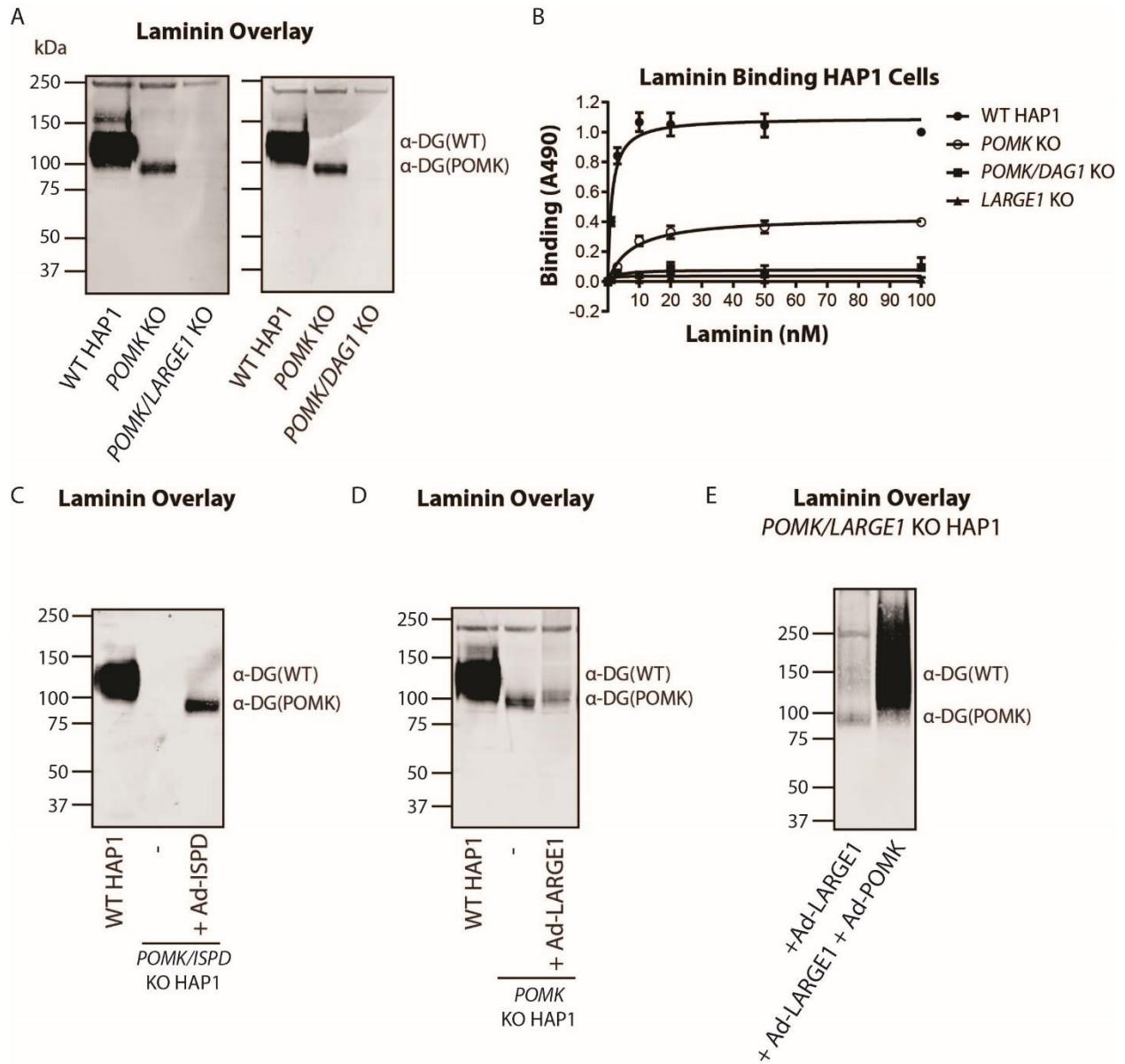


241

242 **Figure 6.** POMK D204N lacks Catalytic Activity. **A**, POMK or **B**, LARGE1 activity in *POMK*
 243 KO HAP1 cells transduced with adenoviruses encoding POMK D204N, D204A, or POMK WT.
 244 Triple asterisks: statistical significance (p -value <0.0001) compared to *POMK* KO alone using
 245 One-Way ANOVA with Dunnett's Test for Multiple Comparisons (three replicates, 95%
 246 Confidence intervals for *POMK* KO vs. WT HAP1: -106.7 to -81.0, *POMK* KO vs. *POMK* KO +
 247 POMK WT: -84.25 to -58.54). **C**, Laminin overlay of *POMK* KO HAP1 cells expressing the
 248 indicated POMK mutants. **D**, **E**, Mass Spectrometry (MS)-based *O*-glycomics analyses of DG
 249 mucin-like domain (DG390TevHis) expressed in *Fukutin* (*FKTN*) (**D**) or *POMK* (**E**) KO HAP1
 250 cells. *O*-glycans were released from the protein backbone and permethylated prior to Matrix-
 251 Assisted Laser Desorption/Ionization time-of-flight (MALDI-TOF) analyses. MS peaks at m/z
 252 779.5 (779.6) correspond to a mixture of core 2 and core M3 *O*-glycan, and at 873.5,
 253 phosphorylated core M3 *O*-glycan (red). MALDI-TOF is unable to determine anomeric or
 254 epimeric configurations of annotated *O*-glycans.

255 To directly test if LARGE1 is required for synthesis of the 90 kDa laminin-binding
256 glycoprotein in *POMK* KO HAP1 cells, we studied *POMK/LARGE1* KO HAP1 cells, which bear
257 a CRISPR/Cas9-mediated deletion in *LARGE1* as well as *POMK*. *POMK/LARGE1* KO HAP1
258 cells demonstrated the absence of the laminin binding at 90 kDa (**Figure 7A; Figure 7-Figure**
259 **Supplement 1A, 1B**), indicating that LARGE1 is required for the synthesis of the matriglycan
260 responsible for laminin binding at 90 kDa. Moreover, *POMK/DAG1* KO HAP1 cells
261 demonstrated a complete absence of laminin binding (**Figure 7A**) and I1H6 immunoreactivity at
262 90 kDa (**Figure 7- Figure Supplement 1C**), demonstrating that α -DG is the glycoprotein that
263 binds laminin in the absence of POMK. We, therefore, refer to this glycoprotein as POMK-null
264 α -DG (α -DG(POMK)). Since the length of matriglycan correlates with its binding capacity for
265 ECM ligands (*Goddeeris et al., 2013*), we hypothesized that, given the MW of α -DG(POMK) at
266 90 kDa, the glycan must be shorter than full-length matriglycan, and therefore, have a lower B_{max}
267 for laminin. We measured the binding capacity of HAP1 α -DG using solid-phase binding assays.
268 B_{max} of α -DG(POMK) for laminin-111 was reduced compared to wild-type α -DG (α -DG(WT))
269 but was greater than that of α -DG from *LARGE1* KO HAP1 cells (**Figure 7B**). *POMK/DAG1*
270 KO HAP1 cells showed a reduction in B_{max} compared to *POMK* KO HAP1 cells, but similar to
271 the low levels observed in *LARGE1* KO HAP1 cells (**Figure 7B**). These data indicate that a
272 short, non-extended form of matriglycan is synthesized on α -DG(POMK), and this short form
273 has a lower binding capacity for laminin-111, thus exhibiting a reduced level of α -DG receptor
274 function.

275



276

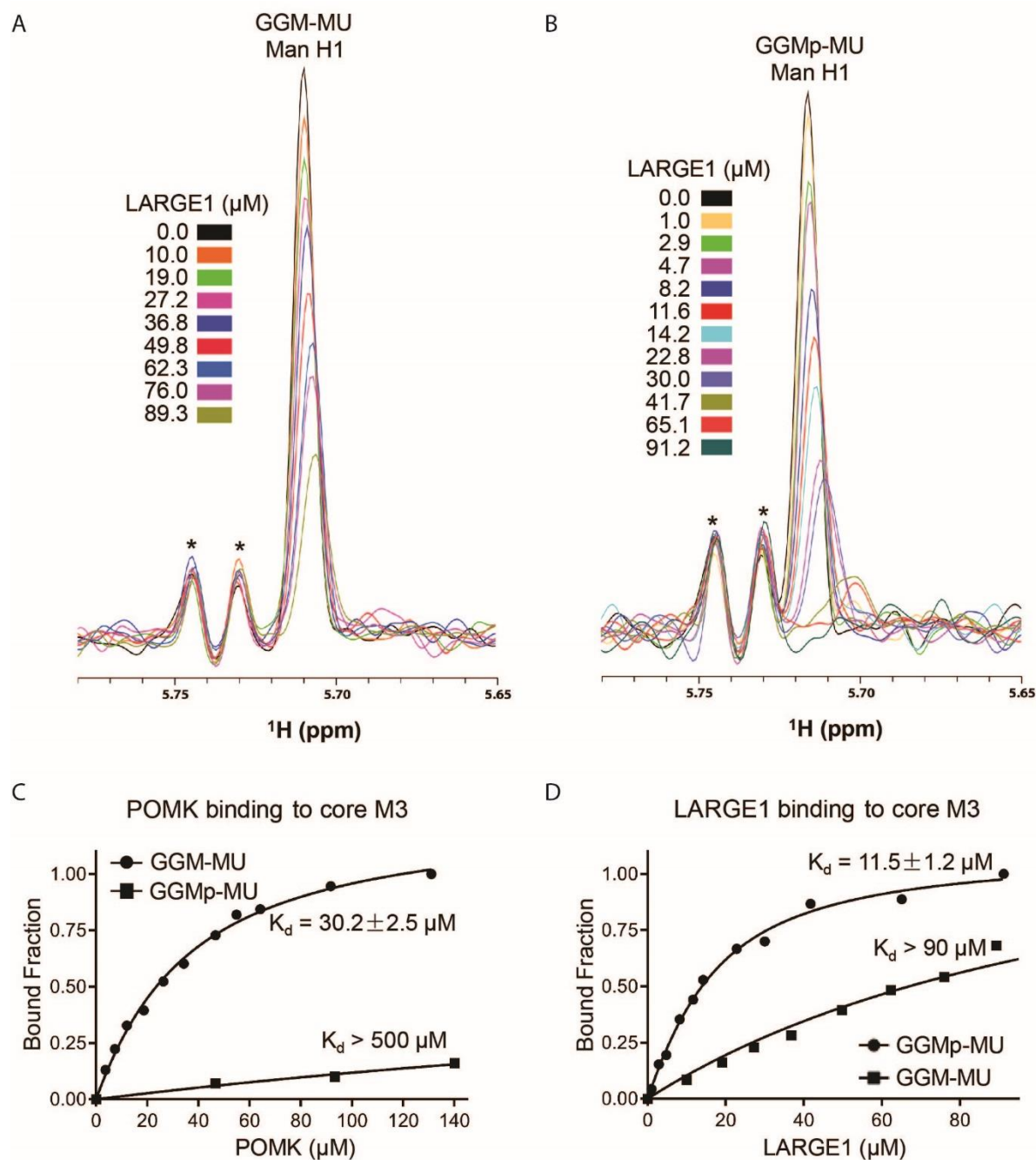
277 **Figure 7.** LARGE1 requires POMK to Elongate Matriglycan. **A**, WT, *POMK* KO, and
 278 *POMK/LARGE1* KO HAP1 cells (left) or *POMK/DAG1* KO HAP1 cells (right) (three
 279 replicates). **B**, Solid phase analysis of WT, *POMK* KO, *POMK/DAG1* KO, and *LARGE1* KO
 280 HAP1 cells (three replicates). **C**, **D**, **E**, Laminin overlays of the following KO HAP1 cells (three
 281 replicates): *POMK/ISPD* expressing Ad-ISP (C); *POMK* expressing Ad-LARGE1 (D);
 282 *POMK/LARGE1* expressing Ad-LARGE1 with or without Ad-POMK (E).

283 After POMK phosphorylates core M3, Fukutin (FKTN) modifies GalNac with ribitol-
284 phosphate for synthesis of full-length matriglycan (*Figure 1*) (*Yoshida-Moriguchi et al., 2015*;
285 *Hohenester, 2019; Kanagawa et al., 2016*). Overexpression in *POMK* KO HAP1 cells of
286 Isoprenoid Synthase Domain-Containing (ISPD), which synthesizes the substrate (CDP-ribitol)
287 of FKTN (*Figure 1*), increases the amount of matriglycan (without changing its MW)
288 responsible for laminin binding at 90 kDa (*Figure 7-Figure Supplement 2A, 2B, 2C*) (*Willer et*
289 *al., 2012; Gerin et al., 2016; Riemersma et al., 2015*). HAP1 cells lacking both *POMK* and
290 *ISPD* do not express matriglycan, and adenoviral transduction of these cells with ISPD restores
291 the 90 kDa laminin binding (*Figure 7C; Figure 7- Figure Supplement 2D, 2E*). FKTN
292 overexpression in *POMK* KO HAP1 cells also increased the 90 kDa laminin binding (*Figure 7-*
293 *Figure Supplement 3A, 3B, 3C*). These experiments collectively support a requirement for CDP-
294 ribitol for synthesis of the non-extended form of matriglycan. This synthesis also requires the N-
295 terminal domain of α -DG (DGN) (*Hara et al., 2011; Kanagawa et al., 2004*), as a DG mutant
296 lacking the DGN (DGE) expressed in *POMK/DAG1* KO HAP1 cells did not show laminin
297 binding at 90 kDa (*Figure 7-Figure Supplement 4A, 4B, 4C*). Similar experiments also
298 indicated that synthesis of the non-extended matriglycan in HAP1 cells requires threonine-317 of
299 the mucin-like domain of α -DG (*Figure 7-Figure Supplement 4A, 4B, 4C*).

300 Overexpression of LARGE1 can rescue the defect in matriglycan synthesis in distinct
301 forms of CMD as well as in *LARGE1* KO HAP1 cells by generating very high molecular weight
302 matriglycan (*Figure 7-Figure Supplement 5A*) (*Barresi et al., 2004*). However, overexpression
303 of LARGE1 in *POMK* or *POMK/LARGE1* KO HAP1 cells did not produce very high molecular
304 weight matriglycan (*Figure 7D, 7E; Figure 7- Figure Supplement 5B, 5C, 5D*). Only the rescue
305 of *POMK/LARGE1* KO HAP1 cells with *POMK* enabled LARGE1 to synthesize high molecular

306 weight matriglycan (*Figure 7E; Figure 7- Figure Supplement 5D*). These findings indicate that
307 LARGE1 requires phosphorylated core M3 to extend matriglycan on α -DG to its mature and
308 high molecular weight forms.

309 To understand why phosphorylated core M3 is needed for LARGE1 to elongate
310 matriglycan, we measured the binding affinity of LARGE1, as well as POMK, for the
311 phosphorylated core M3 using solution NMR. We previously showed that the unphosphorylated
312 core M3 binds to POMK with high affinity (*Zhu et al., 2016*). The mannose anomeric proton
313 (Man H1) is well resolved and its intensity decreases only slightly with increasing POMK
314 protein concentration (*Figure 8- Figure Supplement 1A*). By fitting the intensity changes of the
315 Man H1 peak as a function of POMK concentration, we obtained a dissociation constant of $>$
316 $500 \mu\text{M}$ (*Figure 8C; Figure 8- Figure Supplement 1A, 1B*). These results indicate that,
317 compared to the unphosphorylated core M3 of GGM-MU, the phosphorylated core M3 of
318 GGMP-MU binds to POMK with a much weaker affinity. Then, we measured the binding
319 affinities of LARGE1 for GGMP-MU and GGM-MU in a similar manner. Our results showed
320 that LARGE1 binds with greater affinity to GGMP-MU compared to GGM-MU ($K_d = 11.5 \pm 1.2$
321 μM for GGMP-MU compared to $K_d > 90 \mu\text{M}$ for GGM-MU) (*Figure 8A, 8B, 8D*). This
322 indicates that the core M3 phosphate increases the binding affinity of LARGE1 for core M3 and
323 could explain the ability of LARGE1 to elongate matriglycan in the presence of POMK.



324
 325 **Figure 8.** NMR Analyses of POMK and LARGE1 Binding to GGM-MU and GGMp-MU. **A, B,**
 326 1D ^1H NMR spectra of the anomeric region of GGM-MU (**A**) and GGMp-MU (**B**) were acquired
 327 for the glycan concentration of $10.0 \mu\text{M}$ in the presence of various concentrations of LARGE1 as
 328 indicated. The peak Man H1 is derived from the mannose anomeric H1 proton. Stars indicate
 329 impurity peaks derived from buffer. **C, D,** Fitting of the NMR binding data of POMK (**C**) and
 330 LARGE1 (**D**) to core M3 glycans of GGM-MU and GGMp-MU, respectively. The bound
 331 fraction was obtained from the NMR titration data by measuring the difference in the peak
 332 intensity of the anomeric proton Man H1 in the absence (free form) and presence (bound form)
 333 of POMK or LARGE1, then divided by the peak intensity of the free form.
 334

335 **Discussion**

336 POMK is a novel muscular dystrophy gene that phosphorylates mannose of the core M3
337 trisaccharide (GalNac- β 1,3-GlcNac- β 1,4-Man) on α -DG during synthesis of the *O*-mannose-
338 linked polysaccharide ending in matriglycan. LARGE1 is responsible for the synthesis of
339 matriglycan, and addition of matriglycan enables α -DG to serve as a predominant ECM receptor
340 in many tissues, in particular, skeletal muscle and brain. Over eighteen genes are implicated in
341 matriglycan synthesis, and complete loss-of-function mutations in these genes abrogate synthesis
342 of the *O*-mannose linked modification and preclude the addition of matriglycan, thereby leading
343 to dystroglycanopathies, congenital and limb-girdle muscular dystrophies with or without
344 structural brain and eye abnormalities. Here, we have used a multidisciplinary approach to show
345 that the absence of POMK activity does not preclude addition of matriglycan. Instead, in the
346 absence of core M3 phosphorylation by POMK, LARGE1 synthesizes a short, non-extended
347 form of matriglycan on α -DG (~90 kDa). However, in order to generate full-length mature
348 matriglycan on α -DG (~150 kDa), LARGE1 requires phosphorylation of core M3 by POMK
349 (*Figure 8- Figure Supplement 2A, 2B*).

350 Our study shows that the short form of matriglycan is able to bind to laminin with high
351 affinity and thus enables α -DG (POMK) to function as an ECM receptor. Given the very small
352 increase in apparent MW in α -DG(POMK) compared to α -DG from cells and muscle lacking
353 LARGE1 (*Figure 5-Figure Supplement 2A; Figure 7-Figure Supplement 1A; Figure 8-Figure*
354 *Supplement 3A*), the short, non-extended form of matriglycan likely contains few Xyl-GlcA
355 repeats. However, it can still bind laminin since only a single Xyl-GlcA repeat is needed for
356 laminin binding (*Briggs et al., 2016*), but it cannot function as an ECM scaffold. This short
357 matriglycan likely attenuates muscular dystrophy in patient NH13-284 with a complete loss-of-

358 function mutation in POMK, preventing the severe CMD phenotype that is observed in the
359 complete absence of the other known dystroglycanopathy genes.

360 Muscle-specific POMK KO mice express the short, non-extended form of matriglycan on
361 ~90 kDa α -DG and develop a mild muscular dystrophy phenotype. Muscle physiology studies
362 demonstrate that the short matriglycan expressed in the absence of POMK can maintain specific
363 force but cannot prevent eccentric contraction-induced force loss or skeletal muscle pathology.
364 Interestingly, missense mutations in FKRP that cause LGMD2I also show reduced expression of
365 matriglycan (*Yoshida-Moriguchi et al., 2015*) and exhibit a milder muscular dystrophy. Thus,
366 M-POMK KO mice are an excellent model of milder forms of dystroglycanopathy in which short
367 matriglycan is expressed and will be useful for future studies of these forms of
368 dystroglycanopathy.

369 α -DG is composed of three domains: the DGN, which undergoes cleavage at arginine-
370 312 by a furin-like convertase during α -DG post-translational processing, a central mucin-like
371 domain, and a C-terminus (*Kanagawa et al., 2004; Singh et al., 2004*). The natural C-terminal
372 domain boundary of DGN, arginine-312 in humans, is proximal to three sites of matriglycan
373 synthesis (threonines-317, 319, 379) within the mucin-like domain of α -DG. Biochemical
374 studies using various *POMK* KO HAP1 cell lines demonstrated that the synthesis of the short,
375 non-extended form of matriglycan occurs on threonine-317 of the mucin-like domain and, like
376 full-length matriglycan, requires LARGE1, DGN, and CDP-ribitol. Cell biological experiments
377 demonstrated that the DGN is necessary for synthesis of the short form of matriglycan. As the
378 binding of LARGE1 to the DGN is essential for the synthesis of full-length matriglycan on α -
379 DG (*Kanagawa et al., 2004; Hara et al., 2011*), it is required for synthesis of the short form of
380 matriglycan as well. Solution NMR studies revealed that LARGE1 binds to core M3, and the

381 binding affinity increases in the presence of the mannose phosphate. The phosphorylated core
382 M3, could, therefore serve to recruit DGN-bound LARGE1 to the proper residue during the
383 initiation of full-length matriglycan synthesis. In the absence of the mannose phosphate, the
384 DGN-bound LARGE1 may instead act only upon the matriglycan acceptor added to threonine-
385 317, the threonine nearest to the DGN. Synthesis of full-length matriglycan may, therefore,
386 proceed through a complex of DGN, LARGE1, and phosphorylated core M3. The
387 phosphorylated core M3 may also serve to anchor LARGE1 to α -DG during matriglycan
388 elongation. In the absence of POMK, the binding of LARGE1 to the DGN and the
389 unphosphorylated core M3 may only be sufficient for synthesis of a short form of matriglycan.
390 Further structural and biochemical studies will be required to understand the precise interactions
391 between DGN, LARGE1, and the phosphorylated core M3. Taken together, our results indicate
392 that LARGE1 requires DGN to synthesize the short, non-extended form of matriglycan but needs
393 both the DGN and the phosphorylated core M3 to generate full-length matriglycan on α -DG.

394 Our study demonstrates that POMK is required for the synthesis of full-length and high-
395 molecular weight forms of matriglycan (*Figure 8- Figure Supplement 2A*). In the absence of
396 POMK, LARGE1 generates a short, non-extended form of matriglycan (*Figure 8- Figure*
397 *Supplement 2B*). Collectively, our work provides the first insights into the pathogenic
398 mechanism behind POMK-deficient muscular dystrophy and better elucidates how full-length
399 matriglycan is synthesized so it can act as a scaffold for ECM proteins, thereby enabling proper
400 skeletal muscle function and preventing muscular dystrophy.

401 **Methods**402 **Patient Information**

403 Patient NH13-284 received a diagnosis of congenital muscular dystrophy (CMD) with brain
404 malformations.

405 **Generation of *Pomk*^{LoxP/LoxP} Mice**

406 The *Pomk* gene consists of five exons, exons 1, 2, and 3, which are non-coding and exons 4 and
407 5, which are coding (*Zhu et al., 2016; Di Costanzo et al., 2014*). We used Clustered Regularly
408 Interspersed Short Palindromic Repeats (CRISPR)-Cas9 to insert LoxP sites around exon 5.

409 *Pomk*_5P1 TTCTTTCTGTGATGTGTGCTTATTC

410 *Pomk*_5P2 CAGACACTCACCCCTTACCTTAG

411 Wildtype: 197 bp

412 Targeted: 235 bp

413

414 *Pomk*_3P1 AGCCACACCTTCCTACAGTC

415 *Pomk*_3P2 AAGCTCTGCCCAGAGAGAAG

416 Wildtype: 123 bp

417 Targeted: 162 bp

418

419 *Pomk*_5'_guide(601) CGTGTCCCGCCAGGAATGAA

420 *Pomk*_3'_guide(3P1) TCAGGAGGCGGCTCCCAGTG

421

422 *Pomk*_5'_donor(601; PAGE purified)

423 TCCTCATCTTCTCCCTGTGCAGTCAATCTGCACAGCTCCCTGCACACATGGCTTATAG

424 AGTGGTTCTCACCCCGCCCTTCATAACTTCGTATAGCATAACATTATACGAAGTTATG

425 GTACCTCCTGGCGGGACACGAATAAGCACACATCACAGAAAGAAGTCTGTTGTCTT

426 GACTGCCCAGCCCTCCGCAGCTGCCACCC

427 *Pomk*_3'_donor(3P1; PAGE purified)

428 AGTGTGAGATTCAAGTGTGGATATGCAGTGATCCTCTGGCCACACTTGTGAGCAGCC

429 ACACCTTCCTACAGTCCCTCACTATAACTTCGTATAGCATAACATTATACGAAGTTATG

430 GATCCGGGAGCCGCCTCCTGAGCCCTGCTGTGTAACCCACCTACCTTCCCTCCTTTCA

431 CACTAGAAGCTGAGAGCTCTTCTCTTC

432

433 **Animals**

434 B6SJLF1/J mice were purchased from Jackson Labs (100012; Bar Harbor, ME). Male mice older
435 than 8 weeks were used to breed with 3-5-week-old super-ovulated females to produce zygotes

436 for electroporation. Female ICR (Envigo, Indianapolis, IN; Hsc:ICR(CD-1)) mice were used as
 437 recipients for embryo transfer.

438 Mice expressing *Cre* under the *mouse creatine kinase (Mck)* promoter,
 439 B6.FVB(129S4)-Tg(Ckmm-cre)5Khn/J (stock no. 006475) (**Brüning et al., 1998**) and the
 440 *Pax7* promoter, *Pax7*^{tm1(cre)Mrc}/J, (stock no. 010530) (**Keller et al., 2004**) were purchased from the
 441 Jackson Laboratory. Male mice expressing the *Mck-Cre* transgene were bred to female mice
 442 homozygous for the floxed *Pomk* allele (*Pomk*^{LoxP/LoxP}). Male F1 progeny with the genotype
 443 *Mck*^{Cre}; *Pomk*^{LoxP/+} were bred to female *Pomk*^{LoxP/LoxP} mice. A *Cre* PCR genotyping protocol was
 444 used to genotype the *Cre* allele using standard *Cre* primers. The primers used were Sense:
 445 TGATGAGGTTCGCAAGAACC and Antisense: CCATGAGTGAACGAACCTGG.

446 Sanger sequencing of tail DNA was performed by the University of Iowa Genome Editing Core
 447 Facility to confirm incorporation of 5' and 3' LoxP sites. PCR probes were developed at
 448 Transnetyx to genotype mice expressing both *Pax7-Cre* and *Mck-Cre*. Genotyping of *Mck*^{Cre};
 449 *Pax7*^{Cre}; *Pomk*^{LoxP/LoxP} mice was performed by Transnetyx using real-time PCR.

450 All mice were socially housed in a barrier-free, specific pathogen-free conditions as
 451 approved by the University of Iowa Animal Care and Use Committee (IACUC). All animals
 452 were maintained in a climate-controlled environment at 25°C and a 12/12 light/dark cycle.
 453 Animal care, ethical usage, and procedures were approved and performed in accordance with the
 454 standards set forth by the National Institutes of Health and IACUC. For studies with *Mck*^{Cre};
 455 *Pomk*^{LoxP/LoxP} mice, N=3 mice of each genotype (*Pomk*^{LoxP/LoxP} and *Mck*^{Cre}; *Pomk*^{LoxP/LoxP}) were
 456 used. For studies with *Mck*^{Cre}; *Pax7*^{Cre}; *Pomk*^{LoxP/LoxP} mice, animals of varying ages were used as
 457 indicated, and N=3 each of *Pomk*^{LoxP/LoxP} and *Mck*^{Cre}; *Pax7*^{Cre}; *Pomk*^{LoxP/LoxP} were used.
 458 Littermate controls were employed whenever possible. The number of animals required was

459 based on previous studies (*de Greef et al., 2016; Goddeeris et al., 2013*) and experience with
460 standard deviations of the given techniques.

461 **Preparation of Cas9 RNPs and the microinjection mix**

462 Chemically modified CRISPR-Cas9 crRNAs and CRISPR-Cas9 tracrRNAs were purchased
463 from Integrated DNA Technologies (IDT) (Alt-R® CRISPR-Cas9 crRNA; Alt-R® CRISPR-
464 Cas9 tracrRNA (Cat# 1072532)). The crRNAs and tracrRNA were suspended in T10E0.1 and
465 combined to 1 µg/µL (~29.5 µM) final concentration in a 1:2 (µg: µg) ratio. The RNAs were
466 heated at 98°C for 2 minutes and allowed to cool slowly to 20°C in a thermal cycler. The
467 annealed cr:tracrRNAs were aliquoted to single-use tubes and stored at -80°C.

468 Cas9 nuclease was also purchased from IDT (Alt-R® S.p. HiFi Cas9 Nuclease). Cr:tracr:Cas9
469 ribonucleoprotein complexes were made by combining Cas9 protein and each cr:tracrRNA; final
470 concentrations: 60 ng/µL (~0.4 µM) Cas9 protein and 60 ng/µL (~1.7 µM) cr:tracrRNA). The
471 Cas9 protein and annealed RNAs were incubated at 37°C for 10 minutes. The two RNP mixes
472 were combined and incubated at 37°C for an additional 5 minutes. The single stranded
473 oligonucleotide donors (ssODN) were purchased from IDT as Ultramers. The ssODNs were
474 added to the RNPs and the volume adjusted to the final concentrations in the injection mix were
475 10 ng/µL each ssODN; 20 ng/µL each guide RNA and 40 ng/µL Cas9 Protein.

476 **Collection of embryos and microinjection**

477 Pronuclear-stage embryos were collected using previously described methods (*Pinkert et al.,*
478 *2002*). Embryos were collected in KSOM media (Millipore, Burlington, MA; MR101D) and
479 washed 3 times to remove cumulous cells. Cas9 RNPs and ssODNs were injected into the
480 pronuclei of the collected zygotes and incubated in KSOM with amino acids at 37°C under 5%

481 CO2 until all zygotes were injected. Fifteen to 25 embryos were immediately implanted into the
482 oviducts of pseudo-pregnant ICR females.

483 Insertion of loxP1 (5') and loxP2 (3') sites was confirmed by cloning and sequencing of genomic
484 PCR products (Figure S2) from tail DNA of filial 0 (F0) *Pomk*^{LoxP/+} mice using primers flanking
485 the 5' loxP site, ACTCCAGTTGGTTTCAGGAAG and GAGGGAAGAGAAGTCAGGAAAG.
486 For the 3' loxP site, primers of sequence ACCGAGTGTGAGATTCAAGTG and
487 GGTTGCTGGTAGGGTTAAGAG were used. The 5' loxP site contains a *KpnI* cleavage site,
488 and the 3' loxP site contains a *BamHI* site. The screen of the 5' loxP site gives a product of 803
489 base pairs for the *LoxP* allele when uncut. *KpnI* digestion of the 5' loxP site gives 3 products of
490 381, 355, and 67 base pairs. A screen of the 3' loxP site gives a product of 396 base pairs for the
491 uncut allele with loxP site, while *BamHI* digestion of the 3' loxP site gives products of 273 and
492 123 base pairs.

493 Genotyping was carried out using primers flanking the exon 5 loxP1 site or the
494 (TTCTTTCTGTGATGTGTGCTTATTC) or loxP2 (CAGACACTCACCTTTACCTTAG) site.
495 The wild-type allele is 197 bp while the floxed allele is 235 bp. *Pomk*^{LoxP/+} mice were
496 backcrossed five generations onto a C57BL/6J background and backcrossed mice used whenever
497 possible.

498 **Forelimb Grip Strength Test**

499 Forelimb grip strength was measured at 1 month and 4 months of age using previously published
500 methods (*de Greef et al., 2016*). A mouse grip strength meter (Columbus Instruments,
501 Columbus, OH) was mounted horizontally, with a nonflexible grid connected to the force
502 transducer. The mouse was allowed to grasp the grid with its two front paws and then pulled
503 away from the grid by its tail until the grip was broken. This was done three times over five

504 trials, with a one-minute break between each trial. The gram force was recorded per pull, and any
505 pull where only one front limb or any hind limbs were used were discarded. If the mouse turned,
506 the pull was also discarded. After 15 pulls (5 sets of 3 pulls), the mean of the three highest pulls
507 of the 15 was calculated and reported. Statistics were calculated using GraphPad Prism 8
508 software. Student's T-Test was used (two-sided). Differences were considered significant at a p-
509 value less than 0.05. Graph images were also created using GraphPad Prism and the data in the
510 present study are shown as the means +/- SD unless otherwise indicated.

511 **Creatine Kinase Assay**

512 Creatine Kinase levels were measured in 8-week old mice 2 hours after mild downhill run (3
513 meters per minute for 5 minutes followed by 15 meters per minute for 10 minutes) at a 15-
514 degree downhill incline as previously described (*de Greef et al., 2016; Goddeeris et al., 2013*).
515 Blood was collected by tail vein bleeds from non-anesthetized, restrained mice using a
516 Microvette CB300 (Sarstedt AG & Co, Newton, NC). Samples were centrifuged at 12,000 rpm
517 for 10 minutes and prepared using an enzyme-coupled CK kit (Stanbio Laboratory, Boerne, TX)
518 using the manufacturer's instructions. Absorbance was measured using a plate reader at 340 nm
519 every 30 seconds for 2 minutes at 37°C. Statistics were calculated using GraphPad Prism
520 software and Student's T-Test was used (two-sided). Differences were considered significant at a
521 p-value less than 0.05. Graph images were also created using GraphPad Prism 8 and the data in
522 the present study are shown as the means +/- SD unless otherwise indicated.

523 **Body Weight Measurements**

524 Mice were weighed as previously described (*de Greef et al., 2016*). Weights were measured after
525 testing grip strength using a Scout SPX222 scale (OHAUS Corporation, Parsippany, NJ), and the
526 tester was blinded to genotype. Statistics were calculated using GraphPad Prism 8 software and

527 Student's T-Test was used (two-sided). Differences were considered significant at a p-value less
528 than 0.05. Graph images were also created using GraphPad Prism and the data in the present
529 study are shown as the means +/- SD unless otherwise indicated.

530 **Measurement of *in vitro* muscle function**

531 To compare the contractile properties of muscles, extensor digitorum longus (EDL) muscles
532 were surgically removed as described previously (*Rader et al., 2016; de Greef et al., 2016*). The
533 muscle was immediately placed in a bath containing a buffered physiological salt solution
534 (composition in mM: NaCl, 137; KCl, 5; CaCl₂, 2; MgSO₄, 1; NaH₂PO₄, 1; NaHCO₃, 24;
535 glucose, 11). The bath was maintained at 25°C, and the solution was bubbled with 95% O₂ and
536 5% CO₂ to stabilize pH at 7.4. The proximal tendon was clamped to a post and the distal tendon
537 tied to a dual mode servomotor (Model 305C; Aurora Scientific, Aurora, ON, Canada). Optimal
538 current and whole muscle length (L₀) were determined by monitoring isometric twitch force.
539 Optimal frequency and maximal isometric tetanic force (F₀) were also determined. The muscle
540 was then subjected to an eccentric contraction (ECC) protocol consisting of 8 eccentric
541 contractions (ECCs) at 3-minute intervals. A fiber length (L_f)-to-L₀ ratio of 0.45 was used to
542 calculate L_f. Each ECC consisted of an initial 100 millisecond isometric contraction at optimal
543 frequency immediately followed by a stretch of L₀ to 30% of L_f beyond L₀ at a velocity of 1 L_f/s
544 at optimal frequency. The muscle was then passively returned to L₀ at the same velocity. At 3,
545 15, 30, 45, and 60 minutes after the ECC protocol, isometric tetanic force was measured. After
546 the analysis of the contractile properties, the muscle was weighed. The cross-sectional area
547 (CSA) of muscle was determined by dividing the muscle mass by the product of L_f and the
548 density of mammalian skeletal muscle (1.06 g/cm³). The specific force was determined by
549 dividing F₀ by the CSA (kN/mm²). 18-20 week-old male mice were used, and right and left EDL

550 muscles from each mouse were employed whenever possible, with n=5 to 8 muscles used for
551 each analysis. Each data point represents an individual EDL. Statistics were calculated using
552 GraphPad Prism 8 software and Student's unpaired T-Test was used (two-sided). Differences
553 were considered significant at a p-value less than 0.05.

554 **H&E and Immunofluorescence Analysis of Skeletal Muscle**

555 Histology and immunofluorescence of mouse skeletal muscle were performed as described
556 previously (*Goddeeris et al., 2013*). Mice were euthanized by cervical dislocation and directly
557 after sacrifice, quadriceps muscles were isolated, embedded in OCT compound and then snap
558 frozen in liquid nitrogen-cooled 2-methylbutane. 10 μ M sections were cut with a cryostat (Leica
559 CM3050S Research Cryostat; Amsterdam, the Netherlands) and H&E stained using conventional
560 methods. Whole digital images of H&E-stained sections were taken by a VS120-S5-FL Olympus
561 slide scanner microscope (Olympus Corporation, Tokyo, Japan). For immunofluorescence
562 analyses, a mouse monoclonal antibody to glycoepitopes on the sugar chain of α -DG (IIH6,
563 1:100 dilution, Developmental Studies Hybridoma Bank, University of Iowa; RRID:
564 AB_2617216) was added to sections overnight at 4°C followed by Alexa Fluor®-conjugated
565 goat IgG against mouse IgM (Invitrogen, Carlsbad, CA, 1:500 dilution), for 40 minutes. The
566 sections were also stained with rabbit polyclonal antibody to β -DG (AP83; 1:50 dilution)
567 followed by Alexa Fluor®-conjugated 488 Goat anti-rabbit IgG (1:500). Whole sections were
568 imaged with a VS120-S5-FL Olympus slide scanner microscope. Antibody IIH6 is a monoclonal
569 to the glycoepitope of α -DG (*Ervasti et al., 1991*), and AP83 is a polyclonal antibody to the c-
570 terminus of β -DG (*Ervasti et al., 1991*), both of which have been described previously.

571 For histologic analysis of human skeletal muscle, H&E staining on 10 μ m frozen section was
572 performed using the Leica ST5020 Multistainer workstation (Leica Biosystems, Buffalo Grove,

573 IL) according manufacturer's instructions. For immunofluorescence analysis, unfixed frozen
574 serial sections (7 μm) were incubated with primary antibodies for 1 hour, and then with the
575 appropriate biotinylated secondary antibodies for 30 minutes followed by streptavidin conjugated
576 to Alexa Fluor 594 (ThermoFisher Scientific, UK) for 15 minutes. Primary antibodies used were
577 mouse monoclonal: α -DG I1H6 (clone I1H6C4) (*Ervasti et al., 1991*), β -DG (Leica, Milton
578 Keynes, UK; clone 43DAG1/8D5). All washes were made in PBS and incubations were
579 performed at room temperature. Sections were evaluated with a Leica DMR microscope
580 interfaced to MetaMorph (Molecular Devices, Sunnyvale, CA).

581 **Tissue Biochemical Analysis**

582 30 slices of 30 μm thickness were taken with a with a cryostat (Leica CM3050S Research
583 Cryostat) from skeletal muscle or heart that had been frozen in liquid nitrogen-cooled 2-
584 methylbutane. For biochemical analysis of murine skeletal muscle, quadriceps muscle were used.
585 Samples were solubilized in 500 μL of 1% Triton X-100 in 50 mM Tris pH 7.6 and 150 mM
586 NaCl with protease inhibitors (per 10 mL buffer: 67 μL each of 0.2 M
587 Phenylmethylsulfonylfluoride (PMSF), 0.1 M Benzamidine and 5 μL of each of Leupeptin
588 (Sigma/Millipore) 5 mg/mL, Pepstatin A (Millipore) 1 mg/mL in methanol, Aprotinin (Sigma-
589 Aldrich) 5 mg/mL, Calpeptin (Fisher/EMD Millipore) 1.92 mg/mL in Dimethyl Sulfoxide
590 (DMSO), Calpain Inhibitor 1 (Sigma-Aldrich) 1.92 mg/mL in DMSO). Samples were vortexed
591 for 4 minutes and solubilized for 2.5 hours at 4°C with rotation. Samples were then spun down at
592 12,000 rpm for 30 minutes at 4°C on a Beckman Tabletop Centrifuge. The supernatant was
593 incubated with 100 μL WGA-Agarose slurry (Vector Biolabs, Malvern, PA, AL-1023) overnight
594 at 4°C with rotation. The next day samples were washed three times in 50 mM Tris pH 7.6 and
595 150 mM NaCl with 0.1% TX-100 and protease inhibitors. 100 μL of 5X Laemmli Sample Buffer

596 (LSB) was added, samples boiled for 10 minutes, and 125 μ L of this was loaded in each lane of
597 gels for western blotting.

598 **Fibroblast Growth and Flow Cytometry**

599 Fibroblasts used for biochemical analyses were grown in 20% Fetal Bovine Serum (FBS, Life
600 Technologies, Carlsbad, CA) and 1% penicillin/streptomycin (Invitrogen). Cells were split at 1:2
601 every 2 days using Trypsin-EDTA (ThermoFisher Scientific, Waltham, MA).

602 For flow cytometry analyses, fibroblasts cultured from skin biopsies were grown in Dulbecco's
603 modified Eagles medium (Invitrogen) with 20% fetal bovine serum (FBS, Life Technologies),
604 1% glutamax (Thermo Fisher Scientific) and 1% penicillin/streptomycin (Sigma-Aldrich). Upon
605 approximately 90% confluence, cells were washed with PBS without Ca and Mg, detached with
606 non-enzymatic dissociation solution (Sigma-Aldrich cat. C5914) and fixed in 2%
607 paraformaldehyde for 10 minutes. Cells were subsequently incubated on ice with the following
608 antibodies diluted in PBS/0.1% FBS: anti- α -DG I1H6 (Millipore) for 30 minutes, anti-mouse
609 biotinylated IgM (Vector Labs, Burlingame, CA) for 20 minutes, Streptavidin-Phycoerythrin
610 (BD Pharmingen) for 15 minutes. Negative controls for each fibroblast population were
611 incubated with 0.1% FBS/PBS without the primary antibodies. Cells were washed twice and
612 centrifuged at 1850g for 4 minutes, after each incubation step. After the last wash, cell pellets
613 were re-suspended in 500 μ L of PBS. A total of 10,000 event were acquired using the Cyan ADP
614 analyser (Beckman Coulter, Brea, CA) and analysed using FlowJo software version 7.6.5 (Tree
615 Star, USA).

616 **Generation and Characterization of HAP1 Mutant Cell Lines**

617 HAP1 cells (RRID: [CVCL_Y019](#)) are a haploid human cell line with an adherent, fibroblast-like
618 morphology, originally derived from parent cell line KBM-7 (RRID: [CVCL_A426](#)). Wild-

619 type (WT) C631 cells (a diploid cell line containing duplicated chromosomes of HAP1) were
620 purchased from Horizon Discovery, and gene-specific knockout (KO) HAP1 cells were
621 generated by Horizon Discovery. Absence of the gene was confirmed via PCR amplification and
622 Sanger sequencing. The identity of the cells has been authenticated by the company using the
623 STR profiling method. Mycoplasma testing of the cells was performed on a routine basis to
624 ensure the cells are not contaminated. HAP1 KO cell lines have complete loss of gene function
625 and are validated in the lab by performing western blot analysis before and after gene transfer
626 with the appropriate gene. For each HAP1 KO cell line, a matched WT control parental cell
627 line (WT C631) was provided, ensuring that phenotypes can be attributed directly to the genetic
628 modification. These cells are cultured in Iscove's Modified Dulbecco's Medium (IMDM)
629 supplemented with 10% fetal calf serum and 1% Pen-Strep antibiotics.

630 *POMK* knockout (KO) HAP1: HAP1 cells bearing a 10 bp deletion of exon 4 of the *POMK*,
631 generated using the CRISPR/Cas9 system, were purchased from Horizon Discovery
632 (HZGHC001338c004, clone 1338–4) and were previously described (*Zhu et al., 2016*). *POMK*
633 knockout (KO) HAP1 cells lack the single copy of the wild-type *POMK* allele and are therefore
634 null at the *POMK* locus. The sequence of the guide RNA used is
635 TGAGACAGCTGAAGCGTGTT. Absence of the wild-type *POMK* allele was confirmed by
636 Horizon Discovery via PCR amplification and Sanger sequencing. PCR primers used for DNA
637 sequencing are *POMK* Forward 5'-ACTTCTTCATCGCTCCTCGACAA-3', and *POMK*
638 Backward 5'- GGATGCCACACTGCTTCCCTAA-3'. The identity of the cells has been
639 authenticated by the company using the STR profiling method. Mycoplasma testing of the cells
640 were performed on a routine basis to ensure the cells are not contaminated.

641 *POMK/DAG1* KO HAP1: HAP1 cells lacking both *POMK* and *DAG1* expression (*POMK/DAG1*
642 KO HAP1 cells) were generated using CRISPR/Cas9 by Horizon Discovery. A 16 bp deletion in
643 the *DAG1* gene (exon 2) was introduced into the *POMK* KO HAP1 line (HZGHC001338c004).
644 The sequence of the Guide RNA is CCGACGACAGCCGTGCCATC; NM_004393. PCR
645 primers for DNA sequencing were forward TAGCAAGACTATCGACTTGAGCAA and
646 reverse GCAATCAAATCTGTTGGAATGGTCA.

647 *POMK/LARGE1* KO HAP1: HAP1 cells lacking both *POMK* and *LARGE1* expression
648 (*POMK/LARGE1* KO HAP1 cells) (HZGHC007364c011) were generated using CRISPR/Cas9
649 by Horizon Discovery. A 43 bp deletion of exon 3 of *LARGE1* was introduced into the *POMK*
650 KO HAP1 line (HZGHC001338c004). The guide RNA sequence was
651 CTCGGCGATGGGATGGGGCT and the primer sequence was PCR forward
652 GAGGCATGGTTCATCCAGATTAAG and PCR reverse
653 CTTTACCTCGCATTTCTCCACGA.

654 *POMK/ISPD* KO HAP1: HAP1 cells containing a 1 bp insertion of exon 4 of the *POMK* gene,
655 generated using the CRISPR/Cas9 system, were purchased from Horizon Discovery
656 (HZGHC001338c001, clone 1338-1). The mutation in *POMK* is predicted to lead to a
657 frameshift. These cells also lacked expression of *ISPD*. The Guide RNA sequence was
658 TGAGACAGCTGAAGCGTGTT. The sequences of PCR primers were PCR forward
659 ACTTCTTCATCGCTCCTCGACAA and PCR reverse GGATGCCACACTGCTTCCCTAA.

660 *LARGE1* KO HAP1: HAP1 cells (clone 122-6, HZGHC000122c006) were purchased from
661 Horizon Discovery. Cells were generated using a CRISPR/Cas9-mediated 1 bp deletion of exon
662 3. The guide RNA sequence was GCTCTCGCGCTCCCGCTGGC and the primer sequence for

663 122-7 was PCR forward ATGGAGTAGGTCTTGGAGTGGTT and PCR reverse
 664 GAGGCATGGTTCATCCAGAGTTAAAG.

665 *FKTN* KO HAP1: HAP1 cells (clone 721-10, catalog number 32597-10) were purchased from
 666 Horizon Discovery. CRISPR/Cas9 was used to introduce 16 bp deletion of exon 3. The sequence
 667 of the guide RNA was CAGAACTTGTCAGCGTTAAA and the sequences of PCR forward
 668 CAGATCAAAGAATGCCTGTGGAAAT and PCR reverse
 669 TGCAAAGAGAAGTGTGATCAGAAAA.

670 **Adenovirus Production**

671 DGE (Delta H30- A316) was generated and described previously (*Hara et al., 2011; Kanagawa*
 672 *et al., 2004; Kunz et al., 2001*). DG T317A, DG T319A, and DG T317A/T319A were first
 673 subcloned into an Fc-tagged DG construct (DGFc3) (*Hara et al., 2011; Kanagawa et al., 2004;*
 674 *Kunz et al., 2001*). The *KpnI-XhoI* fragments from the DGFc3 mutants corresponding to the
 675 mutant constructs (DG T317A, DG T319A, or DG T317A/T319A) were then subcloned into
 676 pAd5RSVK-NpA (obtained from the University of Iowa Viral Vector Core) as was the *XhoI-*
 677 *XbaI* fragment from an adenovirus encoding dystroglycan WT. *E1*-deficient recombinant
 678 adenoviruses (Ad5 RSV DG WT, DG T317/T319, DG T317A, DG T319A, DGE, Ad-POMK
 679 WT) were generated by the University of Iowa Viral Vector Core (VVC) using the RAPAd
 680 system (*Anderson et al., 2000*). Assays for replication competence of adenoviruses were
 681 performed to check for contamination. Ad-POMK WT and Ad-POMK D204A were generated
 682 by ViraQuest Inc. (North Liberty, IA) using the RAPAd system and was described previously
 683 (*Zhu et al., 2016*). Ad-POMK D204N was also generated by ViraQuest Inc. Absence of the viral
 684 *E1* DNA sequence was confirmed by ViraQuest Inc. after PCR amplification of the viral DNA
 685 and staining on DNA agarose gel electrophoresis. Replication competence of adenoviruses was

686 negative as assessed by plaque forming assays in cells performed from 10^9 viral particles up to
687 14 days. Adenoviral Fukutin (FKTN) and Isoprenoid Synthase Domain-Containing (ISPD) have
688 been described previously (*Willer et al., 2012*). Adenoviral LARGE1 has been described
689 previously (*Barresi et al., 2004*). DGFc340TEV was cloned into the pUC57-mini vector by
690 GenScript (*Hara et al., 2011; Kanagawa et al., 2004; Kunz et al., 2001*). The insert includes
691 TEV protein cleavage site between amino acids (AAs) 1-340 of rabbit DG and human IgG1 Fc.
692 The insert was subcloned in pcDNA3 expression vector with *EcoRI*. Subsequently, *FseI*-x-340
693 AAs DG-TEV-6xHis-*NotI* fragment was obtained using pcDNA3DGFc340TEV as a PCR
694 template. *FseI*-x-340 AAs DG-TEV-6xHis-*NotI* was ligated into pcDNA3DGFc340TEV
695 digested with *FseI* and *NotI* to construct DG340TEVHis, which includes 1-340 AAs of rabbit
696 DG, TEV site, and 6x Histidine. The construct was also inserted in pacAd shuttle plasmid from
697 the VVC to generate the adenoviral vector. Next, *FseI*-x-390 AAs-TEV-6xHis-*NotI* was
698 obtained using pcDNA3rbdDG as a PCR template and ligated into the pcDNA3DG340TEVHis
699 digested with *FseI* and *NotI* to construct DG390TEVHis, which includes 1-390 AAs of rabbit
700 DG, TEV site, and 6x Histidine. The construct was also inserted in pacAd shuttle plasmid from
701 the VVC to generate the Ad virus vector. *E1*-deficient recombinant adenoviruses were generated
702 by the University of Iowa Viral Vector Core using the RAPAd system (*Kunz et al., 2001*).

703 **HAP1 Cell Culture and Adenovirus Infection**

704 HAP1 cells were maintained at 37°C and 5% CO₂ in Iscove's Modified Dulbecco's Medium
705 (IMDM, Gibco) supplemented with 10% Fetal Bovine Serum (FBS) and 1%
706 penicillin/streptomycin (Invitrogen). Cells were split every 3 days at 1:10 using Trypsin-EDTA
707 (ThermoFisher Scientific). On day 1 for adenovirus transfection experiments, media was
708 changed to 2% IMDM, and an average of 5.9×10^6 *POMK* KO HAP1 cells were infected at the

709 indicated multiplicity of infection (MOI) with the indicated adenovirus. On day 2, infection
710 medium was replaced with 10% IMDM, and on day three the cells were processed for
711 biochemical analyses.

712 **Glycoprotein Isolation and Biochemical Analyses from Cultured Cells**

713 For western blots and laminin overlay, HAP1 cells and fibroblasts were washed twice in ice-cold
714 Dulbecco's Phosphate-Buffered Saline (DPBS, Gibco). The second PBS wash contained the
715 protease inhibitors (0.23 mM PMSF and 0.64 mM Benzamidine). Plates were scraped, spun
716 down for 5 minutes at 14, 000 rpm at 4°C, and pellets were solubilized in 1% Triton X-100 in
717 Tris-buffered saline (TBS, 50 mM Tris-HCl pH 7.6, 150 mM NaCl) with protease inhibitors
718 (0.23 mM PMSF and 0.64 mM Benzamidine) for 1 hour at 4°C. Samples were then spun down at
719 14,000 rpm for 5 minutes, and supernatants incubated in 200 µL wheat-germ agglutinin (WGA)-
720 agarose (Vector Laboratories, AL-1023) as previously described (*Michele et al., 2002;*
721 *Goddeeris et al., 2013*). The following day, WGA beads were washed three times with 0.1%
722 Triton X-100-TBS plus protease inhibitors and heated to 99°C for 10 minutes with 250 µL of 5X
723 Laemmli sample buffer. Samples were run on SDS-PAGE and transferred to PVDF-FL
724 membranes (Millipore) as previously published (*Michele et al., 2002; Goddeeris et al., 2013*).

725 **Immunoblotting and Ligand Overlay**

726 The mouse monoclonal antibody against α -DG (IIH6, Developmental Studies Hybridoma Bank,
727 University of Iowa; RRID: AB_2617216) was characterized previously and used at 1:100
728 (*Ervasti et al., 1991*). The polyclonal antibody, AF6868 (R&D Systems, Minneapolis, MN;
729 RRID: AB_10891298), was used at a concentration of 1:200 for immunoblotting the core α -DG
730 and β -DG proteins, and the secondary was a Donkey anti-Sheep (LI-COR Bioscience, Lincoln,
731 NE) used at 1:2000 concentration. Anti-POMK (Novus Biologicals, Littleton, CO, 6f10) was

732 used at 1:500, and the secondary was 1:2000 Goat anti-Mouse IgG1 (LI-COR Bioscience). The
733 antibody against the Na/K ATPase (BD Biosciences, San Jose, CA, 610993) was used at 1:1000
734 in 5%-milk Blotto, and the secondary was 1:10,000 Goat anti-Mouse IgG1 (LI-COR
735 Bioscience). Anti-myc (Millipore Sigma, Clone 4A6) was used at 1:2,000 in 2% milk and the
736 secondary was 1:2,000 Goat anti-Mouse IgG1 (LI-COR Bioscience). Blots were developed with
737 infrared (IR) dye-conjugated secondary antibodies (LI-COR Bioscience) and scanned using the
738 Odyssey infrared imaging system (LI-COR Bioscience). Blot images were captured using the
739 included Odyssey image-analysis software.

740 Laminin overlay assays were performed as previously described (*Michele et al., 2002;*
741 *Goddeeris et al., 2013*). PVDF-FL membranes were blocked in laminin binding buffer (LBB: 10
742 mM triethanolamine, 140 mM NaCl, 1 mM MgCl₂, 1 mM CaCl₂, pH 7.6) containing 5% milk
743 followed by incubation with mouse Engelbreth-Holm-Swarm (EHS) laminin (ThermoFisher,
744 23017015) overnight at a concentration of 7.5 nM at 4°C in LBB containing 3% bovine serum
745 albumin (BSA) and 2 mM CaCl₂. Membranes were washed and incubated with anti-laminin
746 antibody (L9393; Sigma-Aldrich 1:1000 dilution) followed by IRDye 800 CW dye-conjugated
747 donkey anti-rabbit IgG (LI-COR, 926-32213) at 1:2500 dilution.

748 **EDTA Treatment of Ligand Overlays**

749 EDTA treatment of laminin overlay assays were performed as described above for laminin
750 overlays; however, calcium was excluded from all buffers made with LBB (i.e. 5% milk-LBB,
751 3% BSA-LBB) and 10 mM EDTA was added to all LBB-based buffers, including LBB wash
752 buffer, 5% milk-LBB, and 3% BSA-LBB buffers.

753 **POMK Assay**

754 HAP1 cells were washed twice in ice-cold PBS, scraped, and spun down at 14,000 rpm for 5
755 minutes at 4°C. After removing supernatant, the cell pellet was resuspended in 0.1 M MES buffer
756 pH 6.5 with 1% Triton X-100 with Protease Inhibitors (0.23 mM PMSF and 0.64 mM
757 Benzamidine) for 1 hour at 4°C rotating. Samples were spun down again, and the supernatant
758 was incubated with 200 µL of WGA-agarose beads (Vector Biolabs, AL-1023) overnight at 4°C
759 with rotation. Samples were washed the next day three times in 0.1 M MES pH 6.5 with 0.1%
760 Triton X-100 and protease inhibitors, and 100 µL of the beads were resuspended in 100 µL of
761 the wash buffer.

762 For fibroblast POMK activity measurements, cells were processed as above and solubilized in
763 1% TX-100 in 50 mM Tris and 150 mM NaCl pH 7.6 with protease inhibitors as described above
764 and incubated with WGA-agarose beads. The next day, WGA beads were washed three times
765 and resuspended in 0.1% TX-100 in 0.1 M MES pH 6.5 buffer with protease inhibitors.

766 For measurement of mouse and human skeletal muscle POMK activity, 30 slices of 30 µM
767 thickness were taken using a Leica 3050s cryostat from quadriceps muscle frozen in liquid
768 nitrogen-cooled 2-methylbutane. Samples were solubilized in 250 µL of 1% Triton X-100 in 0.1
769 M MES pH 6.5 with protease inhibitors (per 10 mL buffer: 67 µL each of 0.2 M PMSF, 0.1 M
770 Benzamidine and 5 µL/10 mL of buffer of Leupeptin (Sigma/Millipore) 5 mg/mL, Pepstatin A
771 (Millipore) 1 mg/mL in methanol, Aprotinin (Sigma-Aldrich) 5 mg/mL, Calpeptin (Fisher/EMD
772 Millipore) 1.92 mg/mL in Dimethyl Sulfoxide (DMSO), Calpain Inhibitor 1 (Sigma-Aldrich)
773 1.92 mg/mL in DMSO). Samples were solubilized for 2.5 hours at 4°C on a rotator. Samples
774 were then spun down at 14, 000 rpm for 30 minutes at 4°C on a Beckman Tabletop Centrifuge.
775 The supernatant (total lysate) was separated from the pellet, and 10 µL of this was used for
776 POMK assays.

777 For POMK reaction in HAP1 cells and fibroblasts, 20 μ L slurry (consisting of 10 μ L beads and
778 10 μ L MES buffer) was incubated with reaction buffer for a final reaction volume of 40 μ L. For
779 POMK assay from skeletal muscle, 10 μ L of total lysate was incubated with 20 μ L of reaction
780 buffer for a reaction volume of 30 μ L. The final reaction concentration was 10 mM ATP, 10 mM
781 $MnCl_2$, 10 mM $MgCl_2$, 10 μ M GGM-MU, 0.1% TX-100 in 0.1 M MES Buffer pH 6.5.
782 Reactions were run at 37°C for 24 hours for HAP cells, 48 hours for fibroblasts, or 16 hours for
783 skeletal muscle. Experiments were done in triplicate, with each replicate representing a separate
784 plate of cells or animal. After POMK reaction, 6 μ L 0.5 M EDTA was added to 30 μ L of
785 reaction supernatant, and the mixture boiled for 5 minutes. 25 μ L of this mixture and added to 30
786 μ L ddH₂O in HPLC vial and run on an LC18 column of a reverse-phase HPLC (Shimadzu
787 Scientific, Columbia, Maryland) with a 16% B med sensitivity gradient. The reaction was
788 analyzed using a 4.6 x 250 mm Supelcosil LC-18 column (Supelco). Solvent A was 50 mM
789 ammonium formate (pH 4.0), and solvent B was 80% acetonitrile in solvent A. Elution of the
790 MU derivative was monitored by fluorescence detection (325 nm for excitation, and 380 nm for
791 emission) and peak area used as a measure of activity. The enzymatic activity was calculated as
792 the peak area of the product.

793 **B4GAT1 Assay**

794 For the assessment of endogenous B4GAT1 activity in skeletal muscle, Triton X-100-solubilized
795 lysates (10 μ l for human skeletal muscle or 40 μ L for mouse skeletal muscle) were incubated in
796 a volume of 50 μ L (human skeletal muscle) for 12 hours at 37°C, with 0.4 mM Xylose- β -MU
797 (Xyl- β -MU) and 10 mM Uridine diphosphate glucuronic acid (UDP-GlcA) in 0.1 M MES buffer,
798 pH 6.0, at 5 mM $MnCl_2$, 5 mM $MgCl_2$, and 0.05% Triton X-100 (*Willer et al., 2014*). The
799 reaction was terminated by adding 25 μ L of 0.1 M EDTA and boiling for 5 minutes, and the

800 supernatant was analyzed using an LC-18 column. Both the substrate Xyl- β -MU and the product
801 GlcA-Xyl- β -MU were separated on a 16% acetonitrile isocratic gradient. Elution of the MU
802 derivative product was monitored by fluorescence detection (325 nm for excitation, and 380 nm
803 for emission). The percent conversion of substrate to product was used as the activity of the
804 B4GAT1 in the 10 μ L sample. The B4GAT1 activity then was normalized against the amount of
805 protein measured in the 10 μ L of sample using the DC Protein Assay (Bio-Rad, Hercules, CA)
806 with BSA as the standard.

807 For assessment of B4GAT1 activity in HAP cells, the HAP WGA beads were incubated in a
808 volume of 80 μ L for 26 h at 37°C, with 0.4 mM Xyl- β -MU and 10 mM UDP-GlcA in 0.1 M
809 MES buffer, pH 6.0, at 5 mM MnCl₂, 5 mM MgCl₂, and 0.05% Triton X-100. The reaction was
810 terminated by adding 25 μ L of 0.1 M EDTA and boiling for 5 minutes, and the supernatant was
811 analyzed using an LC-18 column. Elution of the MU derivative was monitored by fluorescence
812 detection (325 nm for excitation, and 380 nm for emission) and peak area used as a measure of
813 activity. The percent product was determined by taking the product peak area and dividing by the
814 total peak areas of substrate plus product peak. Then this number was taken and multiplied by
815 100 for percent conversion to product.

816 **LARGE1 Assay**

817 For the assessment of endogenous LARGE1 GlcA-T activity in skeletal muscle, Triton X-100-
818 solubilized lysates were incubated in a volume of 25 μ L for 3 h at 37°C, with 0.4 mM Xyl- α 1,3-
819 GlcA- β -MU and 10 mM UDP-GlcA in 0.1 M MES buffer, pH 6.0, at 5 mM MnCl₂, 5 mM
820 MgCl₂, and 0.5% Triton X-100. The reaction was terminated by adding 25 μ L of 0.1 M EDTA
821 and boiling for 5 minutes, and the supernatant was analyzed using an LC-18 column. Elution of
822 the MU derivative was monitored by fluorescence detection (325 nm for excitation, and 380 nm

823 for emission) and peak area used as a measure of activity. The GlcA-T activity was assessed by
824 subtracting the background observed in the negative control sample without donor sugar and
825 normalized against the amount of protein measured using the DC Protein Assay (Bio-Rad).

826 For assessment of LARGE1 enzymatic activity in HAP cells, the Triton X-100 solubilized HAP
827 cells were loaded onto WGA beads and processed as described for POMK assay above. The next
828 day after wash, beads were incubated in a volume of 90 μ L with 0.4 mM Xyl- α 1,3-GlcA- β -MU
829 and 10 mM UDP-GlcA in 0.1 M MOPS buffer, pH 6.0, at 5 mM MnCl₂, 5 mM MgCl₂, and
830 0.05% Triton X-100. The samples were run for 46 h at 37°C. The reaction was terminated by
831 adding 25 μ L of 0.25 M EDTA and boiling for 5 minutes, and the supernatant was analyzed
832 using an LC-18 column.

833 For the assessment of endogenous LARGE1 activity in fibroblasts, supernatants from Triton X-
834 100 solubilized fibroblasts were (20 μ L) directly used. Supernatants were incubated in a volume
835 of 100 μ L for 24 h at 37°C, with 0.4 mM Xyl- α 1,3-GlcA- β -MU and 10 mM UDP-GlcA in 0.1 M
836 MES buffer, pH 6.0, at 5 mM MnCl₂, 5 mM MgCl₂, and 0.5% Triton X-100. The reaction was
837 terminated by adding 25 μ L of 0.1 M EDTA and boiling for 5 minutes, and the supernatant was
838 analyzed using an LC-18 column.

839 Elution of the MU derivative was monitored by fluorescence detection (325 nm for excitation,
840 and 380 nm for emission) and peak area used as a measure of activity. The percent product was
841 determined by taking the product peak area and dividing by the total peak areas of substrate plus
842 product peak. Then this number was taken and multiplied by 100 for percent conversion to
843 product.

844 **B3GALNT2 Assay**

845 To assess B3GALNT2 activity in HAP1 cells, 20 μ L of the WGA beads from HAP1 cells were
846 incubated with a 20 μ L volume of the reaction mix. The final volume of reaction buffer was 40
847 μ L (30 μ L reaction mixture and 10 μ L WGA-beads). The final concentrations were 10 mM
848 $MgCl_2$, 10 mM $MnCl_2$, 0.1 M MES pH 6.5, 10 μ M GM-MU, and 10 mM UDP-GalNac.
849 Reactions were run at 37°C for 72 hours. Experiments were done in triplicate, with each replicate
850 representing a separate plate of cells. After B3GALNT2 reaction, 6 μ L 0.5 M EDTA was added
851 to 30 μ L of reaction supernatant, and the mixture boiled for 5 minutes. 25 μ L of this mixture and
852 added to 30 μ L ddH₂O in HPLC vial and run on an LC18 column of a reverse-phase HPLC
853 (Shimadzu Scientific) with a 16% B med sensitivity gradient. The reaction was analyzed using a
854 4.6 x 250 mm Supelcosil LC-18 column (Supelco, Bellefonte, PA). Solvent A was 50 mM
855 ammonium formate (pH 4.0), and solvent B was 80% acetonitrile in solvent A. Elution of the
856 MU derivative was monitored by fluorescence detection (325 nm for excitation, and 380 nm for
857 emission) and peak area used as a measure of activity. The enzymatic activity was calculated as
858 the peak area of the product.

859 **Digestion of α -DG with Exoglycosidases**

860 Exoglycosidase treatment was carried out as described previously (*Briggs et al., 2016; Salleh et*
861 *al., 2006; Moracci et al., 2000*). *T. maritima* β -glucuronidase (*Salleh et al., 2006; Moracci et*
862 *al., 2000*) (Bgus) and *S. solfataricus* α -xylosidase (Xylsa), both bearing a His-tag were
863 overexpressed in *E. coli*, and purified using TALON metal affinity resin as described and activity
864 determined as described (*Salleh et al., 2006; Moracci et al., 2000*) with some modifications.
865 Briefly, the cell pellet was resuspended in 20 mM HEPES buffer (pH 7.3), 150 mM NaCl, 0.1%
866 NP-40 and sonicated. After centrifugation (30 minutes at 40,000 x g), the crude extract was

867 incubated with Benzonase (Novagen) for 1 hour at room temperature and then heat-fractionated
868 for 10 minutes at 75°C. The supernatant was purified by using Talon metal affinity resin.
869 Samples to be digested by Bgus and Xylsa were exchanged into 150 mM sodium acetate (pH
870 5.5) solution and mixed with Bgus (0.45 U) and/or Xylsa (0.09 U), or no enzymes, and incubated
871 overnight at 65°C. Samples were then run on SDS-PAGE, transferred to PVDF-FL (Millipore),
872 and probed with anti- α -DG core antibody (AF6868) and anti- α -DG glycan antibody (IIH6).
873 Enriched rabbit α -DG (100 μ L of the 150 mM sodium acetate (pH 5.5) solution) was mixed with
874 Bgus (0.45 U) and/or Xylsa (0.09 U), or no enzymes, and incubated overnight at 65°C. Samples
875 were then run on SDS-PAGE, transferred to PVDF-FL (Millipore), and subjected to
876 immunoblotting.

877 **Solid Phase Assay**

878 Solid phase assays were performed as described previously (*Michele et al., 2002; Goddeeris et*
879 *al., 2013*). Briefly, WGA eluates were diluted 1:50 in TBS and coated on polystyrene ELISA
880 microplates (Costar 3590) overnight at 4°C. Plates were washed in LBB and blocked for 2 hours
881 in 3% BSA/LBB at RT. The wells were washed with 1% BSA/LBB and incubated for 1 hour
882 with L9393 (1:5,000 dilution) in 3% BSA/LBB followed by incubation with Horseradish
883 Peroxidase (HRP)-conjugated anti-rabbit IgG (Invitrogen, 1:5,000 dilution) in 3% BSA/LBB for
884 30 minutes. Plates were developed with o-phenylenediamine dihydrochloride and H₂O₂, and
885 reactions were stopped with 2 N H₂SO₄. Absorbance per well was read at 490 nm by a
886 microplate reader.

887 **Statistics**

888 The included Shimadzu post-run software was used to analyze POMK, LARGE1, and B4GAT1
889 activity in fibroblasts and mouse skeletal muscle, and the percent conversion to product was

890 recorded. The means of three experimental replicates (biological replicates, where each replicate
891 represents a different pair of tissue culture plates or animals, i.e. control and knockout) were
892 calculated using Microsoft Excel, and the mean percent conversion to product for the WT or
893 control sample (Control human fibroblasts or *Pomk*^{LoxP/LoxP} skeletal muscle, respectively)
894 reaction was set to 1. Percent conversion of each experimental reaction was subsequently
895 normalized to that of the control, and statistics on normalized values were performed using
896 GraphPad Prism 8. For analysis of POMK and LARGE1 activity in fibroblasts and mouse
897 skeletal muscle, Student's T-Test was used (two-sided). Differences were considered significant
898 at a p-value less than 0.05. Graph images were also created using GraphPad Prism and the data
899 in the present study are shown as the means +/- SD unless otherwise indicated. The number of
900 sampled units, n, upon which we report statistics for *in vivo* data, is the single mouse (one mouse
901 is n=1).

902 For measure of POMK activity in HAP1 cells, the percent conversion from GGM-MU to
903 GGM(P)-MU was first calculated using the included Shimadzu analysis software. The means
904 plus standard deviations of the percent conversion to GGM(P)-MU for three experimental
905 replicates was calculated using GraphPad Prism 8. One-way ANOVA with the Dunnett's
906 Method for Multiple Comparisons was performed, and the data for the *POMK* KO HAP1 sample
907 set as the control. Differences were considered significant at a p-value less than 0.05. Graph
908 images were created in GraphPad and show mean +/- SD.

909 To measure POMK activity in control and NH13-284 skeletal muscle, we only performed one
910 experimental replicate due to the limited amount of sample available. To measure B4GAT1
911 activity, two technical replicates were performed from skeletal muscle. Protein concentration
912 from control and NH13-284 skeletal muscle was also measured using two technical replicates.

913 The percent conversion to product for the B4GAT1 reaction was divided by the protein
914 concentration, and the values for these two technical replicates graphed using GraphPad Prism 8.
915 The graph reported is shown as the mean +/- SD.

916 For flow cytometry analyses, six experimental replicates were performed, and the mean
917 fluorescence intensity (MFI) reported. Statistics were performed using the Student's unpaired T-
918 test, two-sided in GraphPad Prism 8 and the values reported as mean +/- SD.

919 **NMR Spectroscopy**

920 1D ^1H NMR spectra of the core M3 trisaccharides GGM-MU and GGMP-MU in the absence and
921 presence of POMK or LARGE1 were acquired at 25°C on a Bruker Avance II 800 MHz NMR
922 spectrometer equipped with a sensitive cryoprobe by using a 50 ms T_2 filter consisting of a train
923 of spin-lock pulses to eliminate the broad resonances from the protein (*Mayer et al., 2001*).
924 *Danio rerio* POMK titrations were performed in 25 mM Tris (pH 8.0), 180 mM NaCl, and 10
925 mM MgCl_2 in 98% D_2O . LARGE1 titrations were performed in 20 mM HEPES, 150 mM NaCl,
926 pH 7.3 in 90% $\text{H}_2\text{O}/10\%$ D_2O . The ^{13}C and ^1H resonances of the trisaccharides were reported
927 previously (*Yoshida-Moriguchi et al., 2010*). The ^1H chemical shifts are referenced to 2,2-
928 dimethyl-2-silapentane-5-sulfonate. The NMR spectra were processed using NMRPipe (*Delaglio*
929 *et al., 1995*) and analyzed using NMRView (*Johnson et al., 1994*). The glycan binding affinity
930 to POMK and LARGE1 was determined using glycan-observed NMR experiments as described
931 previously (*Briggs et al., 2016*). For the resolved anomeric trisaccharide peak, the bound fraction
932 was calculated by measuring the difference in the peak intensity in the absence (free form) and
933 presence (bound form) of POMK or LARGE1, and then dividing by the peak intensity of the free
934 form. To obtain dissociation constant, the data were fitted to the standard quadratic equation
935 using GraphPad Prism (GraphPad Software). The standard deviation from data fitting is reported.

936 **Mass Spectrometry**

937 In order to generate DG fusion proteins for MS analyses, HAP cells were grown in IMDM with
938 10% FBS and 1% penicillin/streptomycin on p150 plates. When plates were 80% confluent, cells
939 were washed twice with DPBS, media changed to serum-free IMDM with 1%
940 penicillin/streptomycin (Invitrogen), and cells infected at high MOI (250-1000) of adenovirus
941 expressing DG390TEVHis. Three days later, the media was harvested and stored at 4°C until
942 samples were ready for MS analysis.

943 Reductive elimination. Glycans were reductively eliminated from DG390 proteins and purified
944 on a 50WS8 Dowex column, and the purified glycans were subjected to permethylation and
945 purified according to published methods (*Jang-Lee et al., 2006; Zhang et al., 2014*). Briefly, the
946 freeze-dried DG390 sample was dissolved in 55 mg/mL potassium borohydride in 1 mL of a 0.1
947 M potassium hydroxide solution. The mixture was incubated for 18 hours at 45°C and quenched
948 by adding five to six drops of acetic acid. The sample was loaded on the Dowex column and
949 subsequently eluted with 5% acetic acid. The collected solution was concentrated and
950 lyophilized, and excessive borates were removed with 10% methanolic acetic acid.

951 Permethylation. For the permethylation reaction, three to five pellets per sample of sodium
952 hydroxide were crushed in 3 mL dry dimethyl sulfoxide. Methyl Iodine (500 µL) as well as the
953 resulting slurry (0.75 mL) were added to the sample. The mixture was agitated for 15 minutes
954 and quenched by adding 2 mL ultrapure water with shaking. The glycans were extracted with
955 chloroform (2 mL) and washed twice with ultrapure water. Chloroform was removed under a
956 stream of nitrogen. The permethylated glycans were loaded on a C18 Sep-pak column, washed
957 with 5 mL ultrapure water and successively eluted with 3 mL each of 15, 35, 50 and 75% aq.
958 acetonitrile. The solutions were collected and lyophilized. The lyophilized 35% and 50%

959 fractions were dissolved in 50% aqueous solution of methanol and combined for MALDI
960 analysis.

961 Mass spectrometry. A Bruker Autoflex III MALDI TOF/TOF was used for acquisition of all
962 MALDI MS data. An in-house made BSA digest was used to calibrate the MS mode. 3,4-
963 diaminobenzophenone was used as the matrix. Permethylated samples were dissolved in 10 mL
964 of methanol, and 1 μ L of this solution was premixed with 1 μ L matrix. 1 μ L of this mixture was
965 spotted on the plate.

966 **Data Availability**

967 All data generated or analyzed during this study are included in this published article. The raw
968 mass spectrometry data are included as a supplement.

969 **Acknowledgements**

970 The BRC/ MRC Centre for Neuromuscular Diseases Biobank is acknowledged for providing
971 patients' serum and biopsy samples. The Muscular Dystrophy UK support to the GOSH
972 Neuromuscular Centre is also gratefully acknowledged. We wish to thank Norma Sinclair,
973 Patricia Yarolem, JoAnn Schwarting and Rongbin Guan for their technical expertise in
974 generating transgenic mice.

975 **Ethics**

976 Animal experimentation: This study was performed in strict accordance with the
977 recommendations in the Guide for the Care and Use of Laboratory Animals of the National
978 Institutes of Health. All animal experiments were approved by the Institutional Animal Care and
979 Use Committee (IACUC) protocols of the University of Iowa (#0081122). All procedures
980 performed in this study involving human participants were in accordance with the ethical
981 standards of NHS Health Research Authority (REC ref: 06/Q0406/33). We acknowledge and
982 thank the BRC/MRC Centre for Neuromuscular Diseases Biobank for providing patients' serum
983 and biopsy samples. We confirm that informed consent was provided to the patient and family
984 regarding the nature of the genetic studies to be performed upon collection of samples and is
985 available for our patient.

986

987

988 **Competing Interests**

989 The authors declare no competing financial interests. Correspondence and requests for materials
990 should be addressed to K.P.C. (kevin-campbell@uiowa.edu).

991

992 **Funding**

993 This work was supported in part by a Paul D. Wellstone Muscular Dystrophy Specialized
 994 Research Center grant (1U54NS053672 to KPC). S. T and F.M. are supported by the National
 995 Institute for Health Research Biomedical Research Centre at Great Ormond Street Hospital for
 996 Children NHS Foundation Trust and University College London. A.S.W. is a student in the
 997 University of Iowa Medical Scientist Training Program, which is funded by Medical Scientist
 998 Training Program Grant by the National Institute of General Medical Sciences (NIGMS) 5 T32
 999 GM007337. Transgenic mice were generated at the University of Iowa Genome Editing Core
 1000 Facility directed by William Paradee, PhD and supported in part by grants from the NIH and
 1001 from the Roy J. and Lucille A. Carver College of Medicine. KPC is an investigator of the
 1002 Howard Hughes Medical Institute.

1003

1004 **References**

1005 Anderson, R. D., Haskell, R. E., Xia, H., Roessler, B. J., & Davidson, B. L. A simple method for
 1006 the rapid generation of recombinant adenovirus vectors. *Gene Ther.* **7**, 1034-1038 (2000).
 1007 DOI: 10.1038/sj.gt.3301197, PMID: 10871752

1008 Barresi, R., Michele, D.E., Kanagawa, M., Harper, H.A., Dovico, S.A., Satz, J.S., Moore, S.A.,
 1009 Zhang, W., Schachter, H., Dumanski, J.P., Cohn, R.D., Nishino, I., Campbell, K.P. LARGE
 1010 can functionally bypass alpha-dystroglycan glycosylation defects in distinct congenital
 1011 muscular dystrophies. *Nat Med.* **10**, 696-703 (2004). DOI: 10.1038/nm1059, PMID:
 1012 15184894

1013 Briggs, D. C., Yoshida-Moriguchi, T., Zheng, T., Venzke, D., Anderson, M.E., Strazzulli, A.,
 1014 Moracci, M., Yu, L., Hohenester, E., Campbell, K.P. Structural basis of laminin binding to

- 1015 the LARGE glycans on dystroglycan. *Nat Chem Biol.* **12**, 810-814 (2016). DOI:
1016 10.1038/nchembio.2146, PMID: 27526028
- 1017 Brüning, J. C., Michael, M.D., Winnay, J.N., Hayashi, T., Hörsch, D., Accili, D., Goodyear, L.J.,
1018 Kahn, C.R. A muscle-specific insulin receptor knockout exhibits features of the metabolic
1019 syndrome of NIDDM without altering glucose tolerance. *Mol Cell.* **5**, 559-569 (1998). DOI:
1020 10.1016/s1097-2765(00)80155-0, PMID: 9844629
- 1021 Cohn, R.D., Henry, M.D., Michele, D.E., Barresi, R., Saito, F., Moore, S.A., Flanagan, J.D.,
1022 Skwarchuk, M.W., Robbins, M.E., Mendell, J.R., Williamson, R.A., Campbell, K.P.
1023 Disruption of DAG1 in differentiated skeletal muscle reveals a role for dystroglycan in
1024 muscle regeneration. *Cell.* **110**, 639-648 (2002). DOI: 10.1016/s0092-8674(02)00907-8,
1025 PMID: 12230980
- 1026 De Greef, J.C., Hamlyn, R., Jensen, B.S., O'Campo Landa, R., Levy, J.R., Kobuke, K.,
1027 Campbell, K.P. Collagen VI deficiency reduces muscle pathology, but does not improve
1028 muscle function, in the γ -sarcoglycan-null mouse. *Hum. Mol. Genet.* **25**, 1357-1369 (2016).
1029 DOI: 10.1093/hmg/ddw018, PMID: 26908621
- 1030 Delaglio, F., Grzesiek, S., Vuister, G.W., Zhu, G., Pfeifer, J., Bax, A. NMRPipe: a
1031 multidimensional spectral processing system based on UNIX pipes. *J. Biomol. NMR.* **6**, 277-
1032 293 (1995). DOI: 10.1007/BF00197809, PMID: 8520220
- 1033 Di Costanzo, S. Balasubramanian, A., Pond, H.L., Rozkalne, A., Pantaleoni, C., Saredi, S.,
1034 Gupta, V.A., Sunu, C.M., Yu, T.W., Kang, P.B., Salih, M.A., Mora, M., Gussoni, E., Walsh,
1035 C.A., Manzini, M.C. POMK mutations disrupt muscle development leading to a spectrum of
1036 neuromuscular presentations. *Hum Mol Genet.* **23**, 5781-5792 (2014). DOI:
1037 10.1093/hmg/ddu296, PMID: 24925318

- 1038 Ervasti, J. M. & Campbell, K. P. Membrane organization of the dystrophin-glycoprotein
1039 complex. *Cell*. **66**, 1121-1131 (1991). DOI: 10.1016/0092-8674(91)90035-w, PMID:
1040 1913804
- 1041 Gerin, I., Ury, B., Breloy, I., Bouchet-Seraphin, C., Bolsée, J., Halbout, M., Graff, J.,
1042 Vertommen, D., Muccioli, G.G., Seta, N., Cuisset, J.-M., Dabaj, I., Quijano-Roy, S., Grahn,
1043 A., Schaftingen, E.V., Bommer, G.T. ISPD produces CDP-ribitol used by FKTN and FKRP
1044 to transfer ribitol phosphate onto α -dystroglycan. *Nat. Commun.* **7**, 11534 (2016). DOI:
1045 10.1038/ncomms11534, PMID: 27194101
- 1046 Goddeeris, M. M., Wu, B., Venzke, D., Yoshida-Moriguchi, T., Saito, F., Matsumura, K.,
1047 Moore, S.A., Campbell, K.P. LARGE glycans on dystroglycan function as a tunable matrix
1048 scaffold to prevent dystrophy. *Nature*. **503**, 136-140 (2013). DOI: 10.1038/nature12605,
1049 PMID: 24132234
- 1050 Han, R., Kanagawa, M., Yoshida-Moriguchi, T., Rader, E.P., Ng, R.A., Michele, D.E.,
1051 Muirhead, D.E., Kunz, S., Moore, S.A., Iannaccone, S.T., Miyake K., McNeil, P.L., Mayer,
1052 U., Oldstone, M.B.A., Faulkner, J.A., Campbell, K.P. Basal lamina strengthens cell
1053 membrane integrity via the laminin G domain-binding motif of α -dystroglycan. *Proceedings*
1054 *of the National Academy of Sciences*. **106**, 12573-12579 (2009). DOI:
1055 10.1073/pnas.0906545106, PMID: 19633189
- 1056 Hara, Y., Balci-Hayta, B., Yoshida-Moriguchi, T., Kanagawa, M., Beltrán-Valero de Bernabé.,
1057 Gündeşli, H., Willer, T., Satz, J.S., Crawford, R.W., Burden, S.J., Kunz, S., Oldstone,
1058 M.B.A., Accardi, A., Talim, B., Muntoni, F., Topaloglu, H., Dinçer, P., Campbell, K.P. A
1059 dystroglycan mutation associated with limb-girdle muscular dystrophy. *N Engl J Med*. **364**,
1060 939-946 (2011). DOI: 10.1056/NEJMoa1006939, PMID: 21388311

- 1061 Hara, Y., Kanagawa, M., Kunz, S., Yoshida-Moriguchi, T., Satz, J.S., Kobayashi, Y.M., Zhu, Z.,
1062 Burden, S.J., Oldstone, M.B.A., Campbell, K.P. Like-acetylglucosaminyltransferase
1063 (LARGE)-dependent modification of dystroglycan at Thr-317/319 is required for laminin
1064 binding and arenavirus infection. *Proc Natl Acad Sci U S A*. **108**, 17426-17431 (2011). DOI:
1065 10.1073/pnas.1114836108, PMID: 21987822
- 1066 Hohenester, E. Laminin G-like domains: dystroglycan-specific lectins. *Current Opinion in*
1067 *Structural Biology*. **56**, 56-63 (2019). DOI: 10.1016/j.sbi.2018.11.007, PMID: 30530204
- 1068 Hohenester, E., Tisi, D., Talts, J. F., & Timpl, R. The crystal structure of a laminin G-like
1069 module reveals the molecular basis of α -dystroglycan binding to laminins, perlecan, and
1070 agrin. *Mol Cell*. **4**, 783-792 (1999). DOI: 10.1016/s1097-2765(00)80388-3, PMID: 10619025
- 1071 Hudson, BG. Tryggvason, K., Sundaramoorthy, M., Neilson, E.G. Alport's syndrome,
1072 Goodpasture's syndrome, and type IV collagen. *N Engl J Med*. **348**, 2543-2556 (2003). DOI:
1073 10.1056/NEJMra022296, PMID: 12815141
- 1074 Inamori, K., Yoshida-Moriguchi, T., Hara, Y., Anderson, M.E., Yu, L., Campbell, K.P.
1075 Dystroglycan function requires xylosyl- and glucuronyltransferase activities of LARGE.
1076 *Science*. **335**, 93-96 (2012). DOI: 10.1126/science.1214115, PMID: 22223806
- 1077 Jae, L.T., Raaben, M., Riemersma, M., van Beusekom, E., Blomen, V.A., Velds, A., Kerkhoven,
1078 R.M., Carette, J.E., Topaloglu, H., Meinecke, P., Wessels, M.W., Lefeber, D.J., Whelan,
1079 S.P., van Bokhoven, H., Brummelkamp, T.R. Deciphering the glycosylome of
1080 dystroglycanopathies using haploid screens for lassa virus entry. *Science*. **340**, 479-483
1081 (2013). DOI: 10.1126/science.1233675, PMID: 23519211
- 1082 Jang-Lee, J., North, S.J., Sutton-Smith, M., Goldberg, D., Panico, M., Morris, H., Haslam, S.,
1083 Dell, A. Glycomic profiling of cells and tissues by mass spectrometry: fingerprinting and

- 1084 sequencing methodologies. *Meth. Enzymol.* **415**, 59–86 (2006). DOI: 10.1016/S0076-
1085 6879(06)15005-3, PMID: 17116468
- 1086 Johnson, B. A., & Blevins, R. A. NMR View: A computer program for the visualization and
1087 analysis of NMR data. *J. Biomol. NMR.* **4**, 603-614 (1994). DOI: 10.1007/BF00404272,
1088 PMID: 22911360
- 1089 Kanagawa, M., Kobayashi, K., Tajiri, M., Many, H., Kuga, A., Yamaguchi, Y., Many-
1090 Akasaka, K., Furukawa, J.-I., Mizuno, M., Kawakami, H., Shinohara, Y., Wada, Y., Endo,
1091 T., Toda, T. Identification of a Post-translational Modification with Ribitol-Phosphate and Its
1092 Defect in Muscular Dystrophy. *Cell Reports* **9**, 2209-2223 (2016). DOI:
1093 10.1016/j.celrep.2016.02.017, PMID: 26923585
- 1094 Kanagawa, M., Nishimoto, A., Chiyonobu, T., Takeda, S., Miyagoe-Suzuki, Y., Wang, F.,
1095 Fujikake, N., Taniguchi, M., Lu, Zhongpeng, L., Tachikawa, M., Nagai, Y., Tashiro, F.,
1096 Miyazaki, J.-I., Tajima, Y., Takeda, S., Endo, T., Kobayashi, K., Campbell, K.P., Toda, T.
1097 Residual Laminin-Binding Activity and Enhanced Dystroglycan Glycosylation by LARGE in
1098 Novel Model Mice to Dystroglycanopathy. *Hum Mol Genet.* **18**, 621-631 (2009). DOI:
1099 10.1093/hmg/ddn387, PMID: 19017726
- 1100 Kanagawa, M., Saito, F., Kunz, S., Yoshida-Moriguchi, T., Barresi, T., Kobayashi, Y.M.,
1101 Muschler, J., Dumanski, J.P., Michele, D.E., Oldstone, M.B.A., Campbell, K.P. Molecular
1102 recognition by LARGE is essential for expression of functional dystroglycan. *Cell.* **117**, 953-
1103 964 (2004). DOI: 10.1016/j.cell.2004.06.003, PMID: 15210115
- 1104 Keller, C., Hansen, M. S., Coffin, C. M., & Capecchi, M. R. Pax3:Fkhr interferes with
1105 embryonic Pax3 and Pax7 function: implications for alveolar rhabdomyosarcoma cell of
1106 origin. *Genes Dev.* **18**, 2608-2013 (2004). DOI: 10.1101/gad.1243904, PMID: 15520281

- 1107 Kunz, S., Sevilla, N., McGavern, D. B., Campbell, K. P., & Oldstone, M. B. Molecular analysis
1108 of the interaction of LCMV with its cellular receptor α -dystroglycan. *J Cell Biol.* **155**, 301-
1109 310 (2001). DOI: 10.1083/jcb.200104103, PMID: 11604425
- 1110 Mayer, M., & Meyer, B. Group epitope mapping by saturation transfer difference NMR to
1111 identify segments of a ligand in direct contact with a protein receptor. *J. Am. Chem. Soc.* **123**,
1112 6108-6117 (2001). DOI: 10.1021/ja0100120, PMID: 11414845
- 1113 Michele, D. E., Barresi, R., Kanagawa, M., Saito, F., Cohn, R.D., Satz, J.S., Dollar, J., Nishino,
1114 I., Kelley, R.I., Somer, H., Straub, V., Mathews, K.D., Moore, S.A., Campbell, K.P. Post-
1115 translational disruption of dystroglycan-ligand interactions in congenital muscular
1116 dystrophies. *Nature.* **418**, 417-422 (2002). DOI: 10.1038/nature00837, PMID: 12140558
- 1117 Moracci, M., Ponzano, B.C., Trincone, A., Fusco, S., De Rosa, M., van Der Oost, J., Swensen,
1118 C.W., Charlebois, R.L., Rossi, M. Identification and molecular characterization of the first
1119 α -xylosidase from an archaeon. *J. Biol. Chem.* **275**, 22082-22089 (2000). DOI:
1120 10.1074/jbc.M910392199, PMID: 10801892
- 1121 Ohtsubo, K., & Marth, J. D. Glycosylation in cellular mechanisms of health and disease. *Cell.*
1122 **126**, 855-867 (2006). DOI: 10.1016/j.cell.2006.08.019, PMID: 16959566
- 1123 Pinkert, C. A. Ed., *Transgenic Animal Technology: A Laboratory Handbook* (Academic Press,
1124 ed. 2, 2002), pp. 20-31.
- 1125 Rader, E.P, Turk R., Willer T., Beltran D., Inamori K., Peterson, .T.A, Engle, J., Prouty S.,
1126 Matsumura, K., Saito, F., Anderson M.E., Campbell, K.P. Role of dystroglycan in limiting
1127 contraction-induced injury to the sarcomeric cytoskeleton of mature skeletal muscle. *Proc.*
1128 *Natl. Acad. Sci. U.S.A.* **113**, 10992–10997 (2016). DOI: 10.1073/pnas.1605265113, PMID:
1129 27625424

- 1130 Riemersma, M., Froese, S.D., van Tol, W., Engelke, U.F., Kopec, J., van Scherpenzeel, M.,
1131 Ashikov, A., Krojer, T., von Delft, F., Tessari, M., Buczkowska, A., Swiezewska, E., Jae,
1132 L.T., Brummelkamp, T.R., Manya, H., Endo, T., van Bokhoven, H., Yue, W.W., Lefeber,
1133 D.J. Human ISPD Is a Cytidyltransferase Required for Dystroglycan O-Mannosylation.
1134 *Chem Biol.* **12**, 1643-1652 (2015). DOI: 10.1016/j.chembiol.2015.10.014, PMID: 26687144
- 1135 Rowe, R.G. & Weiss, S.J. Breaching the basement membrane: who, when and how? *Trends Cell*
1136 *Biol.* **18**, 560-74 (2008). DOI: 10.1016/j.tcb.2008.08.007, PMID: 18848450
- 1137 Salleh, H. M., Mullegger, J., Reid, S.P., Chan, W.Y., Hwang, J., Warren, R.A.J., Withers, S.G.
1138 Cloning and characterization of *Thermotoga maritima* β -glucuronidase. *Carbohydr. Res.* **341**,
1139 49-59 (2006). DOI: 10.1016/j.carres.2005.10.005, PMID: 16303119
- 1140 Singh, J., Itahana, Y., Knight-Krajewski, S., Kanagawa, M., Campbell, K.P., Bissell, M.J.,
1141 Muschler, J. Proteolytic Enzymes and Altered Glycosylation Modulate Dystroglycan
1142 Function in Carcinoma Cells. *Cancer Res.* **64**, 6152-6159 (2004). DOI: 10.1158/0008-
1143 5472.CAN-04-1638, PMID: 15342399
- 1144 von Renesse, A., Petkova, M.V., Lutzkendorf, S., Heinemeyer, J., Gill, E., Hübner, C., Moers,
1145 A.V., Stenzel, W., Schuelke, M. POMK mutation in a family with congenital muscular
1146 dystrophy with merosin deficiency, hypomyelination, mild hearing deficit and intellectual
1147 disability. *J Med Genet.* **51**, 275-282 (2014). DOI: 10.1136/jmedgenet-2013-102236, PMID:
1148 24556084
- 1149 Willer, T., Inamori, K., Venzke, D., Harvey, C., Morgensen, G., Hara, Y., Beltran Valero de
1150 Bernabe, D., Yu, L., Wright, K.M., Campbell, K.P. The glucuronyltransferase B4GAT1 is
1151 required for initiation of LARGE-mediated α -dystroglycan functional glycosylation. *eLife.* **3**,
1152 e03941 (2014). DOI: 10.7554/eLife.03941, PMID: 25279699

- 1153 Willer, T., Lee, H., Lommel, M., Yoshida-Moriguchi, T., Beltran Valero de Bernabe, D.,
1154 Venzke, D., Cirak, S., Schachter, H., Vajsar, J., Voit, T., Muntoni, F., Loder, A.S., Dobyns,
1155 W.B., Winder, T.L., Strahl, S., Mathews, K.D., Nelson, S.F., Moore, S.A., Campbell, K.P.
1156 ISPD loss-of-function mutations disrupt dystroglycan O-mannosylation and cause Walker-
1157 Warburg syndrome. *Nat Genet.* **44**, 575-580 (2012). DOI: 10.1038/ng.2252, PMID:
1158 22522420
- 1159 Yoshida-Moriguchi, T. & Campbell, K. P. Matriglycan: a novel polysaccharide that links
1160 dystroglycan to the basement membrane. *Glycobiology.* **25**, 702-713 (2015). DOI:
1161 10.1093/glycob/cwv021, PMID: 25882296
- 1162 Yoshida-Moriguchi, T., Willer, T., Anderson, M.E., Venzke, D., Whyte, T., Muntoni, F., Lee,
1163 H., Nelson, S.F., Yu, L., Campbell, K.P. SGK196 is a glycosylation-specific *O*-mannose
1164 kinase required for dystroglycan function. *Science.* **341**, 896-899 (2013). DOI:
1165 10.1126/science.1239951, PMID: 23929950
- 1166 Yoshida-Moriguchi, T., Yu, L., Stalnaker, S.H., Davis, S., Kunz, S., Madson, M., Oldstone,
1167 M.B.A., Schachter, H., Wells, L., Cambell, K.P. *O*-mannosyl phosphorylation of α -
1168 dystroglycan is required for laminin binding. *Science.* **327**, 88-92 (2010). DOI:
1169 10.1126/science.1180512, PMID: 20044576
- 1170 Zhang, H., Zhu, F., Yang, T., Ding, L., Zhou, M., Li, J., Haslam, S.M., Dell, A., Erlandsen, H.,
1171 Wu, H. The highly conserved domain of unknown function 1792 has a distinct
1172 glycosyltransferase fold. *Nat Commun.* **5**, 4339 (2014). DOI: 10.1038/ncomms5339, PMID:
1173 25023666
- 1174 Zhu, Q., Venzke, D., Walimbe, A.S., Anderson, M.E., Fu, Q., Kinch, L.N., Wang, W., Chen, X.,
1175 Grishin, N.V., Huang, N., Yu, L., Dixon, J.E., Campbell, K.P., Xiao, J. Structure of protein

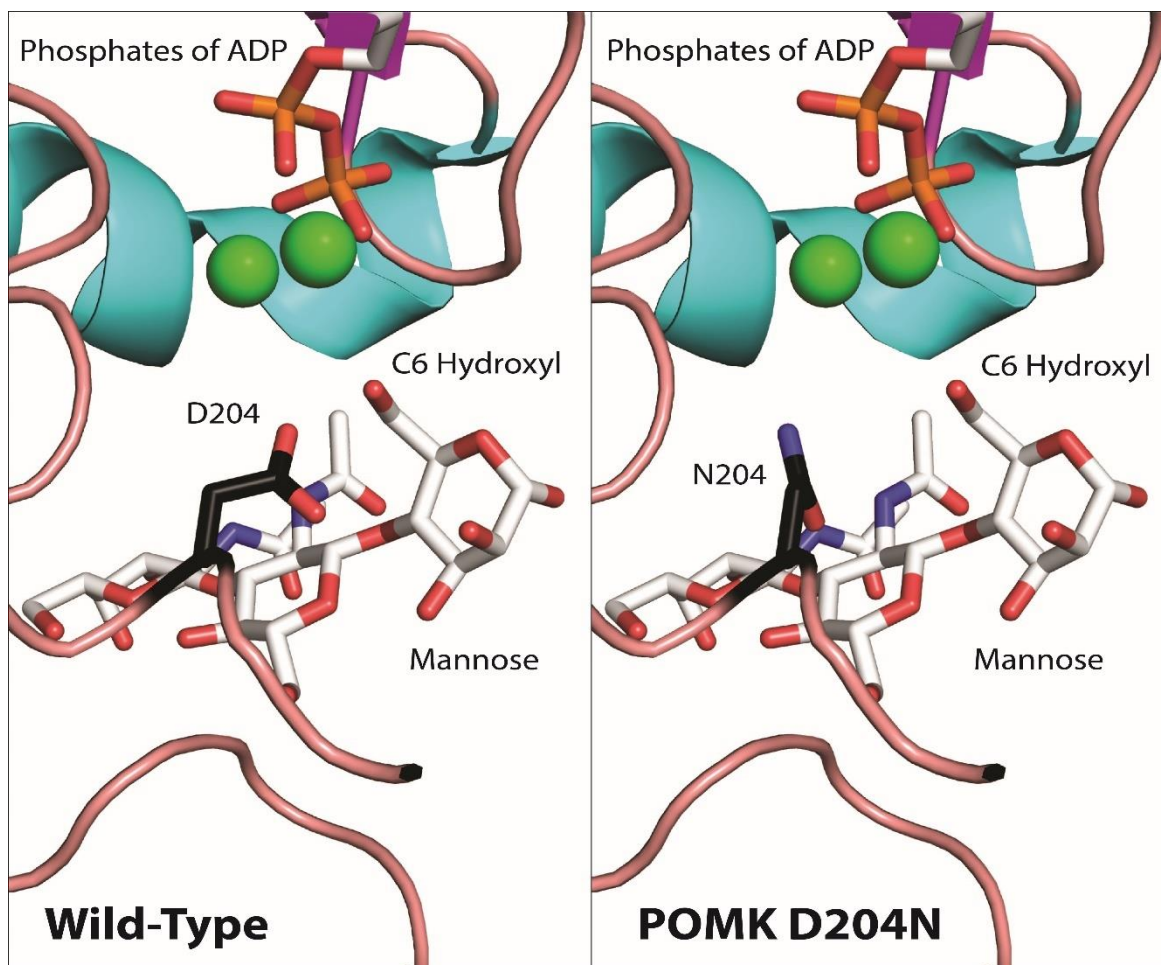
- 1176 *O*-mannose kinase reveals a unique active site architecture. *eLife*. **5**, e22238 (2016). DOI:
1177 10.7554/eLife.22238, PMID: 27879205

1178 SUPPLEMENTARY TEXT

1179 We transduced *POMK/DAG1* KO HAP1 and *POMK* KO HAP1 cells with an adenovirus
1180 expressing wild-type DG (Ad-DG). We observed a return of the laminin binding at 90-100 kDa
1181 in *POMK/DAG1* KO HAP1 cells (**Figure 7-Figure Supplement 4A**) and an increase in the
1182 corresponding IIH6 immunoreactivity and laminin binding in *POMK* KO HAP1 cells (**Figure 7-**
1183 **Figure Supplement 6A, 6B, 6C**), further indicating that the glycoprotein responsible is α -DG.

1184
1185 The binding of a xylose-glucuronic acid repeat of matriglycan to the LG4 domain of laminin α 1
1186 is calcium-dependent (*Yoshida-Moriguchi et al., 2015; Hohenester, 2019; Briggs et al., 2016*).
1187 To test if the binding of the non-extended matriglycan is similarly calcium-dependent, we
1188 performed laminin overlays in the presence of 10 mM EDTA (**Figure 7-Figure Supplement 6D,**
1189 **6E**). In both WT and *POMK* KO HAP1 cells, there was a complete absence of laminin binding
1190 in the presence of EDTA, indicating that laminin binding at 90-100 kDa is calcium-dependent
1191 and the glycan responsible is composed of xylose-glucuronic acid repeats.

1192
1193 Given the higher affinity of POMK for the unphosphorylated core M3 compared to the
1194 phosphorylated form (**Figure 8C; Figure 8-Figure Supplement 1A**), it is possible that POMK
1195 D204N, which is catalytically inactive, binds to GGM and increases the amount of core M3-
1196 modified α -DG in the ER, thereby reducing the amount entering the Golgi. With a reduction in
1197 the amount of core M3-modified α -DG entering the Golgi, FKTN may be able to better modify
1198 GalNac of the unphosphorylated core M3, thus enabling the formation of the matriglycan which
1199 enables laminin binding at 90-100 kDa in the patient's skeletal muscle. In *POMK* KO HAP1 cells
1200 alone, the non-extended matriglycan represents the amount formed when no POMK is present
1201 and transport of core M3-modified α -DG to the Golgi is not reduced. In support of this
1202 hypothesis, overexpression of POMK D204N in *POMK* KO HAP1 cells at a higher multiplicity
1203 of infection (MOI) of 10 leads to higher MW forms of matriglycan despite the catalytic inactivity
1204 of POMK D204N *in vitro* (**Figure 7-Figure Supplement 6F**). The higher MW of this form of
1205 matriglycan resembles that of the POMK D204N skeletal muscle. Alternatively, it is possible
1206 that POMK D204N remains attached to the unphosphorylated core M3 and this binary complex
1207 of POMK D204N and α -DG moves to the Golgi, where it can form a ternary complex with
1208 FKTN. The ternary complex composed of FKTN, POMK D204N, and α -DG enables FKTN to
1209 more efficiently elongate the core M3 leading to formation of the non-extended matriglycan.
1210 Further studies will be needed to determine the precise mechanism.

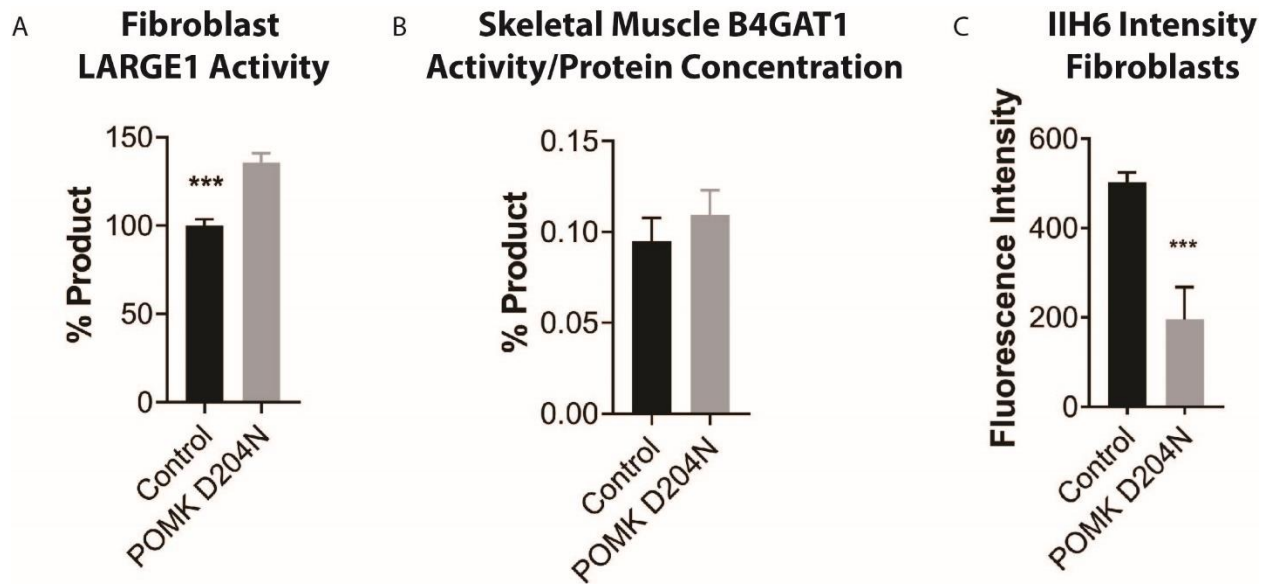


1211 **Supplementary Figures**

1212

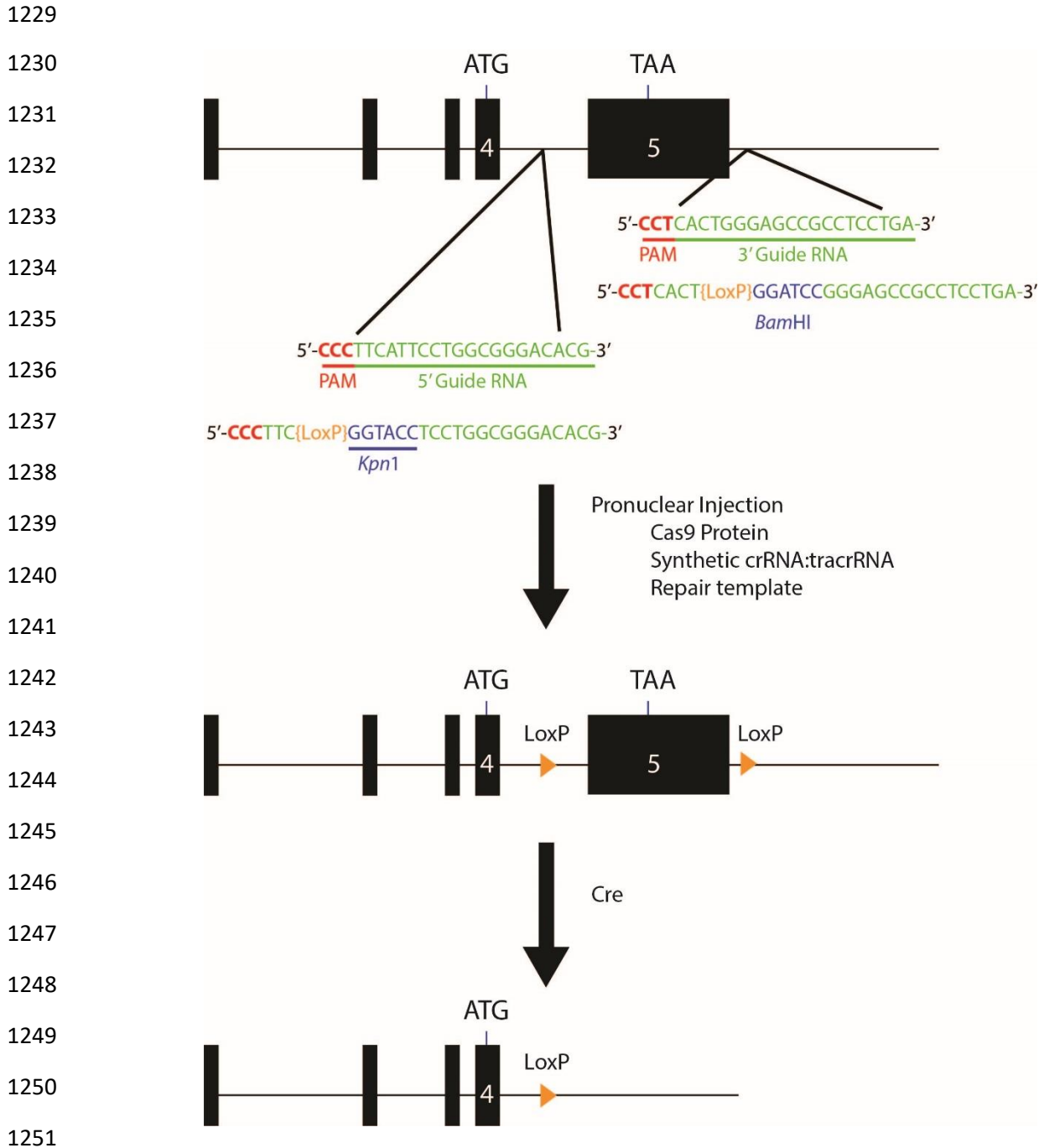
1213 **Figure 2 - Figure Supplement 1.** Structural Modeling of POMK D204N Mutation. This figure
 1214 shows structural modeling of wild-type POMK and the POMK D204N mutation using human
 1215 POMK protein sequence numbering, based on the crystal structure of Zebrafish POMK. The
 1216 green spheres indicate manganese ions. The phosphorous, oxygen, nitrogen, and carbon atoms
 1217 are colored in orange, red, blue, and white, respectively. The D204 and N204 carbon atoms
 1218 are colored dark. The gamma phosphate of ATP is not shown.

1219

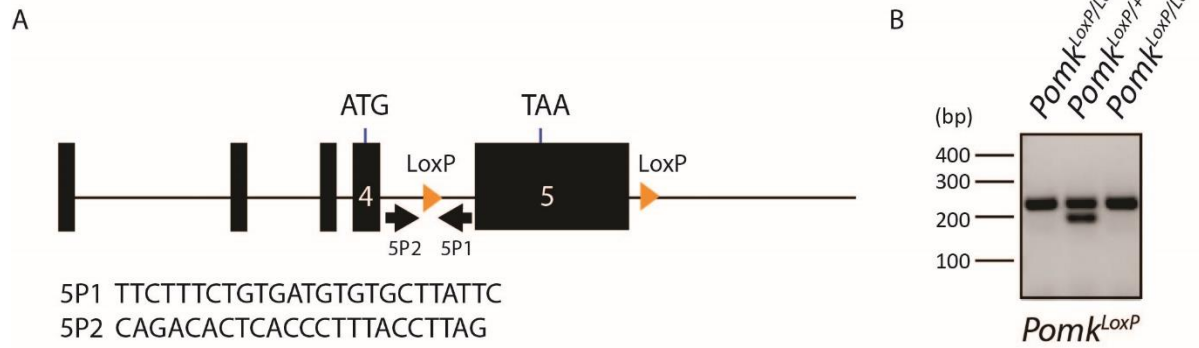


1220

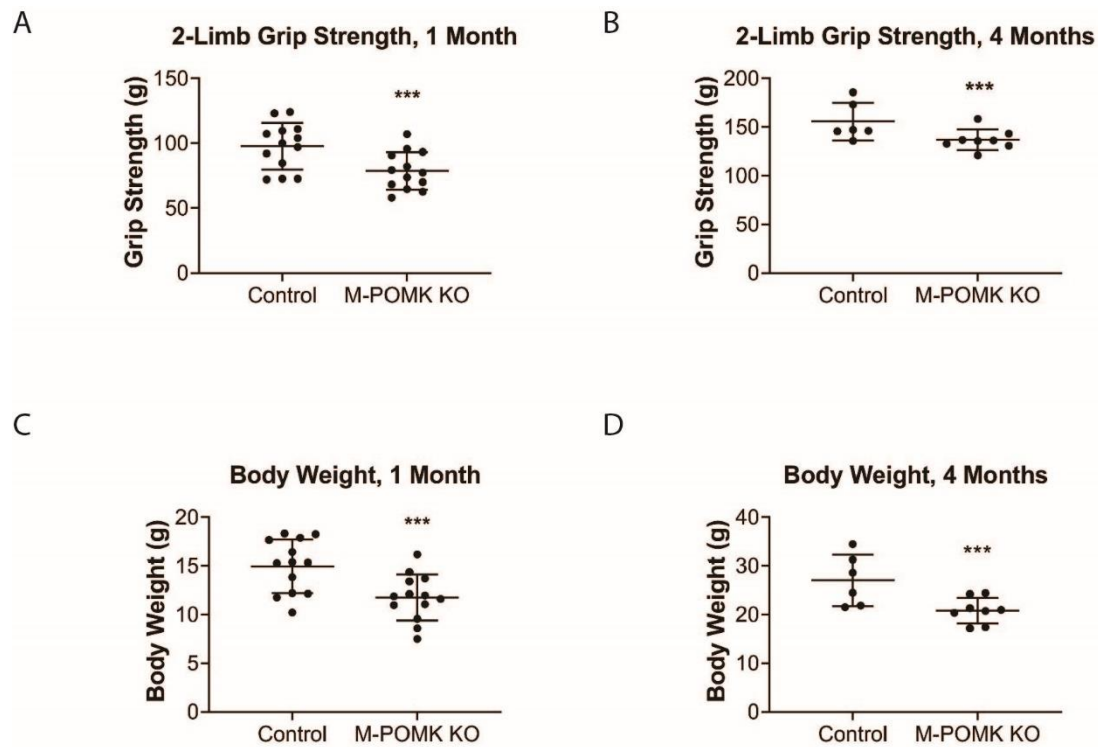
1221 **Figure 2 - Figure Supplement 2.** Supplemental Analysis of POMK D204N Fibroblasts and
 1222 Muscle. **A**, LARGE1 activity in control human fibroblasts and fibroblasts from patient NH13-
 1223 284 (POMK D204N). Triple asterisks indicate statistical significance using Student's unpaired t-
 1224 test (three replicates, p-value=0.0007). **B**, B4GAT1 activity (normalized to protein
 1225 concentration) from control skeletal muscle and POMK D204N muscle. **C**, Mean fluorescence
 1226 intensity of control human fibroblasts and POMK D204N fibroblasts. Flow cytometry analyses
 1227 were performed using an antibody against matriglycan (IIH6). Triple asterisks indicate statistical
 1228 significance using Student's unpaired t-test (three replicates, p-value<0.0001).



1252 **Figure 3 - Figure Supplement 1.** Schematic for Generation of Floxed Alleles of *Pomk*. Map of
 1253 5' and 3' LoxP sites (orange). LoxP sites flanking exon 5 of *Pomk* (large black box), which
 1254 encodes the majority of the kinase domain of POMK, were inserted using CRISPR/Cas9. Cre-
 1255 mediated recombination of the floxed allele of *Pomk* is predicted to lead to a loss of exon 5.

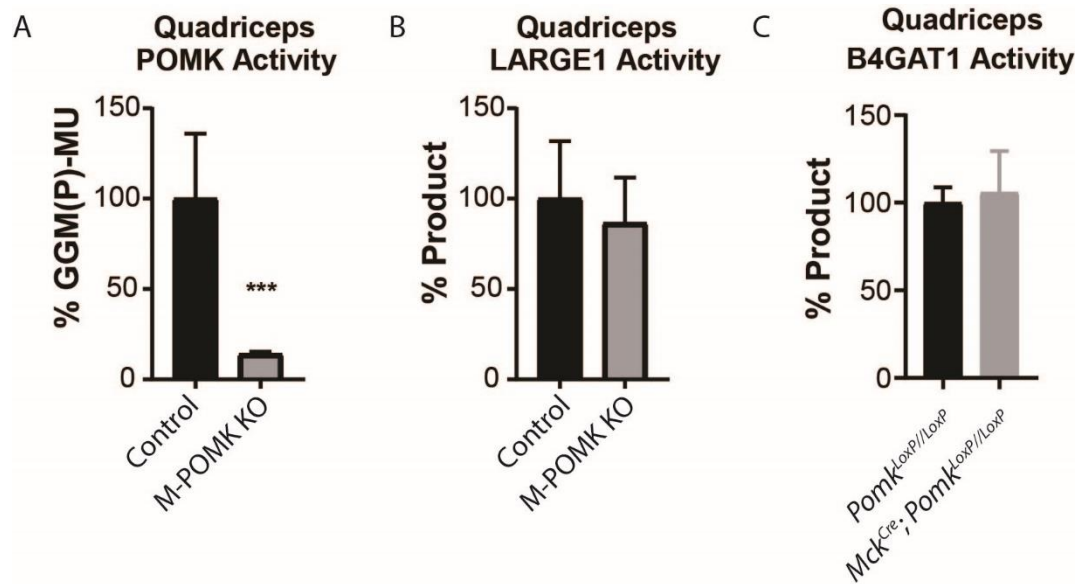


1256 **Figure 3 - Figure Supplement 2.** Results of *Pomk*^{LoxP/LoxP} Genotyping. **A**, Genotyping Strategy
 1257 for floxed *Pomk* Allele. PCR Primers were designed to flank the 5' LoxP site. **B**, The wild-type
 1258 allele of *Pomk* is 197 bp, while the floxed allele is 235 base pairs.



1259

1260 **Figure 3 - Figure Supplement 3.** Muscle-Specific *Pomk* Knockout Mice Have Reduced Grip
 1261 Strength and Body Weight. **A, B**, 2-limb grip strength of 1-month old (**A**) and 4-month old (**B**)
 1262 *Pomk*^{LoxP/LoxP} (Control) and *Mck*^{Cre}; *Pax7*^{Cre}; *Pomk*^{LoxP/LoxP} (M-POMK KO) mice. Triple asterisks
 1263 indicate statistical significance using Student's unpaired t-test, p-value= 0.0069 (A), p-
 1264 value=0.039 (A). **C, D**, Body weights of 1-month old (**C**) and 4-month old (**D**) Control and M-
 1265 POMK KO mice. Triple asterisks indicate statistical significance with p-value < 0.05 using
 1266 Student's unpaired t-test, p-value= 0.0038 (C), p-value=0.0134 (D).

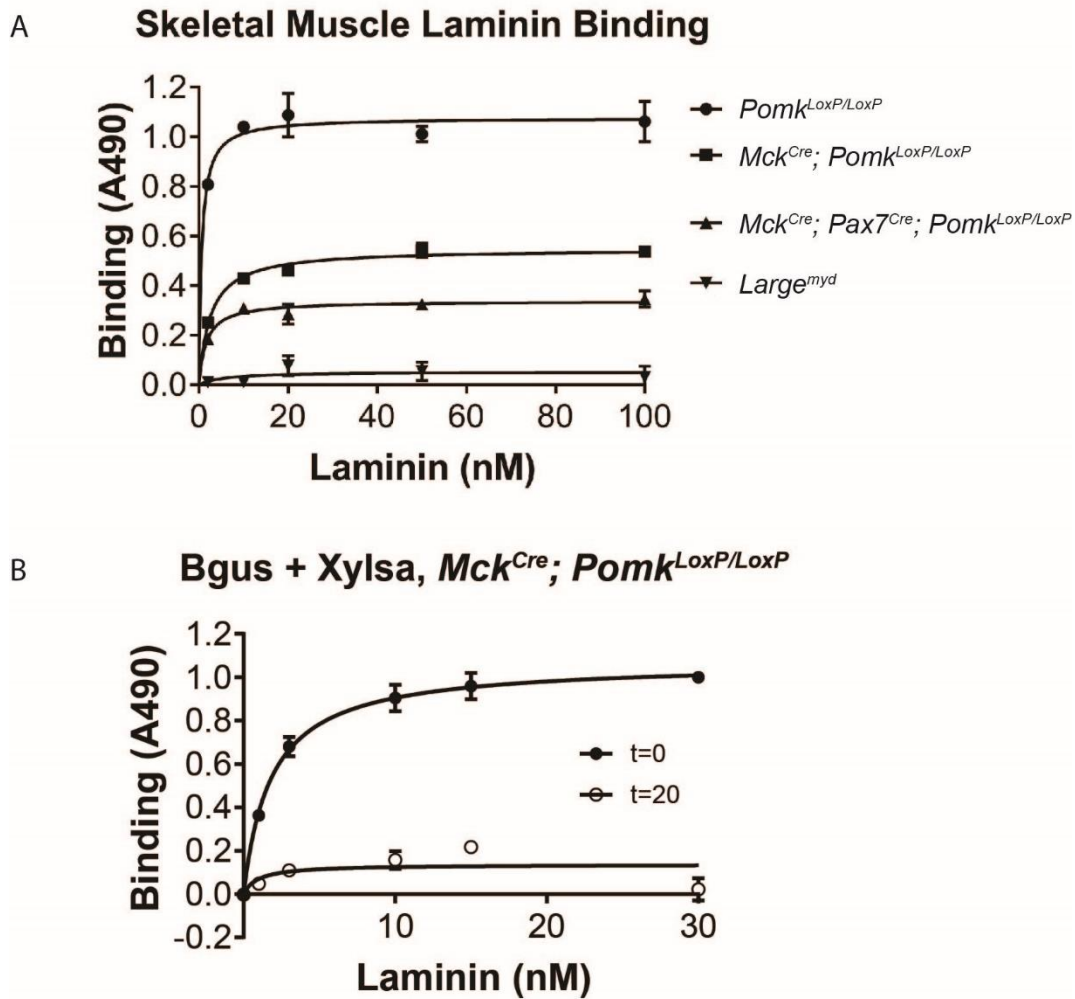


1277

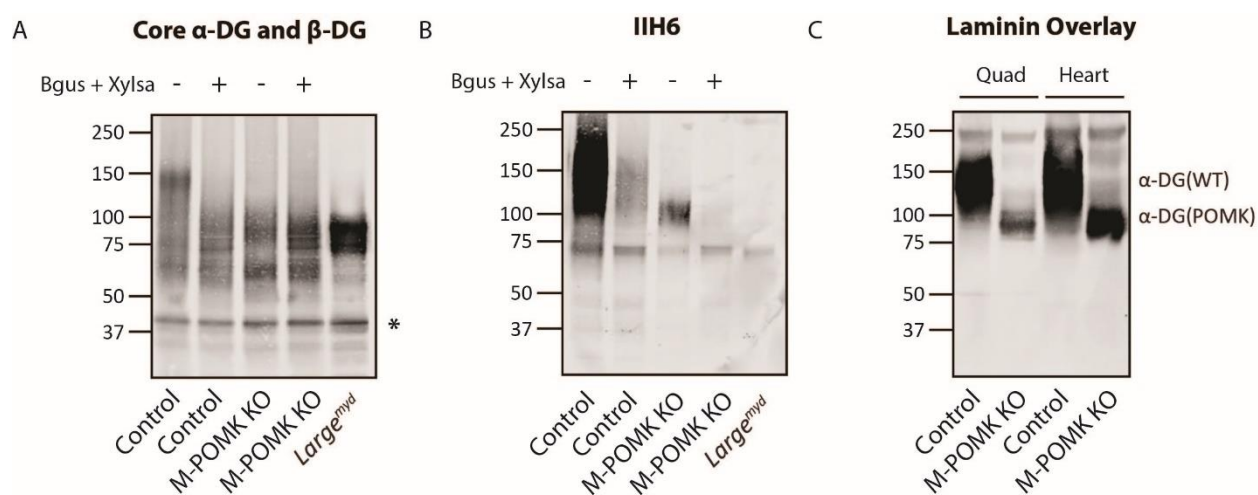
1278 **Figure 3 - Figure Supplement 4.** Supplemental Biochemical Analysis of *Pomk*-null Skeletal
 1279 Muscle. **A, B**, POMK (**A**) and LARGE1 (**B**) activity of M-POMK KO and *Pomk*^{LoxP/LoxP}
 1280 (Control) quadriceps muscle extracts (three replicates). Asterisks indicate statistical significance
 1281 with p-value<0.05 (p-value=0.0144) using Student's unpaired t-test. **C**, B4GAT1 activity in
 1282 *Mck*^{Cre}; *Pomk*^{LoxP/LoxP} and control quadriceps muscle extracts (three replicates).

1283

1284



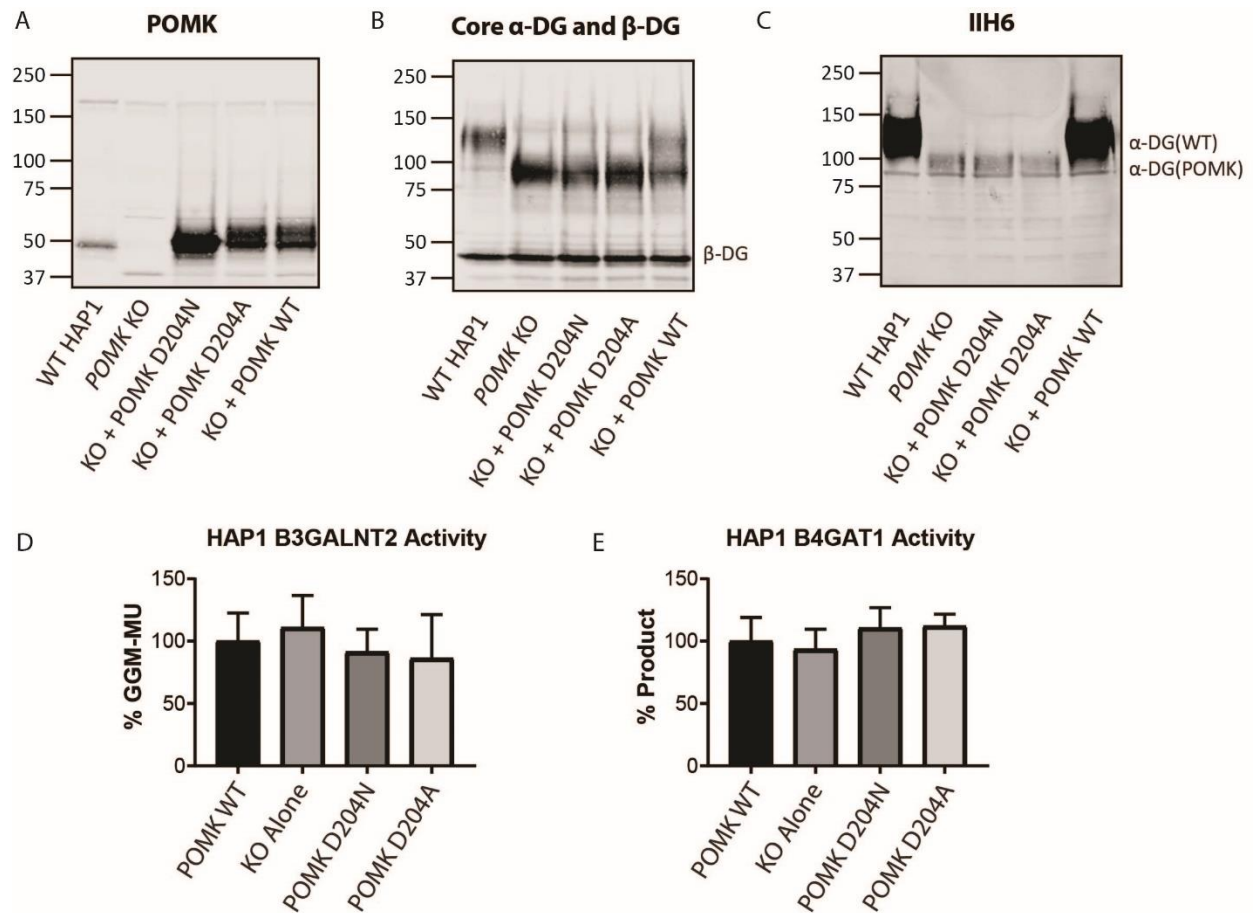
1285 **Figure 5 - Figure Supplement 1.** Solid-Phase Binding Analyses of *Pomk*-null Skeletal Muscle.
 1286 **A**, Solid-phase binding analysis (relative B_{max} for laminin-111) of control, M-POMK KO
 1287 (*Mck*^{Cre}; *Pax7*^{Cre}; *Pomk*^{LoxP/LoxP}), *Mck*^{Cre}; *Pomk*^{LoxP/LoxP}, and *Large*^{myd} skeletal muscle (three
 1288 replicates). Error bars: standard deviation. **B**, Solid-phase binding analysis of *Mck*^{Cre};
 1289 *Pomk*^{LoxP/LoxP} skeletal muscle treated in combination with α -xylosidase (Xylsa) and β -
 1290 glucuronidase (Bgus) for 0 or 20 hours. Results from three independent experiments are shown.
 1291 Error bars: standard deviation.



1292

1293

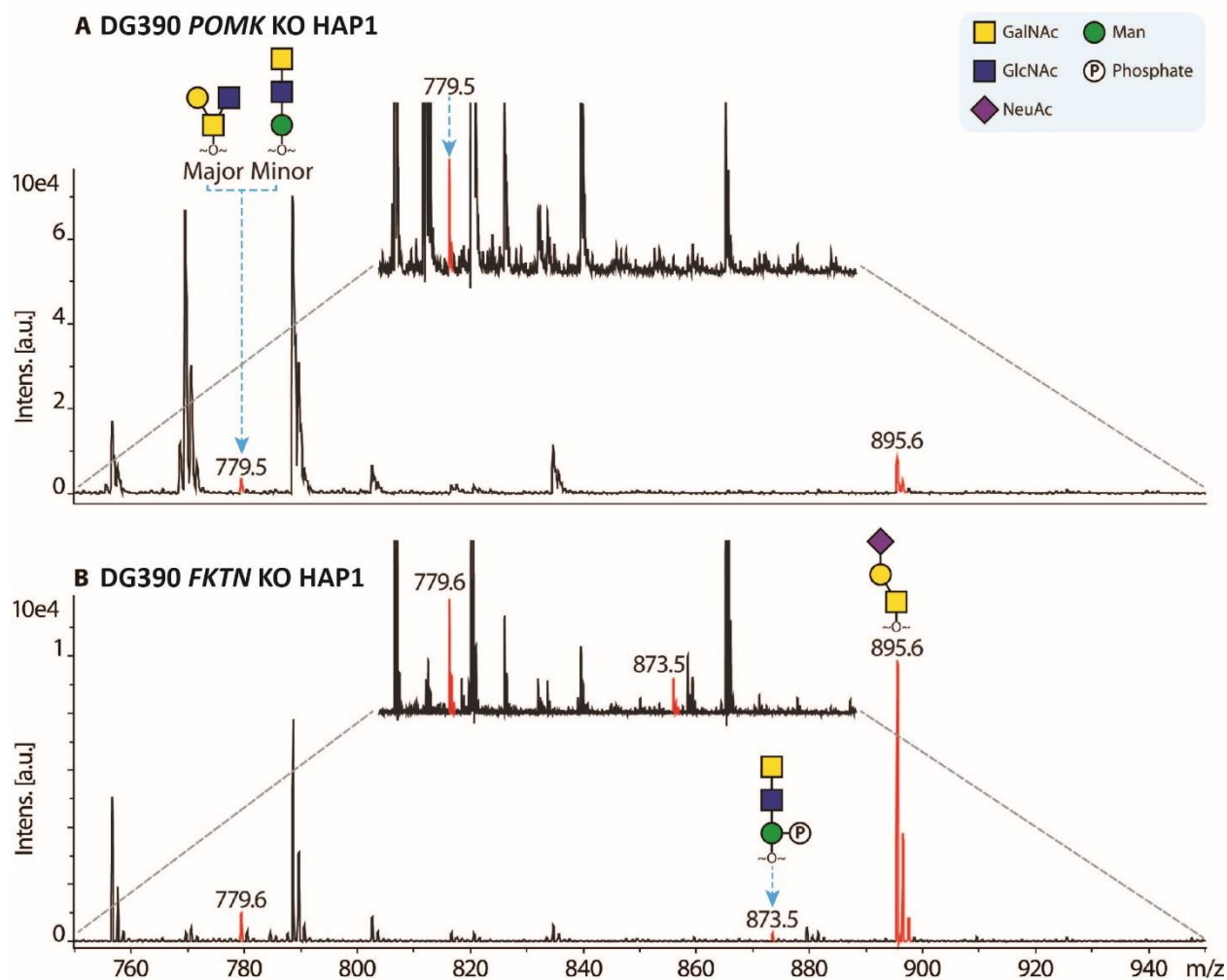
1294 **Figure 5 - Figure Supplement 2. *Pomk*-null Muscle Expresses Matriglycan. **A, B,****
 1295 **Glycoproteins were enriched from skeletal muscles of M-POMK KO, control, and *Large^{myd}* mice**
 1296 **and treated in combination with α -xylosidase (Xylsa) and β -glucuronidase (Bgus).**
 1297 **Immunoblotting was performed with **A,** AF6868 (Core α -DG and β -DG) and **B,** IIH6**
 1298 **(matriglycan). Results from three independent experiments are shown. Asterisk: β -DG. **C, A****
 1299 **laminin overlay was performed of control and M-POMK KO skeletal muscle and heart.**
 1300 **Glycoproteins from heart were enriched as above (three replicates).**



1301

1302

1303 **Figure 6 - Figure Supplement 1.** Supplemental Biochemical Analysis of POMK D204N and
 1304 *POMK* KO HAP1 Cells. **A**, **B**, **C**, *POMK* KO HAP1 cells were transduced with the indicated
 1305 adenoviruses and immunoblotting was performed for: **A**, POMK, **B**, Core α -DG and β -DG, and
 1306 **C**, matriglycan (IIH6), (three replicates). **D**, B3GALNT2 and **E**, B4GAT1 activity of *POMK* KO
 1307 HAP1 cells expressing POMK mutants. Activity of each mutant relative to WT POMK is
 1308 depicted. (Error bars: standard deviation). Results from three independent experiments are
 1309 shown.



1310

1311 **Figure 6- Figure Supplement 2.** Mass spectra of *O*-glycans carried by a DG mucin-like
 1312 domain model (DG390) expressed in *POMK* KO (A) or *Fukutin* (*FKTN*) KO (B) HAP1 cells.
 1313 The glycans were reductively released from the protein backbone and permethylated prior to
 1314 Matrix-Assisted Laser Desorption/Ionization time-of-flight (MALDI-TOF) analyses. Mass
 1315 spectrometry (MS) peaks corresponding to sodiated permethylated *O*-glycans were colored red
 1316 and annotated with glycan structures. The annotation was based on previous knowledge of
 1317 human *O*-glycan structure and biosynthesis. MS peaks at *m/z* 779.5 correspond to a mixture of
 1318 core 2 and core M3 *O*-glycan, and at 873.5, phosphorylated core M3 *O*-glycan. In addition,
 1319 mucin-type core 1 *O*-glycan was also observed (*m/z* 895.6). Non-annotated peaks are
 1320 contaminants from matrix and/or samples. The spectra were further zoomed (the spectra between
 1321 the grey dashed lines) to facilitate the relative intensity comparison between core M3
 1322 and phosphorylated core M3 *O*-glycans in the two samples. Under the current experimental set-
 1323 up, our MALDI-TOF data are not sufficient to determine the stereochemistries of
 1324 monosaccharides in the observed *O*-glycans. Raw MS data has been included as a supplement
 1325 for more information (*Source Data File 1*, *Source Data File 2*).

1326

1327
 1328
 1329
 1330
 1331
 1332
 1333
 1334
 1335
 1336
 1337
 1338
 1339
 1340
 1341
 1342
 1343
 1344
 1345
 1346
 1347
 1348
 1349
 1350
 1351
 1352
 1353
 1354
 1355

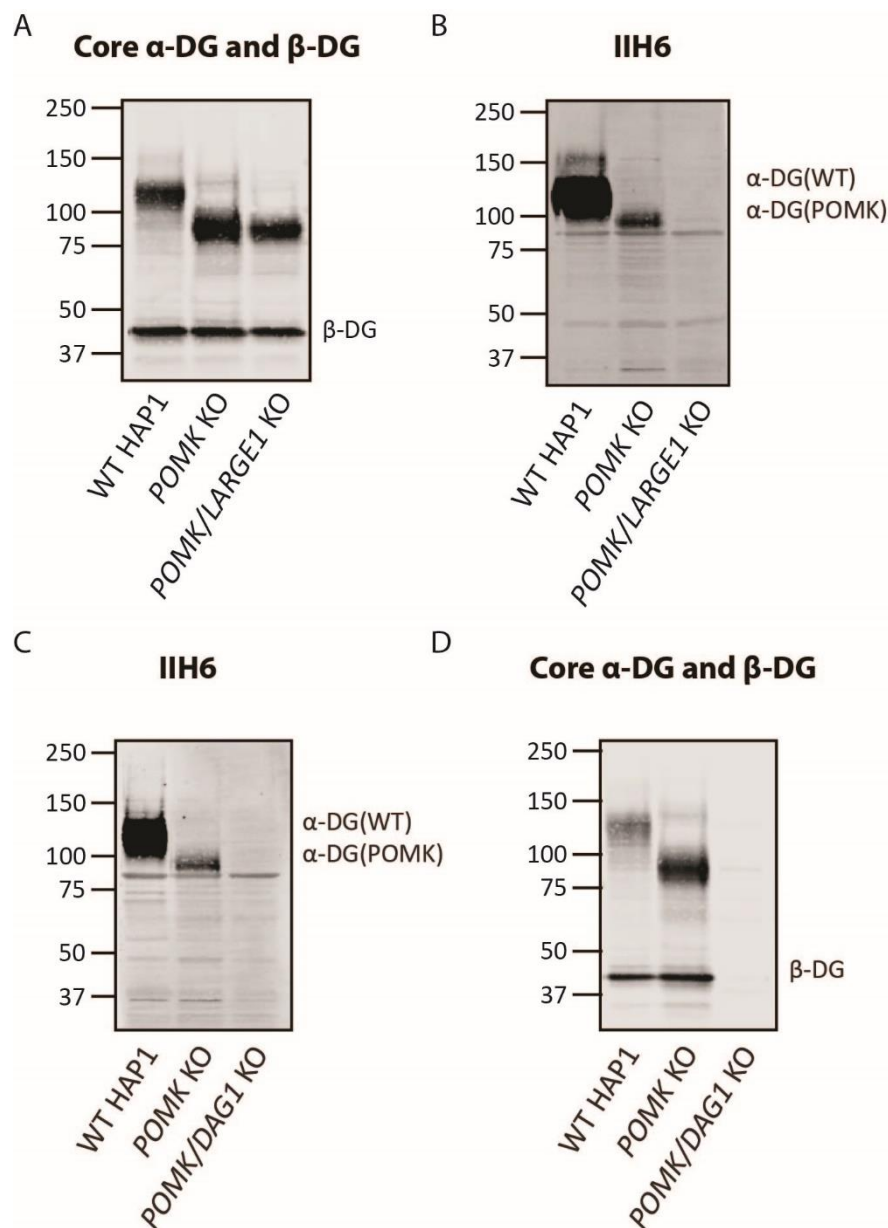
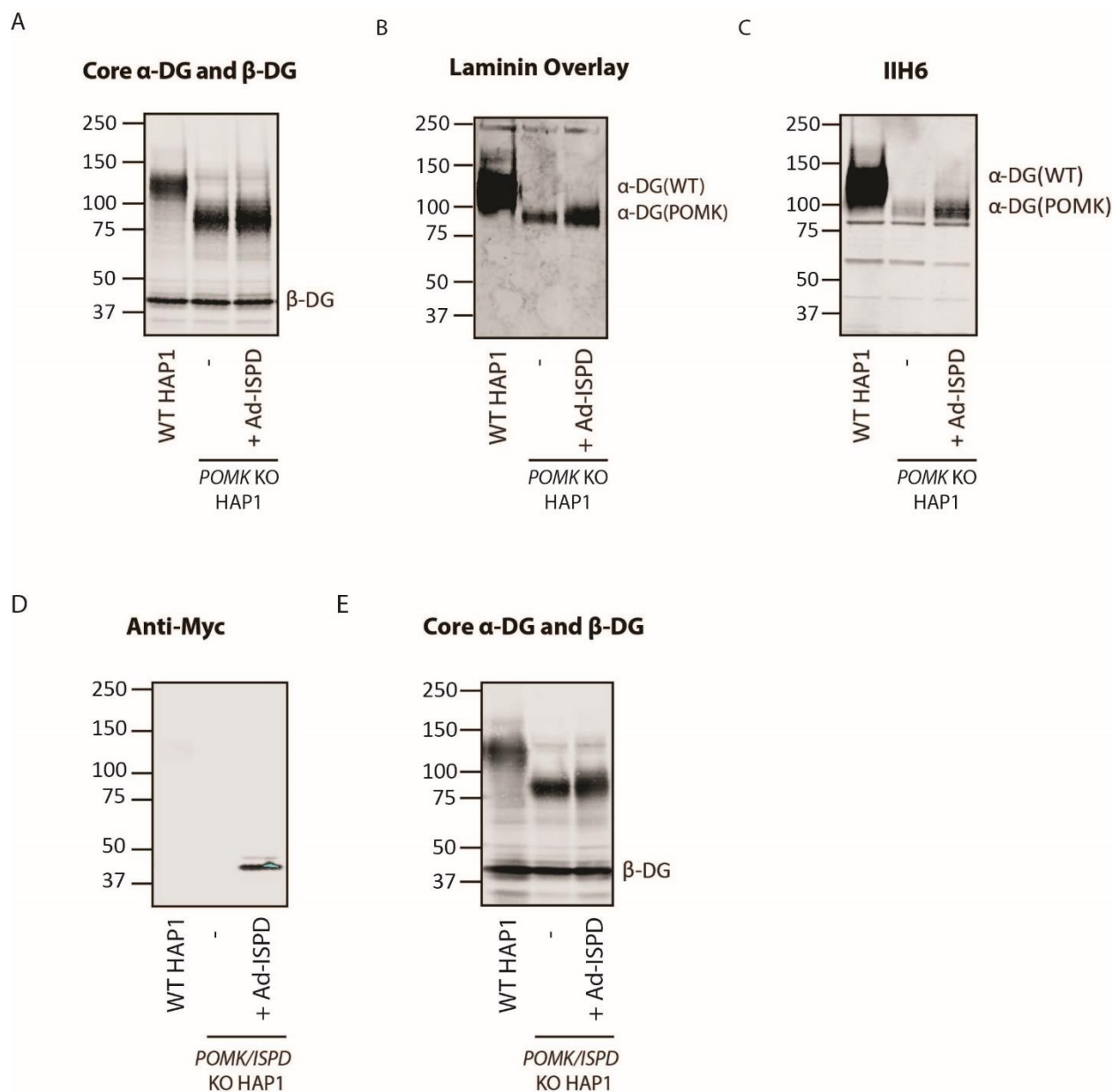
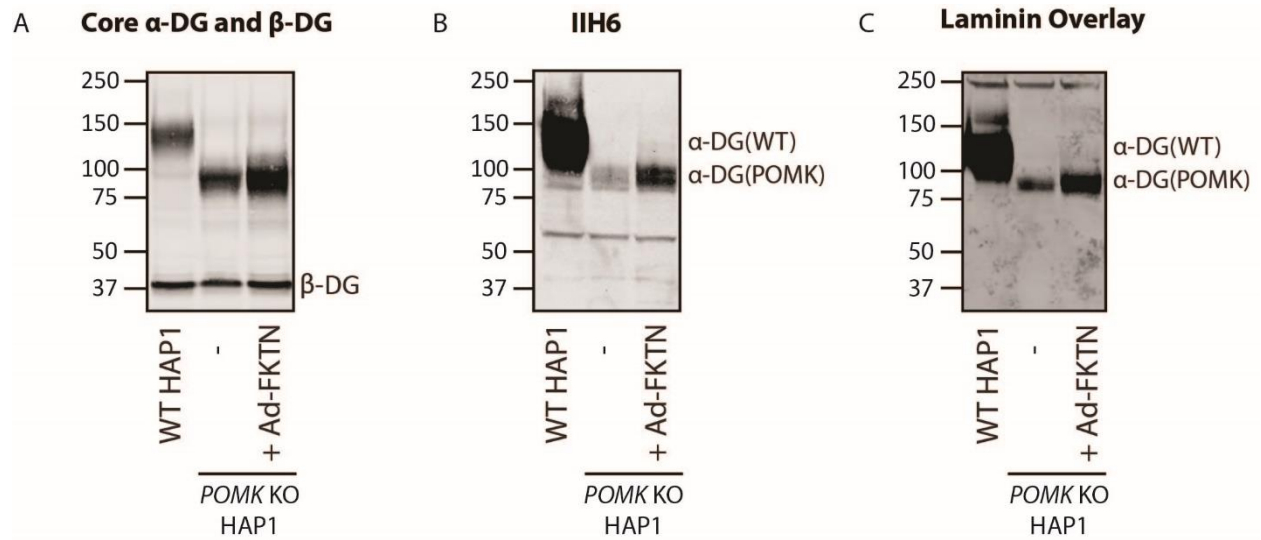


Figure 7 - Figure Supplement 1. Supplemental Biochemical Analysis of *POMK/LARGE1* KO and *POMK/DAG1* KO HAP1 Cells. **A, B** Immunoblotting of WT, *POMK* KO and *POMK/LARGE1* KO HAP1 cells with antibodies AF6868 (**A**) (Core α-DG and β-DG) or IIH6 (**B**). Glycoproteins were enriched using WGA-agarose as described in the Methods. **C, D** Immunoblotting of WT, *POMK* KO, and *POMK/DAG1* KO HAP1 cells with antibodies IIH6 (**C**) or AF6868 (**D**), (Core α-DG and β-DG). Representative results from three independent experiments are shown.

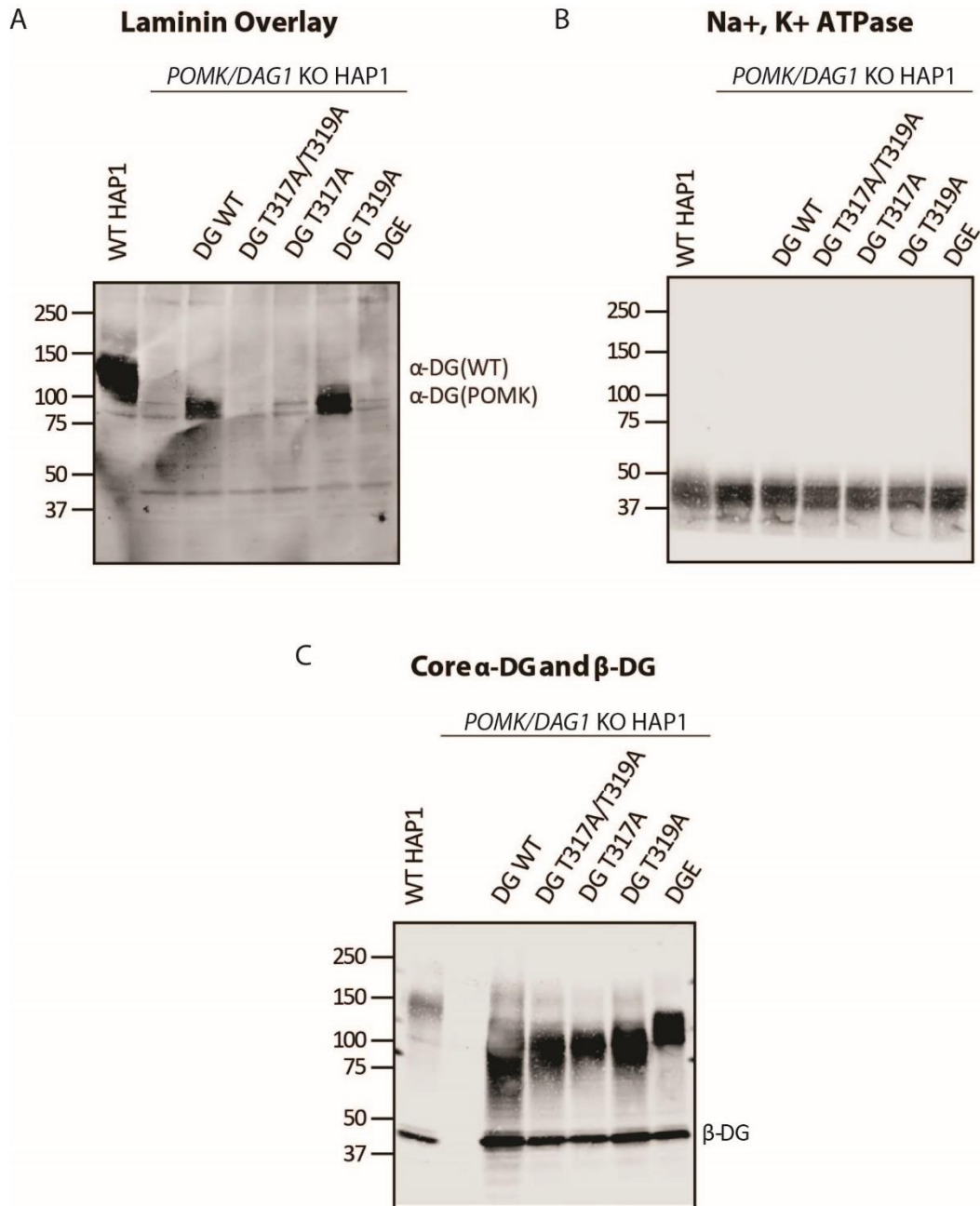


1356 **Figure 7 - Figure Supplement 2.** Requirement for Ribitol-Phosphate in the Synthesis of the
 1357 Non-Extended Form of Matriglycan. **A, B, C,** *POMK* KO HAP1 cells were transduced with an
 1358 adenovirus encoding Isoprenoid Synthase Domain-Containing (Ad-ISPd). Immunoblotting was
 1359 performed using antibodies AF6868 (**A**) or IIH6 (**C**). **B,** A laminin overlay was also performed.
 1360 Representative results from three independent experiments are shown. **D, E,** HAP1 cells lacking
 1361 expression of *ISPd* and *POMK* (*POMK/ISPd* KO) were transduced with Ad-ISPd.
 1362 Immunoblotting was performed with an anti-Myc antibody (**D**) or antibody AF6868 (**E**) (Core α-
 1363 DG and β-DG). Representative results from three independent experiments are shown.



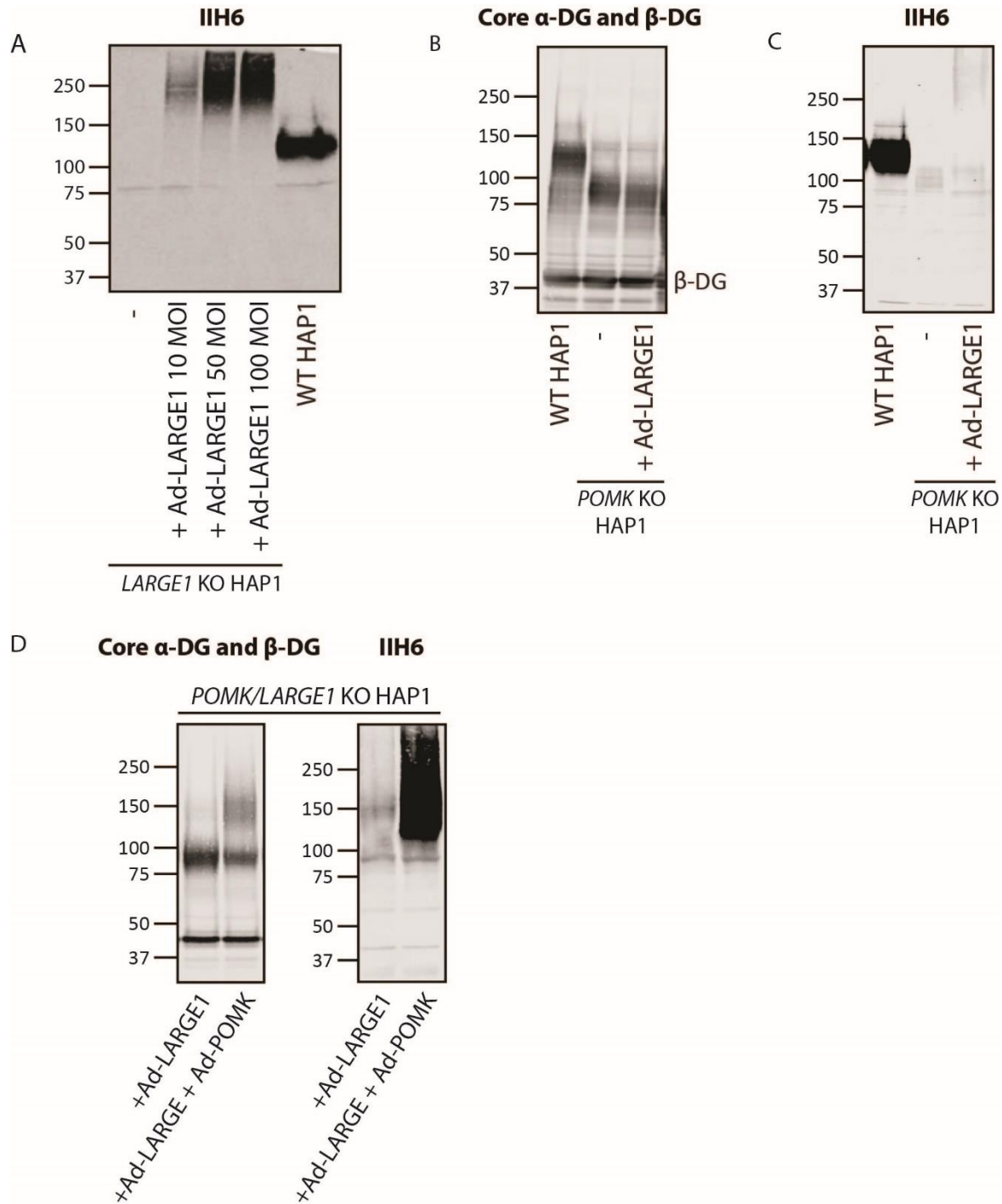
1364

1365 **Figure 7 - Figure Supplement 3.** Fukutin Overexpression Enhances Synthesis of the Non-
 1366 Extended Matriglycan. **A, B, C,** *POMK* KO HAP1 cells transduced with an adenovirus encoding
 1367 Fukutin (FKTN), Ad-FKTN. Immunoblotting was performed using antibodies AF6868 (**A**),
 1368 (Core α -DG and β -DG) or IIH6 (**B**) (three replicates). **C,** A laminin overlay was also performed
 1369 (three replicates).



1370
1371

1372 **Figure 7 - Figure Supplement 4.** T317 is Required for Synthesis of the Non-Extended
1373 Matriglycan. **A, B, C,** Biochemical analysis of *POMK/DAG1 KO HAP1* cells expressing the
1374 indicated adenoviruses (three replicates). DGE is for viral expression of α -DG that lacks the
1375 Dystroglycan N-terminal domain (DGN). **A,** A laminin overlay was performed. Immunoblotting
1376 was performed with an Na⁺/K⁺ ATPase antibody (**B**) and antibody AF6868 (**C**) (Core α -DG and
1377 β -DG).

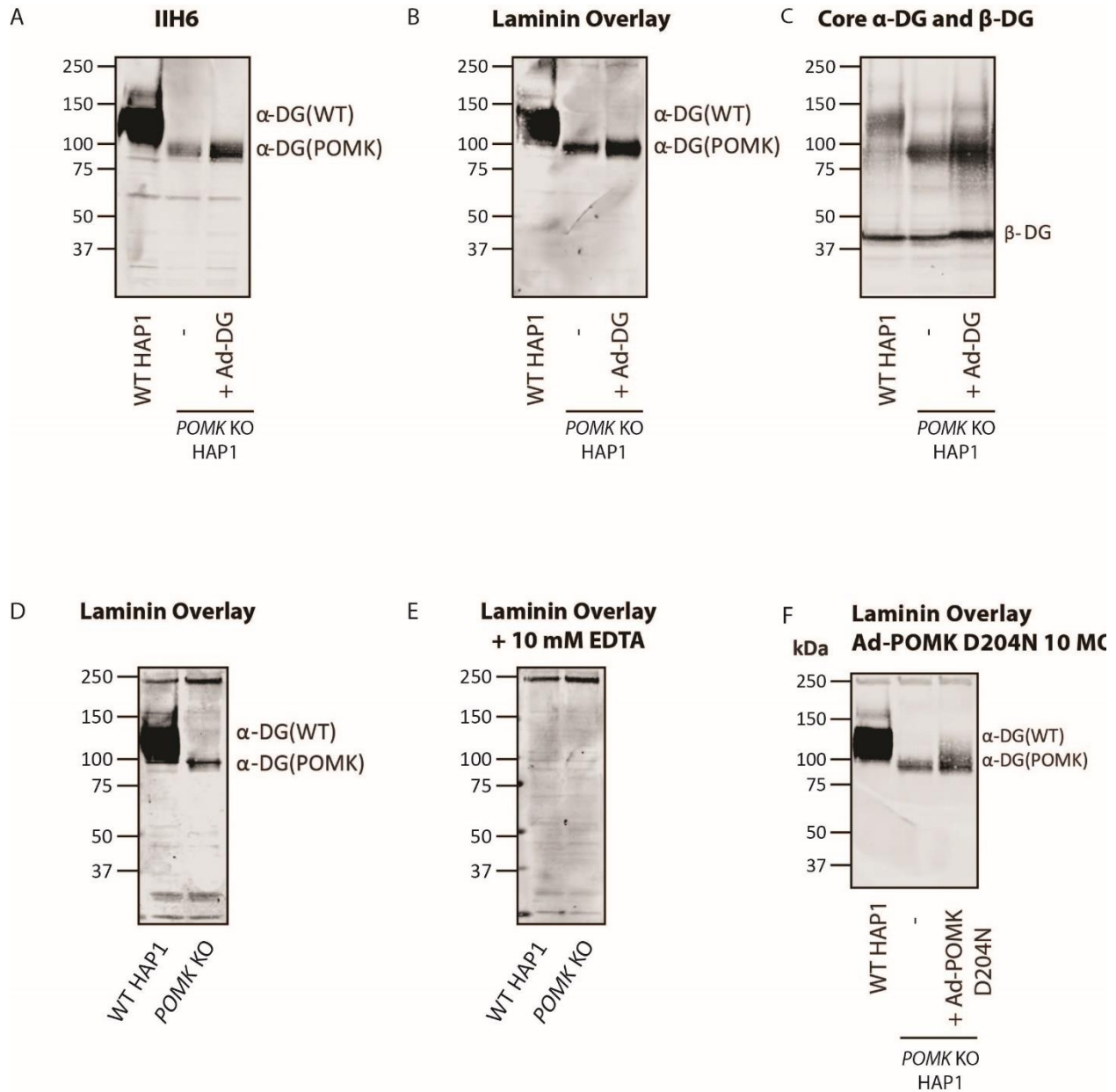


1378

1379

1380 **Figure 7 - Figure Supplement 5.** POMK Enables LARGE1-mediated Elongation of
 1381 Matriglycan. **A, B, C,** Immunoblots of the following HAP1 cells: **A,** *LARGE1* KO,
 1382 overexpressing Ad-LARGE1; **B, C,** *POMK* KO, overexpressing Ad-LARGE1; **D,**
 1383 *POMK/LARGE1* KO, overexpressing Ad-LARGE1 with or without Ad-POMK. Immunoblotting
 1384 was performed with antibodies AF6868 (Core α -DG and β -DG) or IIH6 (three replicates).

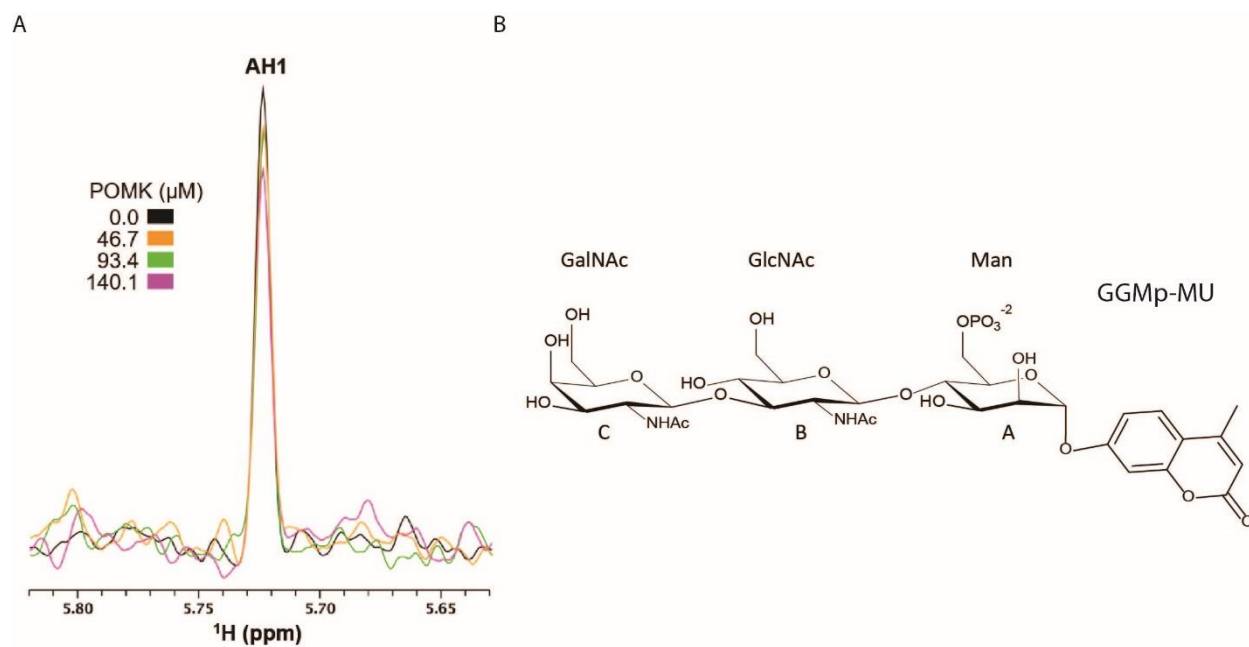
1385



1386

1387

1388 **Figure 7 - Figure Supplement 6.** Supplemental Characterization of POMK-null Matriglycan
 1389 Synthesis. **A, B, C**, *POMK* KO HAP1 cells were transduced with an adenovirus encoding DG
 1390 WT (Ad-DG) and immunoblotting was performed with antibodies IIH6 (**A**) and AF6868 (**C**)
 1391 (three replicates). A laminin overlay was also performed (**B**) (three replicates). **D, E**, Laminin
 1392 overlays of WT and *POMK* KO HAP1 cells were performed without (**D**) or with (**E**) EDTA
 1393 (three replicates). **F**, A laminin overlay of WT HAP1, *POMK* KO HAP1, or *POMK* KO HAP1
 1394 cells transduced with 10 MOI Ad-POMK D204N was performed (three replicates).

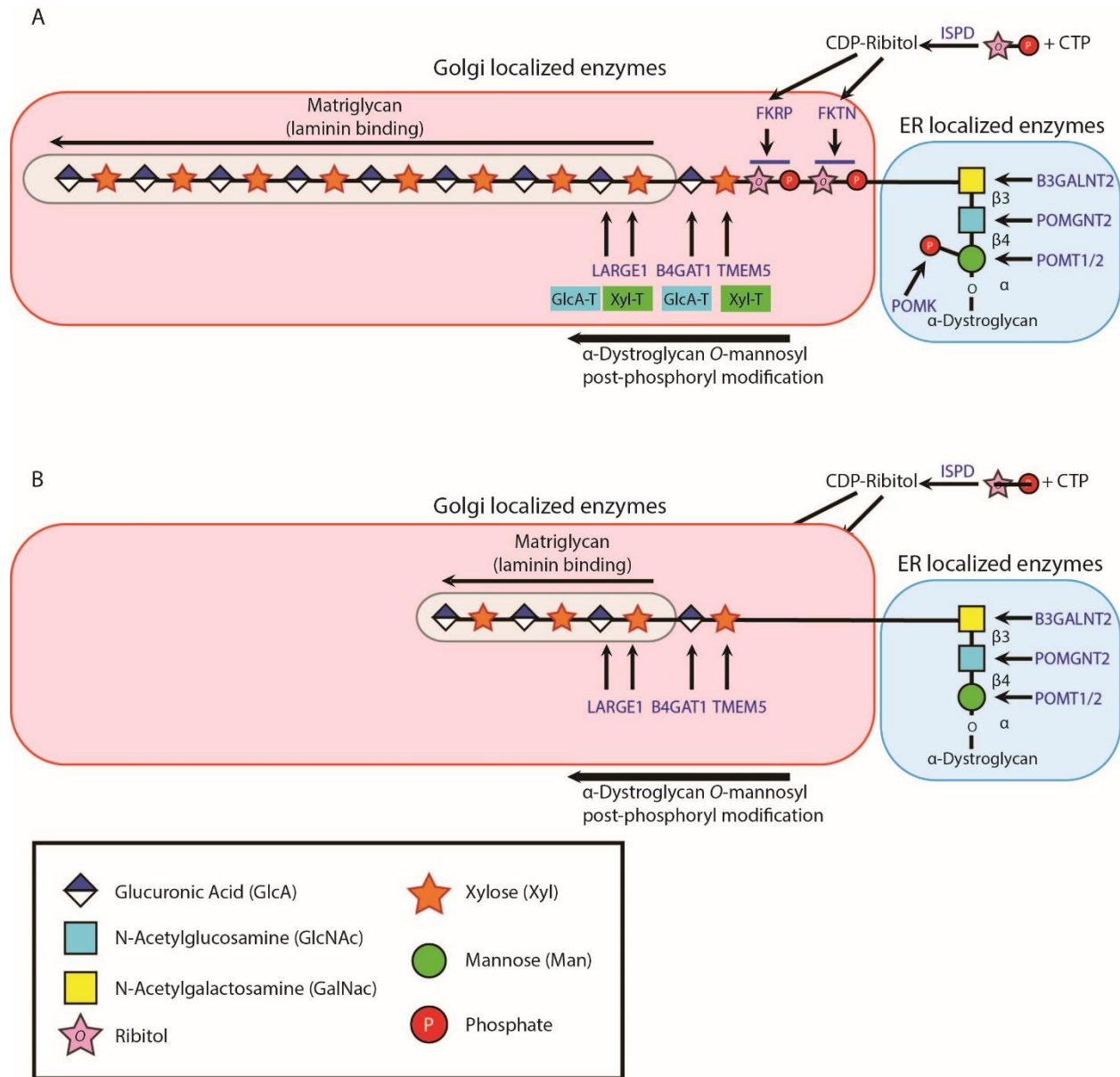


1395

1396

1397 **Figure 8 - Figure Supplement 1.** NMR Spectra of POMK Binding to GGMP-MU and Structure
 1398 of GGMP-MU. **A**, 1D ^1H NMR spectra of the glycan sample (10.0 μM GGMP-MU) were
 1399 acquired in the presence of various concentrations of zebrafish POMK as indicated. The ^{13}C and
 1400 ^1H resonances of GGMP-MU have been assigned before (*Yoshida-Moriguchi et al., 2013*). The
 1401 peak AH1 is derived from the residue A (Man) anomeric H1 proton. **B**, Chemical structure of
 1402 GGMP-MU.

1403



1404

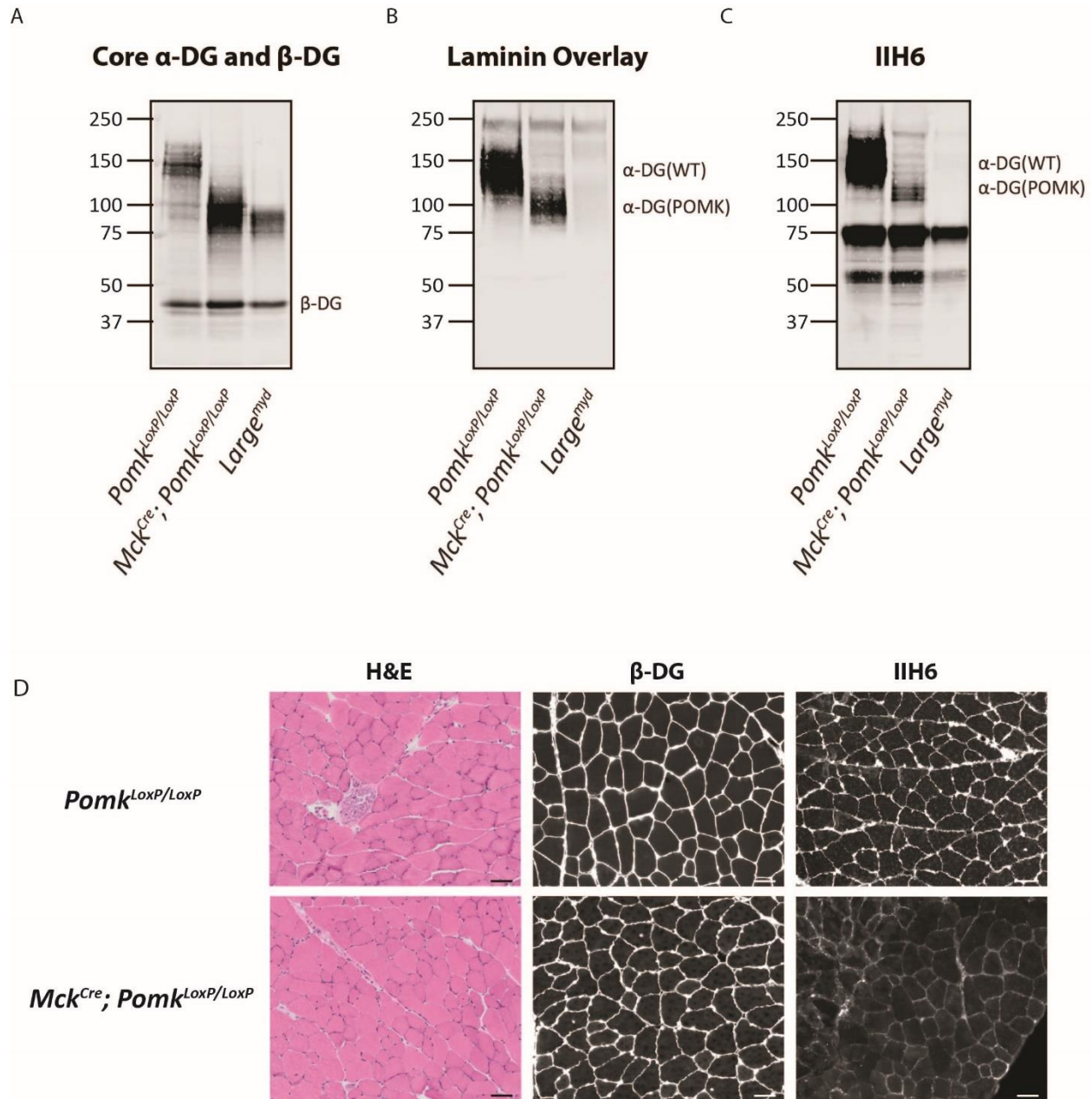
1405 **Figure 8 - Figure Supplement 2.** Model of Full-Length and Non-extended Matriglycan
 1406 Synthesis. **A**, Mature matriglycan is a long polysaccharide that is synthesized by LARGE1. **B**, In
 1407 the absence of the core M3 phosphate added by POMK, LARGE1 generates a shorter, non-
 1408 extended form of matriglycan.

1409

1410

1411

1412



1413

1414

1415 **Figure 8 - Figure Supplement 3.** Biochemical and Histologic Analysis of *Mck^{Cre}; Pomk^{LoxP/LoxP}*
 1416 Quadriceps Muscle. **A, B, C**, Representative biochemical analysis of glycoproteins enriched
 1417 from quadriceps skeletal muscles of *Pomk^{LoxP/LoxP}*, *Mck^{Cre}; Pomk^{LoxP/LoxP}*, and *Large^{myd}* mice
 1418 using WGA-agarose (three replicates). For immunoblotting, antibodies AF6868 (**A**) and IIH6
 1419 (**C**) were used, and a laminin overlay was also performed (**B**). **D**, Immunofluorescence and H&E
 1420 analyses of *Pomk^{LoxP/LoxP}* and *Mck^{Cre}; Pomk^{LoxP/LoxP}* quadriceps muscle sections from 8-month
 1421 old mice. Sections were stained with antibodies against β -DG (middle) and matriglycan (IIH6)

1422 (right). Histologic abnormalities in the sections were evaluated by means of hematoxylin and
1423 eosin (H&E) staining (left). Scale bars- 50 μ M (three replicates).

1424



HAP_FKTN_DG390_0_D21_1.txt

1425

1426 **Source Data File 1.** Raw MALDI-TOF data of DG390 expressed in FKTN KO (**Figure 6-**
1427 **Figure Supplement 2B**) HAP1 cells were exported to the TXT format by FlexAnalysis
1428 3.3 (Bruker Daltonics). The mass spectra in the article were zoomed into the range of m/z 750-
1429 950 to better present MS signals corresponding to CoreM3 glycan structures.



HAP_POMK_DG390_O22.txt

1430

1431 **Source Data File 2.** Raw MALDI-TOF data of DG390 expressed in POMK KO (**Figure 6-**
1432 **Figure Supplement 2A**) HAP1 cells were exported to the TXT format by FlexAnalysis
1433 3.3 (Bruker Daltonics). The mass spectra in the article were zoomed into the range of m/z 750-
1434 950 to better present MS signals corresponding to CoreM3 glycan structures.

Key Resources Table				
Reagent type (species) or resource	Designation	Source or reference	Identifiers	Additional information
Genetic reagent (<i>Mus musculus</i>)	<i>Pomk</i> ^{LoxP/LoxP} ICR	This paper	Campbell Lab	Materials and Methods “Generation of POMK ^{LoxP/LoxP} Mice”
Genetic reagent (<i>Mus musculus</i>)	<i>Pax7</i> ^{Cre} C57BL/6J	The Jackson Laboratory, Bar Harbor ME.	JAX:010530, RRID:IMSR JAX:010530	<i>Pax7</i> ^{tm1(cre)Mrc}
Genetic reagent (<i>Mus musculus</i>)	<i>Mck</i> ^{Cre} C57BL/6J	The Jackson Laboratory, Bar Harbor ME.	JAX:006475, RRID:IMSR_ JAX:006475	B6.FVB(129S4)-Tg(Ckmm-cre)5Khnl/J
Genetic reagent (<i>Mus musculus</i>)	<i>Large</i> ^{myd} C57BL/6J	The Jackson Laboratory, Bar Harbor ME.	JAX:000300, RRID:IMSR_ JAX:000300	MYD/Le-Os +/+ Largemyd/J myd
Antibody	anti-DG (Sheep polyclonal)	R and D Systems	Cat# AF6868, RRID:AB_10891298	WB (1:500)
Antibody	anti-α-DG (IIH6C4) (Mouse monoclonal)	DSHB Campbell Lab	Cat# IIH6C4, RRID:AB_2617216	WB (1:10-1:100)
Antibody	anti-myc clone 4A6 (Mouse monoclonal)	Millipore	Cat# 05-724, RRID:AB_309938	WB (1:2000)

Antibody	anti- α -DG (IIH6C4) (Mouse monoclonal)	Millipore Campbell Lab	Cat# 05- 593, RRID:AB_3 09828	IF (1:1000- 1:2000)
Antibody	anti-Laminin (Rabbit polyclonal)	Sigma-Aldrich	Cat# L9393, RRID:AB_4 77163	WB (1:1000), Solid Phase Assay (1:5000)
Antibody	anti- β -DG (Rabbit polyclonal)	Campbell Lab PMID: 1741056 DOI: 10.1038/35569 6a0	AP83	IF (1:50)
Antibody	anti- β -DG mouse IgM (Mouse monoclonal)	Leica Biosystems	Cat# NCL- b-DG, RRID:AB_4 42043	IF (1:50 to 1:200)
Antibody	anti-Na ⁺ ,K ⁺ ATPase (Mouse monoclonal)	BD Biosciences	Cat# 610993 RRID:AB_3 98306	WB (1:1000)
Antibody	anti-sheep IgG (Donkey polyclonal)	Rockland	Cat# 613- 731-168, RRID:AB_2 20181	WB (1:2000)
Antibody	anti-mouse IgG (H + L) (Donkey polyclonal)	LI-COR Biosciences	Cat# 926- 32212, RRID:AB_6 21847	WB (1:15,000), IF (1:800)
Antibody	anti-rabbit IgG (H + L) (Donkey polyclonal)	LI-COR Biosciences	Cat# 926- 32213, RRID:AB_6 21848	WB (1:15,000), IF (1:800)

Antibody	anti-mouse IgM (Goat polyclonal)	LI-COR Biosciences	Cat# 926-32280, RRID:AB_2814919	WB (1:2500)
Antibody	anti-mouse IgG1 (Goat polyclonal)	LI-COR Biosciences	Cat# 926-32350, RRID:AB_2782997	WB (1:2000, 1:10,000)
Antibody	anti-rabbit IgG (H+L) (Goat polyclonal)	Thermo Fisher Scientific	Cat# A-11034, RRID:AB_2576217	IF (1:1000 to 1:2000)
Antibody	anti-mouse IgM (Goat polyclonal)	Thermo Fisher Scientific	Cat# A-21042, RRID:AB_2535711	IF (1:1000 to 1:2000)
Antibody	anti-human FLJ23356 (Mouse monoclonal)	Novus	Cat# H00084197-M03, RRID:AB_2188284	WB (1:500)
Commercial assay or kit	Creatine Kinase (CK) Liqui-UV™ Test	Fisher Scientific/Stanbio	Cat# 22-022-630	
Cell line (<i>Homo-sapiens</i>)	Parental cell line C631	Horizon Discovery	Cat# C631	Mycoplasma testing passed
Cell line (<i>Homo-sapiens</i>)	<i>POMK/DAG1</i> KO	Horizon Discovery	HZGHC001338c004, RRID:CVC_L_TF19	Authenticated by Sanger sequencing. Mycoplasma testing passed.
Cell line (<i>Homo-sapiens</i>)	<i>POMK/LARGE1</i> KO	Horizon Discovery	HZGHC007364c011	Authenticated by Sanger sequencing.

				Mycoplasma testing passed.
Cell line (<i>Homo-sapiens</i>)	<i>POMK</i> KO	Horizon Discovery	HZGHC001 338c004, RRID:CVC L_TF19	Authenticated by Sanger sequencing. Mycoplasma testing passed.
Cell line (<i>Homo-sapiens</i>)	<i>POMK/ISPD</i> KO	Horizon Discovery	HZGHC001 338c001, RRID:CVC L_TF18	Authenticated by Sanger sequencing. Mycoplasma testing passed.
Cell line (<i>Homo-sapiens</i>)	<i>FKTN</i> KO	Horizon Discovery	HZGHC000 721c010, RRID:CVC L_SN68	Authenticated by Sanger sequencing. Mycoplasma testing passed.
Cell line (<i>Homo-sapiens</i>)	<i>LARGE1</i> KO	Horizon Discovery	HZGHC000 122c007, RRID:CVC L_SV31	Authenticated by Sanger sequencing. Mycoplasma testing passed.
Cell line (<i>Homo-sapiens</i>)	Primary dermal fibroblasts, human	ATCC	PCS-201-012	
Cell line (<i>Homo-sapiens</i>)	Human fibroblasts (POMK D204N)	This paper	NH13-284	Dubowitz Neuromuscular Center, Campbell Lab

Peptide, recombinant protein	β -Glucuronidase	PMID: 16303119 DOI: 10.1016/j.carres.2005.10.005		
Peptide, recombinant protein	α -Xylosidase	PMID: 10801892 DOI: 10.1074/jbc.M910392199		
Biological sample (<i>Homo-sapiens</i>)	Control human skeletal muscle	This paper		Dubowitz Neuromuscular Center, Campbell Lab
Biological sample (<i>Homo-sapiens</i>)	Human skeletal muscle	This paper	(NH13-284, POMK D204N)	Dubowitz Neuromuscular Center, Campbell Lab
Chemical compound, drug	Purified <i>Danio rerio</i> POMK	PMID: 27879205 DOI: 10.7554/eLife.22238		
Chemical compound, drug	Purified mammalian dTMLARGE1	PMID: 22223806 DOI: 10.1126/science.1214115		
Chemical compound, drug	GGM-MU and GGMP-MU	PMID: 23929950 DOI: 10.1126/science.1239951		

Chemical compound, drug	UDP-Xylose	CarboSource	https://www.ccrcc.uga.edu/~carbosource/CSS_substrates.html	
Chemical compound, drug	4-Methylumbelliferyl- β -D-xylopyranoside	Sigma/Millipore	Cat# M7008	
Chemical compound, drug	UDP-Glucuronic acid	Sigma/Millipore	Cat# U6751	
Chemical compound, drug	Uridine 5'-diphospho-N-acetylgalactosamine disodium salt	Sigma/Millipore	Cat# U5252	
Chemical compound, drug	Uridine 5'-diphospho-N-acetylglucosamine sodium salt	Sigma/Millipore	Cat# U4375	
Chemical compound, drug	4-methylumbelliferyl α -(GlcNAc- β (1-4)Man) GM-MU	Sussex Research	https://www.sussex-research.com/	
Chemical compound, drug	Xylose- α 1,3-GlcA- β -MU	Sussex Research	https://www.sussex-research.com/	
Chemical compound, drug	Pepstatin A	Sigma/Millipore	Cat# 516481	
Chemical compound, drug	Calpain Inhibitor I (25mg)	Sigma/Millipore	Cat# A6185	

Chemical compound, drug	Aprotinin from bovine lung	Sigma/Millipore	Cat# A1153	
Chemical compound, drug	Leupeptin (25mg)	Sigma/Millipore	Cat# 108975	
Chemical compound, drug	PMSF	Sigma/Millipore	Cat# P7626-25G	
Chemical compound, drug	Immobilon-FL PVDF	Sigma/Millipore	Cat# IPFL00010	
Chemical compound, drug	Calpeptin	Fisher Scientific	Cat# 03-340-05125M	
Chemical compound, drug	Bis-acrylamide solution-30% (37:1)	Fisher Scientific/Hoef er	Cat# HBGR3375 00X	
Chemical compound, drug	Benzamidine Hydrochloride Hydrate	MP Biochemicals	Cat# 195068	
Chemical compound, drug	WGA agarose bound	Vector Labs	Cat# AL-1023, RRID:AB_2336862)	
Chemical compound, drug	Precision Plus Protein All Blue Standards-500ul	Bio-Rad	Cat# 161-0373	
Software, algorithm	SigmaPlot	SigmaPlot	RRID:SCR_003210	

Software, algorithm	Excel	Microsoft	RRID:SCR_016137	
Software, algorithm	GraphPad Prism	https://www.graphpad.com/scientific-software/prism/	RRID:SCR_002798	Version 8.3
Software, algorithm	FlowJo	https://www.flowjo.com/solutions/flowjo/downloads	RRID:SCR_008520	Version 7.6.5
Software, algorithm	Li-Cor Image Studio Software	https://www.licor.com/bio/image-studio-lite/download	RRID:SCR_015795	
Other	Streptavidin, Alexa Fluor™ 594 conjugate	Thermo Fisher Scientific	Cat# S11227	IF (1:1000 to 1:2000)
Other	Adenovirus: DGC (DG, delta H30-A316)	PMID: 21987822 DOI: 10.1073/pnas.1114836108		
Other	Adenovirus: DG T317A	PMID: 21987822 DOI: 10.1073/pnas.1114836108		
Other	Adenovirus: DG T319A	PMID: 21987822 DOI: 10.1073/pnas.1114836108		

Other	Adenovirus: DG T317A/319A	PMID: 21987822 DOI: 10.1073/pnas. 1114836108		
Other	Adenovirus: DG Wild-Type (WT)	PMID: 21987822 DOI: 10.1073/pnas. 1114836108		
Other	Adenovirus: POMK WT	PMID: 27879205 DOI: 10.7554/eLife. 22238		
Other	Adenovirus: POMK D204A	PMID: 27879205 DOI: 10.7554/eLife. 22238		
Other	Adenovirus: POMK D204N	This paper	Campbell Lab	Materials and Methods "Adenovirus Production"
Other	Adenovirus: DG390TEVHis	This paper	Campbell Lab	Materials and Methods "Adenovirus Production"
Other	Adenovirus: Fukutin	PMID: 22522420 DOI: 10.1038/ng.22 52		

Other	Adenovirus: Isoprenoid Synthase Domain- Containing (ISPD)	PMID: 22522420 DOI: 10.1038/ng.22 52		
Other	Adenovirus: LARGE1	PMID: 22522420 DOI: 10.1038/ng.22 52		
Other	NMR spectrometer	Bruker	Avance II 800 MHz	
Other	Rodent Treadmill	Columbus Instruments	Exer 3/6 Treadmill	
Other	Western Blot Imager	Li-Cor	Odyssey CLx	
Other	Mouse treadmill	Omnitech Electronics	Accupacer Treadmill	
Other	Isolated Mouse Muscle System	Aurora Scientific	1200A	
Other	Mouse Grip Strength Meter	Columbus Instruments	1027 Mouse	
Other	Prominence HPLC	Shimadzu	LC-20 system	

Other	Tabletop ultracentrifuge	Beckman Coulter	Optima max, 130K	
Other	Ultracentrifuge	Beckman Coulter	Optima-L-100 XP	
Other	Centrifuge	Beckman Coulter	Avanti J-E HPC	
Other	HPLC LC18 column	Supelco	58368	